N73-16693
NASA TR R-400

NASA TECHNICAL REPORT

NASA TR R-400

A THEORETICAL AND EXPERIMENTAL INVESTIGATION OF THE LINEAR AND NONLINEAR IMPULSE RESPONSES FROM A MAGNETOPLASMA COLUMN

by Norman Charles Grody

Goddard Space Flight Center

Greenbelt, Md. 20771

NATIONAL AERONAUTICS AND SPACE ADMINISTRATION • WASHINGTON, D. C. • FEBRUARY 1973

1. Report No.	2. Government Accession No.	3. Recipient's Catalog No.
NASA TR R-400		

4. Title and Subtitle	5. Report Date
A Theoretical and Experimental Investigation of the Linear and Nonlinear Impulse Responses From a Magnetoplasma Column	February 1973
	6. Performing Organization Code
7. Author(s)	8. Performing Organization Report No.
Norman Charles Grody	G-1072
9. Performing Organization Name and Address	10. Work Unit No.
Goddard Space Flight Center Greenbelt, Maryland 20771	11. Contract or Grant No.
	13. Type of Report and Period Covered
12. Sponsoring Agency Name and Address	Technical Report
National Aeronautics and Space Administration Washington, D.C. 20546	14. Sponsoring Agency Code

15. Supplementary Notes

16. Abstract

Linear and nonlinear responses of a magnetoplasma resulting from inhomogeneity in the background plasma density are studied. The plasma response to an impulse electric field was measured and the results are compared with the theory of an inhomogeneous cold plasma.

A 120-ps baseband pulse with a maximum peak amplitude of 1860 V was used to impulsively drive the plasma into the nonlinear regime. Because of the extremely short time scale of observation, ionization and electron heating, which alter the plasma background, are absent. The predominant electron relaxation mechanism is caused by plasma inhomogeneity; the observed phenomena arise from the effects produced by the inhomogeneity in the plasma density.

The impulse responses were recorded for the different plasma densities, static magnetic fields, and neutral pressures and generally appeared as modulated, damped oscillations. The frequency spectra of the waveforms consisted of two separated resonance peaks.

For weak excitation, the results correlate with the linear theory of a cold, inhomogeneous, cylindrical magnetoplasma. The damping mechanism is identified with that of phase mixing due to inhomogeneity in plasma density.

With increasing excitation voltage, the nonlinear impulse responses display stronger damping and a small increase in the frequency of oscillation. These results are also observed in the frequency spectra of the waveforms and correlate with the nonlinear theory of a cold, inhomogeneous plasma. The nonlinear mechanism is attributed to electron bunching and multistreaming caused by inhomogeneity.

17. Key Words (Selected by Author(s))	18. Distribution Statement
Linear impulse Nonlinear impulse Magnetoplasma column Inhomogeneous plasma	Unclassified—Unlimited

19. Security Classif. (of this report)	20. Security Classif. (of this page)	21. No. of Pages	22. Price*
Unclassified	Unclassified	68	$3.00

*For sale by the National Technical Information Service, Springfield, Virginia 22151.

CONTENTS

CONTENTS (concluded)

A THEORETICAL AND EXPERIMENTAL INVESTIGATION OF THE LINEAR AND NONLINEAR IMPULSE RESPONSES FROM A MAGNETOPLASMA COLUMN

by
Norman Charles Grody
Goddard Space Flight Center

1. INTRODUCTION

The study of laboratory plasmas has received increased attention within the past few years because of its application to the areas of space and nuclear science. Microwave scattering from plasma columns has been investigated with increasing detail, resulting in a better understanding of the interactions between charged particles and electromagnetic radiation. Correlation between experiment and theory has been increased by improvements in experimental techniques and advances in theory.

Although many contributions have been made, there are a number of questions unanswered, particularly those concerning the nonlinear plasma response to excitation. Unlike the linear response, to which superposition applies, the nonlinear response generally exhibits different plasma properties depending on the form of excitation used. Herein is reported the study of the linear and nonlinear responses of a magnetoplasma to an impulsively applied electric field.

The impulse response has always been recognized as a valuable tool for studying the properties of physical systems. However, because of practical limitations, little experimental work has been done involving the impulsive excitation of a laboratory plasma. The use of sharp, baseband pulses (10^{-9} s) as an experimental tool for plasma studies was first employed by Schmitt in 1964 (References 1 and 2). Later, Baldwin, Henderson, and Hirshfield (Reference 3) also did some work with baseband pulses. However, the strengths for the impulses used ranged from 40 mV in Schmitt's work to about 5 V in the experiments of Baldwin et al., and nonlinear effects were never studied.

To excite the plasma at the nonlinear level, large peak pulse voltage must be employed. A special pulse generator[1] was developed for this purpose and was used throughout this experimental investigation. This generator, called a "bouncing-ball generator" (BBG), is capable of producing baseband pulses with pulse widths of 120 ps at the 3-dB points and peak voltage greater than 1 kV into a 50-Ω load. Because of the availability of this device combined with the utilization of a very fast sampling scope, the nonlinear investigation became feasible. In fact, much of the concern involving signal-to-noise ratio, stability of the system, sensitivity, resolution, etc., proved to be unfounded by the measurements made.

[1] P. Pleshko and I. Palocz: Memorandum M-6, School of Engineering and Science, New York Univ., 1969.

Impulse excitation has many advantages over other forms of excitation when studying plasmas. The following list indicates a few of the important reasons why this form of excitation was chosen for studying the plasma dynamics.

(1) The impulse response serves as a simple method for displaying and analyzing the plasma properties.

(2) At the linear level, the impulse response can be used to obtain the response to other forms of excitation by applying the well-known convolution principle.

(3) At the nonlinear level, the large-amplitude sharp BBG pulse is preferred over continuous microwaves because high-power microwaves result in ionization of the atoms and electron heating, which alter the background plasma density and temperature.

(4) Most of the measurements and observations can be made very quickly (<20 ns) after the application of the impulse. This period is usually short compared to the electron-neutral collision time, thus enabling one to study phenomena predicted by "collisionless" theoretical models.

These items are used to full advantage throughout this work.

Experiments have recently been performed by Sindoris, Grody, and Cheo (Reference 4) using the BBG to observe the plasma responses (with and without a static magnetic field). In this study more detailed measurements of the time responses were obtained and used to identify the oscillations and relaxation properties of the plasma. The linear impulse responses appeared as modulated, damped oscillations, the modulation being produced by the magnetic field. For the BBG voltages exciting the electrons to initial velocities greater than 10^8 cm/s, the nonlinear plasma responses exhibited both an increase in oscillation frequency and stronger damping with increasing excitation. To identify the physical mechanisms characterizing these linear and nonlinear responses, the experimental results are compared with theory.

The linear impulse responses are shown to correlate with those predicted by the linear theory of a cold, inhomogeneous plasma. This theoretical model was studied by Baldwin and Ignat (Reference 5) for an isotropic plasma column and by Henderson (Reference 6) for a magnetoplasma. However, their work was primarily concerned with the plasma responses to continuous microwaves and was extended in this study using approximate techniques to include impulse excitation. At the nonlinear level, the experimental results, i.e., increased oscillation frequency and damping, are shown to be in agreement with the nonlinear theory proposed in this report.

Theoretical Background: Impulse Response of a Cold Magnetoplasma

A magnetoplasma consists of charged particles of various species interacting with each other in the presence of a static magnetic field. The following is a brief account describing the time development of the cold-plasma response to an impulsively applied electric field directed transverse to the static magnetic field.

Impulse excitation results initially in the separation of electrons from a relatively fixed, neutralizing ion charge background. The electron motion is prescribed by the space-charge restoring force

resulting from the fixed ions and the additional force caused by the static magnetic field. In the absence of any thermal motion, these forces cause the electrons to orbit about their initial positions. The resulting stimulated emission of radiation from the plasma has been studied and the following plasma characteristics discerned:

Considering a linear, homogeneous, cold magnetoplasma, the emitted radiation appears as one or two undamped (i.e., neglecting radiation and collisional dampings) oscillations depending on the mode of excitation. Inhomogeneity in either the ion density or magnetic field produces a continuous spread in electron orbital periods, resulting in the damping of the plasma response because of phase mixing. This form of linear damping was first described by Baldwin and Ignat (Reference 5) for an isotropic plasma and by Henderson (Reference 6) for a magnetoplasma. Greenwald (Reference 7) showed that for conditions easily attained in the laboratory, damping resulting from inhomogeneity can exceed that due to radiation and electron-neutral collisions.

In addition to these linear effects, the plasma displays nonlinear behavior for large impulse amplitude. In particular, nonlinearity resulting from plasma inhomogeneity damps the plasma response beyond the linear damping value. The nature of this nonlinear damping mechanism has been indicated by Leavens and Leavens (Reference 8) and also by Schneider and Bers (Reference 9) and is briefly described.

The plasma boundary contains a relatively low ion density with a large spatial gradient. This results in the formation of strong electron bunching at the boundary, followed in time by multistreaming (electron crossover or overtaking). The multistreaming acts to damp the plasma response because, once it starts, it eventually spreads throughout the plasma removing the phase coherence among the different electrons. Because of the amplitude dependence associated with the streaming velocity of propagation, the damping is inherently nonlinear.

The nonlinear response of a plasma to impulse excitation is analyzed in Section 2, where the following properties are noted: For a given time, it is the electrons that previously had not participated in multistreaming that contribute largely to the plasma response. These electrons are generally found near the central region of the plasma where inhomogeneity is small and plasma density is high. Consequently, the nonlinear plasma response arises predominately from the higher frequency orbital electrons, resulting in an increase in oscillation frequency in addition to an increase in damping.

The experimental results are compared with this cold-plasma theory.

Experimental Background: Pulse Excitation of a Laboratory Plasma

Until recently, most experimental investigations used continuous microwaves for studying plasmas. The application of pulse excitation as an experimental tool has been employed only recently, following the development of fractional-nanosecond pulses and sampling scopes capable of detecting them. The following survey describes some of the contributions made by other investigators using this form of excitation.

Initial work involving pulse excitation of plasmas besides that of Schmitt (References 1 and 2) was performed by Hill and Kaplan (Reference 10) in 1965. They applied short (10-ns) microwave pulses having 15-W average power to nonlinearly excite an afterglow plasma immersed in a slightly

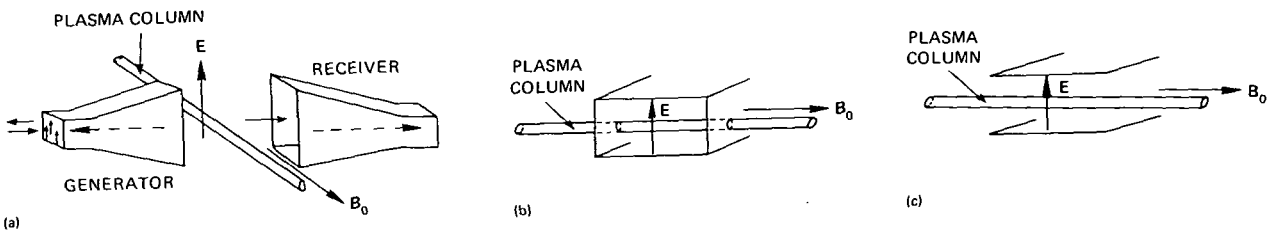

Figure 1—Configurations for plasma excitation. (a) Antenna. (b) Waveguide. (c) Parallel plate.

inhomogeneous magnetic field. The plasma was placed between transmitting and receiving antennas; the orientation of the plasma, static magnetic field B_0, and pulsed electric field E are shown in Figure 1a. The two-pulse response displayed signals (termed echoes) that appeared after the second pulse and depended nonlinearly on the applied pulse amplitudes.

Following the discovery of echoes, other investigators (References 11 to 14) began studying their properties to identify the plasma nonlinearities. This study incorporates single-pulse techniques to investigate the linear and nonlinear plasma properties; the studies referred to in the following paragraphs are related to the problems discussed in this research.

Bruce, Crawford, and Harp (Reference 15) performed experiments with a single microwave pulse incident to an afterglow plasma placed in waveguide as shown in Figure 1b. The linear transient response was recorded for different magnetic field inhomogeneities, plasma densities, and neutral pressures to exhibit the effects of magnetic field inhomogeneity, inhomogeneity in plasma density, and electron-neutral collisions on the single-pulse relaxation. Large-amplitude-pulse measurements were made for the collision-dominated regime, showing that the plasma response nonlinearly damps because of the speed-dependent electron-neutral collisions. Nonlinear measurements were not made for the *collisionless* regime in which inhomogeneity effects become important.

Impulse excitation of a nonmagnetoplasma was performed by Baldwin, Henderson, and Hirshfield (Reference 3) to observe the linear response. An afterglow discharge was used, with the plasma column placed between the plates of a parallel-plate structure as shown in Figure 1c ($B_0 = 0$). The plasma was weakly excited using a 5.0-V, 3.0-ns baseband pulse, resulting in a damped oscillatory response. The oscillation frequency was correlated with the Tonks dipole resonance (Reference 16) measured from the peak in steady-state reflection from the cylindrical plasma column. No identification was made of the damping observed.

In contrast with the work performed by Bruce et al. (Reference 15) and Baldwin et al. (Reference 3), this study observed the impulse response of a low-pressure, continuous-dc-discharge magnetoplasma to both weak and strong excitation. The plasma column was placed within a parallel-plate structure as indicated in Figure 1c and was excited by a fractional-nanosecond baseband pulse having a maximum peak amplitude of 1860 V. Because of the low pressure, electron-neutral collisions were unimportant; the plasma response was dominated by effects resulting from inhomogeneity in plasma density.

One of the most interesting results of this study was the observation of a slight increase in the frequency of oscillation in addition to an increase in damping for strong excitation. These nonlinear

phenomena are not predicted by existing theories (References 11 to 14) and a new mechanism is proposed in Section 2 to account for these effects.

Experimental Techniques

Experiments were conducted to examine the linear and nonlinear impulse response of a low-pressure, continuous-discharge argon magnetoplasma. Unlike the previously mentioned experiments, a fractional-nanosecond baseband pulse having a maximum of 1860 V peak from the BBG was applied to excite the plasma at the linear and nonlinear levels. For all practical purposes, this excitation is equivalent to an impulse and is referred to as such. Detailed measurements were made displaying the impulse responses; the following is a brief description of the experimental setup and the results obtained.

The plasma column was placed between the plates of a broadband parallel-plate transmission structure, and a uniform static magnetic field was directed along the column axis as shown in Figure 1c. This orientation of applied pulsed electric field E and static magnetic field B_0 is used exclusively throughout this work. The plasma parameters pertinent to the experiments performed are $f_c < f_p$ and $\nu \ll f_p$, where f_c, f_p, and ν are the electron-cyclotron, plasma, and electron-neutral collision frequencies, respectively. These parameters are controlled independently by varying the static magnetic field, plasma discharge current, and argon neutral pressure, respectively.

The plasma was impulsively excited by the fractional-nanosecond baseband pulse propagating along the parallel-plate structure that was properly terminated with negligible reflections. A broadband directional coupler was used to separate the low-voltage impulse response from the larger excitation pulse. (Details are given in Section 3.) The impulse response was then transmitted through the coupling port and observed on a sampling scope, or an accompanying X-Y recorder.

The impulse responses of the structure with and without the plasma on are shown in Figure 2 on the same voltage and time scales. Also shown is the power spectrum determined from the plasma impulse response.

In the absence of any plasma, $f_p = 0$, the leakage of the excitation pulse through the coupling port was observed followed in time by the smaller residual reflections due to the cable connectors, glass plasma tube, etc. Excitation of the structure with the plasma on resulted in plasma oscillations that were easily distinguished from the leakage and residual reflections. These measurements were performed using a low-level (50-V) pulse and for the plasma parameters indicated. Additional impulse responses obtained for different plasma parameters are discussed in Section 4.

The impulse response of the magnetoplasma generally appeared as a modulated, damped oscillation and is compared in Section 4 with the linear theory of a cold, inhomogeneous, cylindrical magnetoplasma. This behavior was further displayed by Fourier analyzing the time responses using a digital computer to obtain the power spectrum.

The appearance of the two (split-dipole) resonances in the spectrum was originally obtained from microwave scattering measurements by Tonks in 1931 (Reference 16) and in the 1960's by Messiaen and Vandenplas (Reference 17) and also by Crawford et al. (Reference 18). However, their

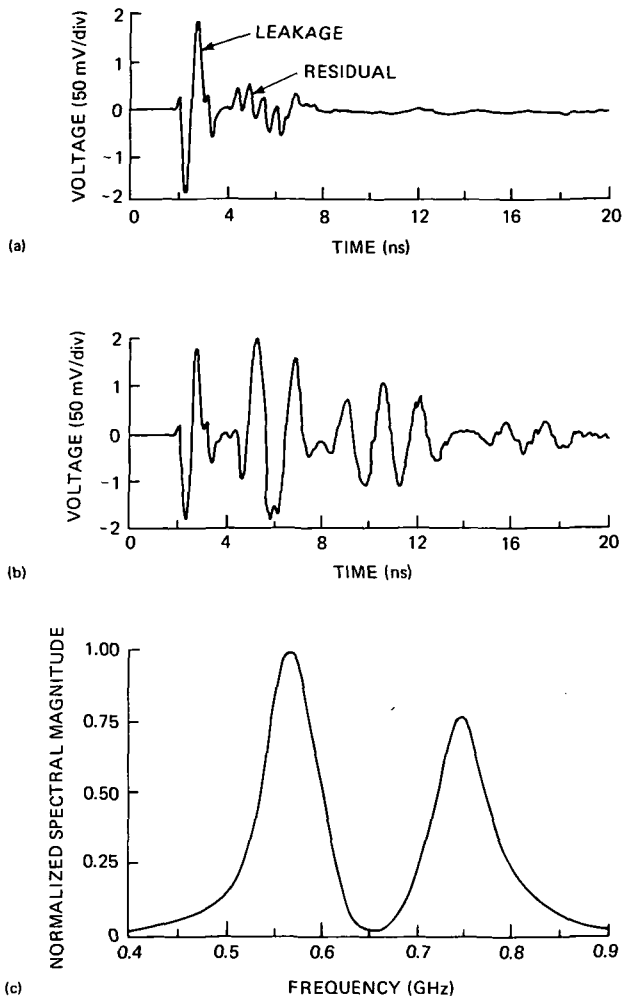

Figure 2—Linear impulse responses and spectrum. (a) Linear impulse response with f_p = 0. (b) Linear impulse response with f_p = 1.1 GHz, ν = 0.03 GHz, and f_c = 0.2 GHz. (c) Power spectrum determined from the plasma impulse response.

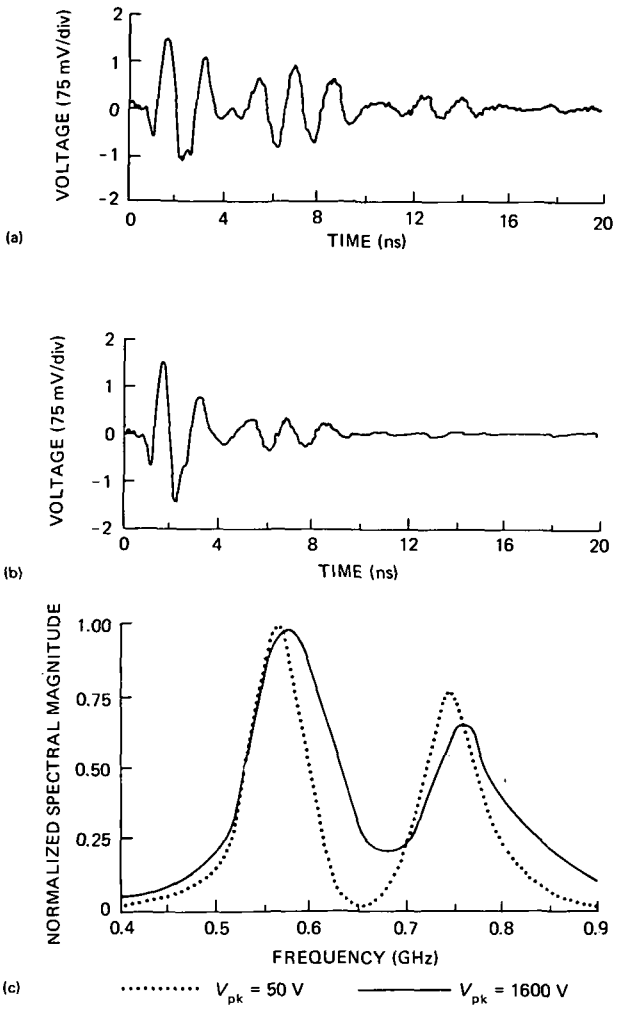

Figure 3—Linear and nonlinear impulse responses and spectra produced by different V_{pk}. (a) Impulse response for V_{pk} = 50 V. (b) Impulse response for V_{pk} = 1600 V. (c) Power spectra determined from the plasma impulse responses.

measurements are not as readily interpreted as those of this study because they were made by sweeping plasma current (consequently changing the plasma density profile) for a fixed microwave frequency. In particular, for studying the damping and frequency shift due to inhomogeneity in plasma density, it is desirable to obtain measurements for a fixed discharge current and varying excitation frequency. Such a series of experiments was performed in this study, with the plasma current as a parameter, and is described in Section 4.

The preceding impulse measurement of Figure 2 was obtained using a low-voltage excitation pulse, resulting in the linear impulse response of the plasma. The nonlinear impulse response was obtained by applying larger excitation. Figure 3 shows the impulse responses for 50- and 1600-V peak pulse

amplitudes V_{pk} for the same overall system gain. The plasma parameters were the same as used previously. It is observed that larger excitation results in a stronger damped response with a small increase in the oscillation frequency. This nonlinear behavior is also exhibited in the power spectra determined from the time responses with a computer. The spectra shown in Figure 3 display the two resonances, although the linear spectrum (V_{pk} = 50 V) contains sharper resonances appearing at slightly lower frequencies than the nonlinear spectrum (V_{pk} = 1600 V). Additional nonlinear impulse responses and their spectra are presented in Section 4.

One objective of this work is to compare the observed nonlinearities with the nonlinear theory of a cold, inhomogeneous plasma.

2. THEORY

The theory concerns the linear and nonlinear responses of a magnetoplasma to an impulsively applied electric field. The analysis entails solving both the dynamical equations for particles and Maxwell's equations subject to appropriate initial and boundary conditions. This general description results in a set of coupled, nonlinear equations for the plasma constituents. To simplify the analysis, assumptions are made that are later correlated with experimentally observed results.

Throughout this discussion, the thermal properties of the plasma are neglected, resulting in a cold-plasma description. The theoretical results are summarized below, and are applied in Section 4 to explain the measurements made.

To obtain an analytical solution for the plasma response, simple geometry and plasma conditions are considered. The equations for a cold, inhomogeneous magnetoplasma slab are developed and the linear results of this theory are presented and shown to be in agreement with those of Henderson (Reference 6). The linear impulse response is observed to appear as an oscillation that damps because of phase mixing resulting from inhomogeneity.

The nonlinear impulse response is then discussed. Applying the theory developed for cold, inhomogeneous magnetoplasmas, two radically different nonlinear mechanisms are observed and are treated separately in the text. Because of the anharmonic electron motion, the plasma response exhibits a decrease in oscillation frequency with increasing impulse amplitude. Nonlinearity also appears in the form of electron bunching, followed in time by electron crossover (multistreaming or overtaking) which randomizes the electron velocities. This phenomenon is shown to appear initially at the plasma boundary where inhomogeneity is maximum, spreading throughout the plasma with an amplitude-dependent propagation velocity. Because the fluid equations used are invalid after electron crossover occurs, numerical results are used to show that the plasma response damps nonlinearly and increases in frequency with increasing impulse amplitude. A comparison is made between the two nonlinear mechanisms, showing that the second form dominates in general. This observation is borne out by experimental results.

The effects due to cylindrical geometry, which is the experimental geometry used, are examined. It is observed that unlike the slab geometry, a cylindrical, cold magnetoplasma supports a dipole mode of excitation. This results in a linear impulse response consisting of two oscillations, which, for a homogeneous plasma, are separated by the electron-cyclotron frequency. This interference between

the two oscillations produces a modulated oscillatory response. Just as for the one-dimensional case, inhomogeneity causes a linear damping of the response because of phase mixing. However, it is shown using approximate techniques that the additional degree of freedom results in a more heavily damped response. The linear results are extended to the nonlinear regime by referring to the results for slab geometry.

Equations for a Cold, Inhomogeneous Magnetoplasma Slab

In this section, the equations for a cold, inhomogeneous magnetoplasma slab are derived. The derivation is similar to that developed by Davidson and Schram (Reference 19) for a homogeneous plasma. The plasma is exactly described in the zero-temperature limit by the following fluid equations:

$$\frac{\partial}{\partial t} n_e(\mathbf{r}, t) + \nabla \cdot n_e(\mathbf{r}, t)\mathbf{v}_e(\mathbf{r}, t) = 0 \tag{1}$$

$$\left[\frac{\partial}{\partial t} + \mathbf{v}_e(\mathbf{r}, t) \cdot \nabla\right] \mathbf{v}_e(\mathbf{r}, t) = -\frac{e}{m_e}\left[\mathbf{E}(\mathbf{r}, t) + \mathbf{v}_e(\mathbf{r}, t) \times \mathbf{B}_0(\mathbf{r})\right] . \tag{2}$$

Equation 1 is denoted as the continuity equation for the electrons, where n_e is the electron density and $\mathbf{v}_e$ is the electron velocity. The dynamical equation for an electron is prescribed by Equation 2, where $\mathbf{E}$ is the electric field as seen by the electron and $\mathbf{B}_0$ is the static magnetic field. In the electrostatic approximation, the electric field is derivable from a scalar potential, so $\mathbf{E} = -\nabla\Phi$. The significance of this approximation is discussed in the section, "Linear Equations for a Cylindrical, Cold Magnetoplasma."

Poisson's equation then supplements Equations 1 and 2:

$$\nabla \cdot \mathbf{E}(\mathbf{r}, t) = -\frac{e}{\epsilon_0}\left[n_e(\mathbf{r}, t) - n_i(\mathbf{r})\right] \tag{3}$$

where $n_i(\mathbf{r})$ is the ion density. The ions are considered relatively fixed compared to the electrons, and merely constitute a neutralizing charge background.

Equations 1 and 3 are combined, eliminating n_e:

$$\nabla \cdot \left\{\left[\frac{\partial}{\partial t}\mathbf{I} + \mathbf{v}_e(\mathbf{r}, t)\nabla\right] \cdot \mathbf{E}(\mathbf{r}, t) - \frac{e}{\epsilon_0} n_i(\mathbf{r})\mathbf{v}_e(\mathbf{r}, t)\right\} = 0 \tag{4}$$

where $\mathbf{I}$ is a unit dyadic.

Equations 1, 2, and 4 represent a set of coupled, nonlinear equations for the plasma constituents n_e, $\mathbf{v}_e$, and $\mathbf{E}$. The solution of these equations subject to appropriate initial and boundary conditions gives the plasma response.

To obtain an analytical solution, a one-dimensional plasma slab is treated as shown in Figure 4, where the plasma constituents are functions of x and t. Inhomogeneity in the background ion density is considered to vary along the x direction. The static magnetic field is in the z direction and is also

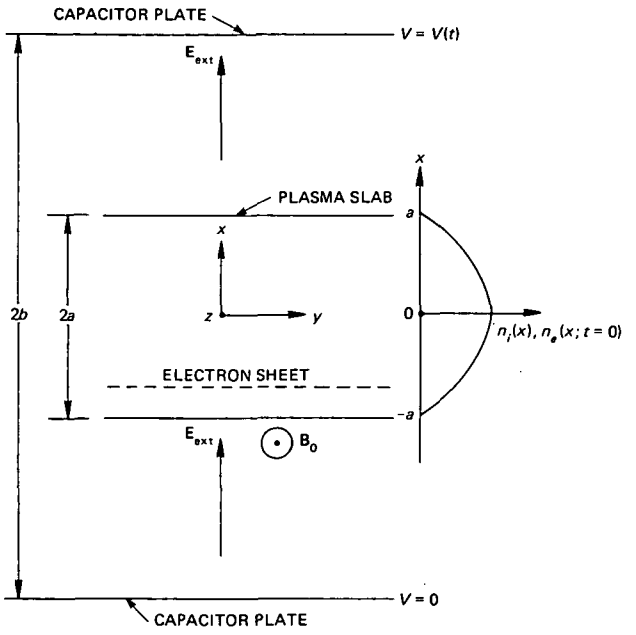

Figure 4—Plasma slab geometry.

considered to vary as a function of x. Then the electric fields external and internal to the plasma are in the x direction and independent of the y and z coordinates to be consistent with the electrostatic approximation; i.e., $\mathbf{E} = -\nabla\Phi(x, t)$.

For this one-dimensional geometry, Equations 1, 2, and 4 become

$$\frac{\partial}{\partial t} n_e(x, t) + \frac{\partial}{\partial x} n_e(x, t) v_x(x, t) = 0 \tag{5}$$

$$\left[\frac{\partial}{\partial t} + v_x(x, t)\ \frac{\partial}{\partial x}\right] v_x(x, t) = -\frac{e}{m_e}\left[E_x(x, t) + v_y(x, t) B_0(x)\right] \tag{6}$$

$$\left[\frac{\partial}{\partial t} + v_x(x, t)\ \frac{\partial}{\partial x}\right] v_y(x, t) = \frac{e}{m_e} v_x(x, t) B_0(x) \tag{7}$$

$$\left[\frac{\partial}{\partial t} + v_x(x, t)\ \frac{\partial}{\partial x}\right] E_x(x, t) = \frac{e}{\epsilon_0} n_i(x) v_x(x, t) + \frac{d}{dt} E_{\text{ext}} \tag{8}$$

where Equation 8 is obtained from Equation 4 after integrating with respect to x (from $-b$ to x). Equation 5 is deduced from Equation 1, and Equations 6 and 7 are a result of Equation 2. Although these results are simpler than the original set of equations, various techniques must be employed to obtain analytical solutions at the nonlinear level.

Equations 5 to 8 are in Eulerian coordinates (x, t) where x and t are independent variables. These equations become simplified when the Lagrangian coordinates (x_0, τ) are introduced as new independent variables (see Reference 19); that is,

where

$$\left.\begin{aligned} \tau &= t \\ x_0 &= x - X, \\ X &= \int_0^{\tau} v_x(x_0, \tau')\, d\tau' . \end{aligned}\right\} \tag{9}$$

As shown in Appendix A, this transformation has the effect of replacing the convective derivative, $\partial/\partial t + v_x\ \partial/\partial x$, by the local derivative, $\partial/\partial\tau$. The transformation physically represents a change of the fixed x, t coordinates to X, τ coordinates following the electron motion from an initial point x_0.

The following trajectory equation is then obtained:

$$\frac{\partial^2 X}{\partial \tau^2} + \int_0^X \omega_p^2(x')\, dX' + \omega_c(x) \int_0^X \omega_c(x')\, dX' = -\frac{e}{m_e} E_{\text{ext}} \tag{10}$$

where $x' = X' + x_0$ and $X(x_0, \tau)$ is the electron displacement in the x direction from its initial position x_0. The parameters $\omega_p(x)$ and $\omega_c(x)$ are the plasma and electron-cyclotron frequencies, respectively, and are defined by the equations

$$\left.\begin{aligned} \omega_p(x) &= \sqrt{\frac{n_i(x)e^2}{\epsilon_0 m_e}} \\ \omega_c(x) &= \frac{e}{m_e} B_0(x) \end{aligned}\right\} \tag{11}$$

The electric field in the plasma $E_x(x_0, \tau)$ and electron density $n_e(x_0, \tau)$ are shown in Appendix A to be

$$E_x(x_0, \tau) = E_{\text{ext}} + \frac{m_e}{e} \int_0^X \omega_p^2(x')\, dX' \tag{12}$$

$$n_e(x_0, \tau) = \frac{n_e(x_0, 0)}{1 + (\partial/\partial x_0) X(x_0, \tau)}\,, \tag{13}$$

where, in the case of impulse excitation, the initial electron density $n_e(x_0, 0)$ is the ion density $n_i(x_0)$.

Equation 10 describes the electron displacement $X(x_0, \tau)$ from an initial point x_0 due to an externally applied excitation. This equation could have been derived by considering the plasma composed of elementary electron sheets (Reference 20), where $X(x_0, \tau)$ is the sheet displacement from its equilibrium position x_0. (A typical electron sheet is shown in Figure 4.) The motion of the sheets is characterized by the space-charge restoring force resulting from the fixed ions and the additional force of the static magnetic field.

Equations 10 and 12 describe the space-time development of the electric field in the plasma caused by an externally applied excitation. To obtain the field in Eulerian (laboratory) x, t coordinates, x_0 and $X(x_0, \tau)$ must be transformed back to x, t. This requires the solution of the nonlinear algebraic equation

$$X(x_0, \tau) + x_0 = x\,, \tag{14}$$

which can only be solved numerically. For the inverse transformation to be unique, it is required that

$$\frac{\partial}{\partial x_0} X(x_0, \tau) > -1\,. \tag{15}$$

The physical significance of this condition is discussed in the following: Considering Equation 13, it is seen that the electron density becomes large (i.e., electron bunching appears) as the denominator approaches zero. Following bunching, the electrons begin to cross over as is determined by the inequality $(\partial/\partial x_0)X \leqslant -1$. Equation 15 defines the x_0, τ coordinates for which there is no overtaking of electrons. When the inequality of Equation 15 is not satisfied, the electron density becomes negative and the use of the fluid equations for describing the processes following electron bunching becomes invalid. The effects of bunching at crossover and the more important randomization following crossover were observed in the numerical simulation work of Schneider and Bers (Reference 9). In a later section of this report, a simple mechanism based on these observations is proposed that is capable of explaining the essential experimental observations of nonlinear impulse responses of plasma columns (with or without magnetic fields) made in this work and in the earlier reported work (Reference 4); i.e., the increase of oscillation frequency and damping.

It is seen that the nonlinearity in the plasma results in a nonlinear trajectory (Equation 10) for the electrons, in addition to the singular behavior (i.e., shock formation) of the electron density. The effects of these two mechanisms on the nonlinear impulse response is discussed later.

Linear Impulse Response

For small amplitude of excitation, the electron displacement $X(x_0, t)$ from its equilibrium position x_0 is small. Equations 10 and 12 are linearized by substituting for x' the linearized value x_0. Also, the transformation equation 14 is linearized resulting in the following linear equations:

$$\left[\frac{\partial^2}{\partial t^2} + \omega_h^2(x)\right] X(x, t) = -\frac{e}{m_e} E_{\text{ext}} \tag{16}$$

$$E_x(x, t) = E_{\text{ext}} + \frac{m_e}{e}\omega_p^2(x)X(x, t)\,, \tag{17}$$

where

$$\omega_h(x) = \sqrt{\omega_p^2(x) + \omega_c^2(x)}$$

is the upper hybrid frequency.

For an excitation in the form of a δ-function pulse, that is,

$$E_{\text{ext}} = Et_p\,\delta(t)\,, \tag{18}$$

the linear trajectory equation (Equation 16) has the solution

$$X(x, t) = \frac{v_p}{\omega_h(x)} \sin \omega_h(x)t\,, \tag{19}$$

where $v_p = (e/m_e)Et_p$ is the electron velocity developed initially from an externally applied pulse of amplitude E and effective width t_p.

The potential $V(t)$ developed across the parallel-plate configuration is obtained from Equation 19 in conjunction with Equation 17; that is,

$$V(t) = \int_{-b}^{b} E_x(x, t)\, dx$$

$$= 2bE_{ext} + V_{pl}(t)\,, \tag{20}$$

where the plasma response $V_{pl}(t)$ is the following well-known result (Reference 6):

$$V_{pl}(t) = \frac{m_e}{e} v_p \int_{-a}^{a} \frac{\omega_p^2(x)}{\omega_h(x)} \sin \omega_h(x) t\, dx\,. \tag{21}$$

The solution of Equation 21 depends on the particular form of density profile and magnetic-field variation in the plasma. For a homogeneous plasma,

$$V_{pl}(t) = 2a \frac{m_e}{e} \frac{\omega_p^2}{\omega_h} \sin \omega_h t\,, \tag{22}$$

which is an undamped oscillation at the upper hybrid frequency. To display the effects of inhomogeneity on the plasma response, one can apply stationary-phase integration to Equation 21 and obtain the following asymptotic response:

$$V_{pl}(t) = \sum_n \frac{(m!)^{1/m}\, \Gamma(1/m)}{m} \frac{\omega_p^2(x_n)}{\omega_h(x_n)} \frac{Et_p}{\left|(\partial^m/\partial x^m)\omega_h(x_n)\right|^{1/m}} \frac{\sin\left[\omega_h(x_n)t - \pi/2m\right]}{t^{1/m}}\,, \tag{23}$$

where the stationary-phase points x_n exist where $(\partial/\partial x)\omega_h(x) = 0$. The integer m denotes the order of the lowest nonvanishing derivative $\omega_h(x)$ evaluated at the stationary-phase points.

Hence, the plasma response consists in general of a series of oscillations at frequencies determined by the extremes of the upper hybrid frequency and is damped according to $t^{-1/m}$. For the important case of a homogeneous magnetic field and an inhomogeneous background ion density, in general there is one stationary-phase point located at the center of the slab where the density is maximum. In this case, the response appears as a single damped oscillation. The asymptotic response oscillates with a frequency $\omega_h(0)$ and damps with a rate depending on the shape of the density profile near the center of the slab. Considering the class of profiles given by

$$\omega_p^2(x) = \omega_p^2(0) \left(1 - \left|\frac{x}{a}\right|^N\right)\,, \tag{24}$$

where N is an integer, the damping varies as $t^{-1/N}$, where it is seen that the damping increases with increasing inhomogeneity; i.e., for N decreasing.

The inhomogeneity is also increased by increasing $\omega_p(0)$. The spatial variation of the density profile (as defined by N) is fixed by the type of discharge employed (Reference 21), whereas the peak density (proportional to $\omega_p(0)$) increases with discharge current. For a low-temperature afterglow plasma, the profile is approximately parabolic, $N = 2$; whereas a continuous dc discharge produces a

quartic profile, $N = 4$. The experiments performed in this study incorporated a continuous dc discharge and measurements were made (and presented in Section 4) for different discharge currents. From Equation 21 it is found that increasing $\omega_p(0)$ results in a stronger damped response. This is first recognized by considering a nonmagnetoplasma and substituting Equation 24 into Equation 21, so that

$$\frac{V_{pl}(T)}{V_0} = \int_0^1 \sqrt{1 - u^N}\, \sin\left(\sqrt{1 - u^N}\, 2\pi T\right) du \,, \tag{25}$$

where

$$V_0 = 2a\omega_p(0)\frac{m_e}{e} v_p \,,$$

$$u = \frac{x}{a} \,,$$

$$T = f_p(0)t \,.$$

Thus, for a specific profile N the response appears as a damped oscillation that is a function of the normalized time $T = \omega_p(0)t/2\pi$. Hence, the response damps with increasing time t or for increasing peak plasma frequency $f_p(0) = \omega_p(0)/2\pi$, as mentioned before. This same form of reasoning can be applied to the magnetoplasma, showing the increase in damping due to increasing $\omega_p(0)$. The damping due to inhomogeneity in plasma density has been observed experimentally by Sindoris, Grody, and Cheo (Reference 4) by measuring the impulse responses of the plasma (with and without magnetic field) for different discharge currents.

The relaxation mechanism resulting from Equation 21 is due to the phase mixing from the spread in plasma and electron-cyclotron frequencies. The integral is generally referred to as a phase-mixing integral and displays the asymptotic behavior shown by Equation 23. Asymptotically, the response oscillates or "rings" at the frequencies $\omega_h(x_n)$ as determined by the extremes of $\omega_h(x)$. This oscillation results because the phase mixing at these points proceeds more slowly than in the rest of the plasma.

A more complete picture of the linear plasma response is presented in a later section, where the effects due to cylindrical geometry are considered.

Nonlinear Impulse Response

A primary objective of this study was to experimentally and theoretically investigate the nonlinear plasma response to impulse excitation. The following sections discuss the analysis of the nonlinear equations for the slab geometry. The analysis was developed in a manner that would explain the results of experiments performed; i.e., both frequency and damping are increased when higher amplitude excitations are used. The results are later expanded to include the effects due to cylindrical geometry, the experimental geometry used.

As previously described, nonlinearity exists because of the electron motion in an inhomogeneous plasma. The nature of the nonlinearity was shown to appear as two distinctly different phenomena; i.e., anharmonic electron motion and electron bunching followed in time by multistreaming. Gould and Blum (Reference 22) analyzed the two-pulse response incorporating the effects of anharmonic electron motion; the results were later used to explain the existence of upper hybrid echoes (Reference 14). This same mechanism is analyzed in the following section to show its effect on the single-pulse response. The additional nonlinear effects due to electron bunching and multistreaming are employed to obtain the resulting impulse response. Comparisons are made of the two nonlinear responses, showing that the effects due to multistreaming generally dominate.

Anharmonic Oscillations

As evident from Equation 10, inhomogeneity associated with either the ion density or magnetic field results in a nonlinear trajectory. To exhibit the nonlinearity due to inhomogeneity, the parameters $\omega_c(x)$ and $\omega_p^2(x)$ are expanded about the point x_0:

$$\left.\begin{aligned} \omega_p^2(x) &= \omega_{p_0}^2 + \omega_{p_0}^{2\prime} X + \frac{1}{2}\omega_{p_0}^{2\prime\prime} X^2 + \cdots \\ \omega_c(x) &= \omega_{c_0} + \omega_{c_0}' X + \frac{1}{2}\omega_{c_0}'' X^2 + \cdots \end{aligned}\right\} \tag{26}$$

The coefficients $\omega_{p_0}^2$, $\omega_{p_0}^{2\prime}$, and $\omega_{p_0}^{2\prime\prime}$ are the plasma frequency squared and its first and second derivatives evaluated at x_0, respectively. Similarly, ω_{c_0}, ω_{c_0}', and ω_{c_0}'' are the electron-cyclotron frequency and its derivatives evaluated at x_0.

Substituting the first three terms of Equation 26 into Equations 10 and 12 produces

$$\left(\frac{\partial^2}{\partial\tau^2} + \omega_{h_0}^2\right) X + \frac{1}{2}(\alpha + \gamma X)X^2 = -\frac{e}{m_e} E_{\text{ext}} \tag{27}$$

$$E_x(x_0, \tau) = E_{\text{ext}} + \frac{m_e}{e}\omega_{p_0}^2 X + \frac{1}{2}\frac{m_e}{e}\omega_{p_0}^{2\prime} X^2 + \cdots, \tag{28}$$

where $\omega_{h_0} = \sqrt{\omega_{p_0}^2 + \omega_{c_0}^2}$ is the upper hybrid frequency evaluated at x_0. The nonlinear parameters α and γ are defined as

$$\left.\begin{aligned} \alpha &= \omega_{h_0}^{2\prime} + \frac{1}{2}\omega_{c_0}^{2\prime} \\ 3\gamma &= \omega_{h_0}^{2\prime\prime} + 2\omega_{c_0}\omega_{c_0}'' + \omega_{c_0}'^2 \end{aligned}\right\} \tag{29}$$

and depend on inhomogeneity.

The first-order perturbation solution (Reference 23) of the nonlinear trajectory equation (Equation 27) for impulse excitation is

$$\left.\begin{aligned} X(x_0, t) &= \frac{v_p}{\omega_{h_0}} \sin \omega t \\ \omega(x_0; v_p) &= \omega_{h_0} + K v_p^2 , \end{aligned}\right\} \tag{30}$$

where the nonlinear frequency coefficient K is

$$K = \frac{1}{16}\left[\frac{3\gamma}{\omega_{h_0}^2} - \frac{5}{3}\left(\frac{\alpha}{\omega_{h_0}^2}\right)^2\right]\frac{1}{\omega_{h_0}} . \tag{31}$$

The electron motion is sinusoidal (neglecting smaller higher order harmonic terms) with an amplitude-dependent frequency of oscillation. This anharmonic motion of the different electrons leads to a nonlinear plasma response that will now be investigated.

The potential across the parallel-plate structure is given by Equation 20. At the nonlinear level, the plasma response is written as

$$V_{\mathrm{pl}}(t) = \frac{m_e}{e}\int_{x_0(-a)}^{x_0(a)} \omega_{p_0}^2 X\left(1 + \frac{\partial X}{\partial x_0}\right) dx_0 , \tag{32}$$

which is obtained using Equation 28 (omitting the smaller harmonic terms) and applying the relationship $dx = (\partial x/\partial x_0)\, dx_0$. The limits of integration are determined from the transformation in Equation 14, substituting the coordinates $\pm a$ for x.

Neglecting electron bunching, i.e., $\partial X/\partial x_0 \gg -1$, and $x_0(\pm a) = \pm a$, the following simple result is obtained:

$$V_{\mathrm{pl}}(t) = \frac{m_e}{e} v_p \int_{-a}^{a} \frac{\omega_p^2(x)}{\omega_h(x)} \sin \omega(x; v_p) t \, dx , \tag{33}$$

where the zero subscripts are omitted.

This equations is similar to the linear response given by Equation 21, except for the amplitude-dependent frequency term $\omega(x; v_p)$. The nonlinear response is a result of the phase mixing of the anharmonic electron oscillations. This leads, asymptotically, to a plasma response having a shift in frequency with impulse amplitude about the upper hybrid frequency. The damping is unchanged from that of the linear response; i.e., it decays as $t^{-1/m}$.

For a homogeneous magnetic field, the frequency shift depends on the inhomogeneity in plasma density. From Equations 30 and 31, the frequency shift is

$$\frac{\omega - \omega_h}{\omega_h} = \frac{v_p^2}{16} \frac{\omega_p^{2\prime\prime}}{\omega_h^4} , \tag{34}$$

where ω_h and $\omega_p^{2\prime\prime}$ are evaluated at the stationary phase point corresponding to $\omega_p' = 0$. This position is at the center of the slab where the density is maximum. Consequently $\omega_p'' < 0$, and there is a negative frequency shift; i.e., the oscillation frequency decreases with increasing impulse amplitude or initial velocity v_p.

The frequency shift given by Equation 34 is generally small. To estimate its magnitude, a parabolic density profile is considered as given by Equation 24 with $N = 2$. Considering a nonmagnetoplasma having a maximum plasma frequency of $2\pi \times 10^9$ rad/s and a slab width of 1 cm, then for an initial velocity of 10^9 cm/s the frequency shift is less than 1 percent, agreeing with the numerical evaluation of Equation 33.

Having shown the frequency shift to be small, the stronger nonlinear effects due to electron bunching and multistreaming are next considered.

Multistreaming Effects

As previously described, the fluid equations predict the formation of electron bunching followed in time by electron crossover (or multistreaming). The condition $\partial X/\partial x_0 = -1$ defines the time t for which an electron having initial position x_0 overtakes an adjacent electron. Using the approximate linearized trajectory given by Equation 19, the crossover condition becomes

$$\frac{v_p \omega_{h_0}'}{\omega_{h_0}^2} (\sin \omega_{h_0} t - \omega_{h_0} t \cos \omega_{h_0} t) = 1 . \tag{35}$$

Expanding the bracketed terms for $\omega_{h_0} t \ll 1$, one finds

$$t = \sqrt[3]{\frac{6}{v_p \left| \omega_{h_0}^{2\prime} \right|}} , \tag{36}$$

where in the opposite limit, $\omega_{h_0} t \gg 1$, keeping only the second term in brackets, then

$$t = \frac{2\omega_{h_0}^2}{v_p \left| \omega_{h_0}^{2\prime} \right|} . \tag{37}$$

Equation 36 gives the approximate crossover time for those electrons near the plasma boundary where the density is low, whereas Equation 37 is applicable in the central region where the density is much larger. Considering a homogeneous magnetic field, the crossover time is longer in the central region where $\omega_{p_0}^{2\prime} \cong 0$ than near the boundary where the density gradient is larger.

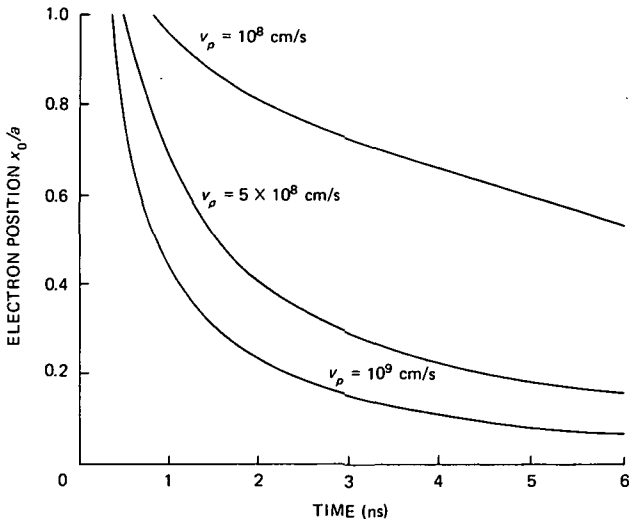

Figure 5—Electron crossover position (approximate), $\omega_p^2(x) = \omega_p^2(0)[1 - (x/a)^2]$.

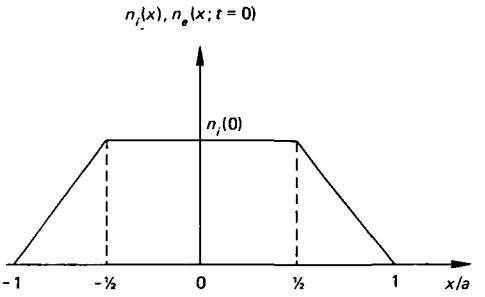

Figure 6—Density in a tapered slab.

The coordinates x_0, t as obtained from Equation 35 are determined approximately using Equations 36 and 37; the results are shown in Figure 5. A nonmagnetoplasma is considered having a parabolic density profile where $\omega_p(0) = 2\pi \times 10^9$ rad/s and $a = 1/2$ cm. Initially, crossover appears near the boundaries (the symmetrical half is not shown) at a time given by Equation 36. At later times, crossover occurs among electrons within the plasma volume, for which Equation 37 gives the crossover time as determined by only the adjacent electrons. Electron crossings approach the center asymptotically, at a rate that is dependent on the impulse amplitude or initial velocity v_p.

To develop the basic concept behind the proposed mechanism for the multistreaming, the simulation work by Schneider and Bers (Reference 9) mentioned earlier is first reviewed. They performed computer experiments to describe the electron motion for a nonmagnetoplasma slab having the density profile shown in Figure 6. The plasma was modeled using 50 electron sheets, each being characterized by the trajectory of Equation 10 ($\omega_c = 0$) prior to sheet crossover and corrected following crossover. The sheets were initially placed at their equilibrium positions x_0 and were perturbed by a uniform displacement δ. This is a different form of excitation than the one with which this study is concerned; i.e., initial velocity, although the electron motion has similar behavior.

Figure 7 displays the electron (sheet) motion for an initial displacement $\delta/a = 0.02$. Crossover appears initially at the boundaries and later in time within the plasma volume. The electron motion exhibits random behavior as a result of rapid electron crossings. It is observed that for short time, the scattered electrons appear to propagate toward the center slower than the movement of the crossover region (i.e., shock front). For this time period, crossings exist among adjacent electrons and the crossover coordinates are determined by the equation $\partial X/\partial x_0 = -1$. At longer times, the scattered electrons move ahead of the shock front causing a randomization of electrons in the center of the plasma slab.

The effect of larger initial displacement, $\delta/a = 0.06$, is clearly exhibited in Figure 8. Compared with the results in Figure 7, there is in this case a quicker randomization of the plasma electrons.

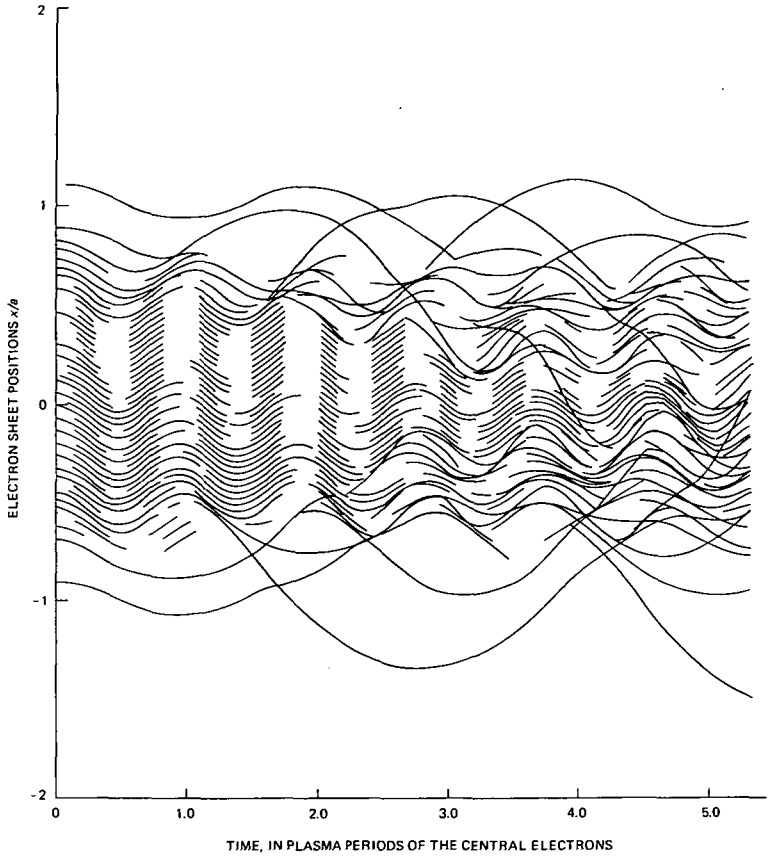

Figure 7—Electron sheet trajectories; initial displacement δ/a = 0.02.

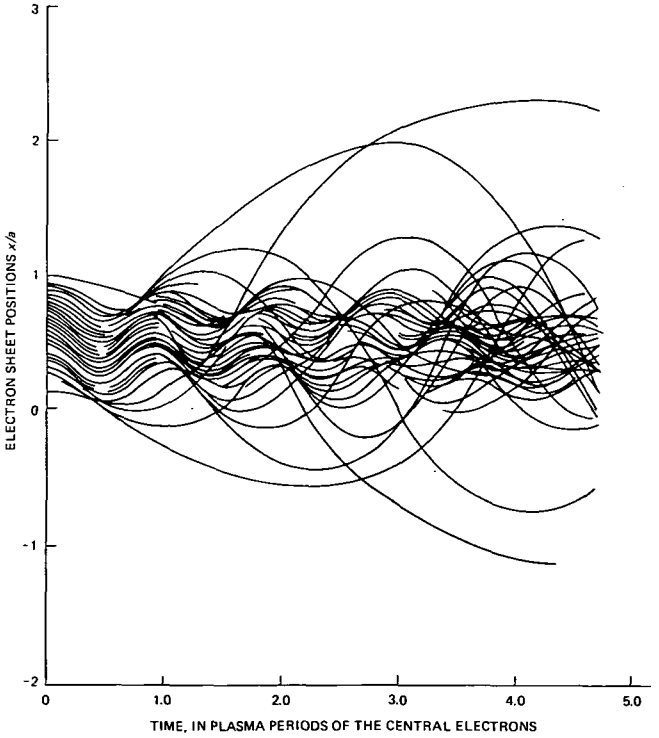

Figure 8—Electron sheet trajectories; initial displacement δ/a = 0.06.

This occurrence of electron randomization after crossover can now be considered when explaining the observed positive frequency shift and increased damping in the nonlinear impulse response of a plasma column.

The plasma response $V_{pl}(t)$ is approximated by obtaining only the contribution due to the nonrandom electrons that appear in the central region of the plasma as shown in Figure 5. This is a reasonable assumption because the scattered electrons randomly mix quickly, leaving only the nonrandom electrons (which have near-linear behavior) to contribute to the plasma response. To obtain the response, the linear response given by Equation 21 is modified as follows:

$$V_{pl}(t) = 2\frac{m_e}{e} v_p \int_0^{x_c(t;\, v_p)} \frac{\omega_p^2(x_0)}{\omega_h(x_0)} \sin \omega_h(x_0) t \, dx_0 \tag{38}$$

where the upper limit a in Equation 21 has been replaced by the crossover position as given by Equation 35. To simplify the analysis, a nonmagnetoplasma is considered having a parabolic density profile. Using Equation 37 to obtain approximately the upper limit, Equation 38 becomes

$$\frac{V_{pl}(T)}{V_0} = \int_0^{\sqrt{(T/\beta)^2+1} - T/\beta} \sqrt{1-u^2} \sin\left(\sqrt{1-u^2}\, 2\pi T\right) du \,, \tag{39}$$

where

$$V_0 = 2a\omega_p(0)\frac{m_e}{e} v_p$$

$$\beta = f_p(0)\frac{2a}{v_p}$$

$$T = f_p(0)t \,.$$

Equation 39 gives the nonlinear impulse response for the plasma under consideration. The integral is a function of the normalized time T and contains a nonlinear parameter β. The numerical evaluation of this response is shown in Figure 9 for the initial velocities of 10^8 and 10^9 cm/s, where $f_p(0) = 10^9$ s^{-1} and $a = 1/2$ cm.

The smaller excitation results in a response comparable to the linear response given by Equation 21. For $f_p(0)t > 1$, the response approaches its asymptotic behavior; i.e., it oscillates at the maximum plasma frequency $f_p(0)$ and slowly damps according to $t^{-1/2}$. This asymptotic behavior is also observed for the larger excitation; however, the initial damping is much larger because of the more rapid decrease in the upper limit; i.e., random mixing. Also noted is that there is a larger initial frequency of oscillation for the larger excitation. This is a consequence of random mixing, which reduces the number of low-frequency oscillating electrons (which are located near the boundaries) contributing to the plasma response resulting in a net increase in response frequency.

Further discussions concerning these nonlinear effects are presented in the discussion of the results due to cylindrical geometry.

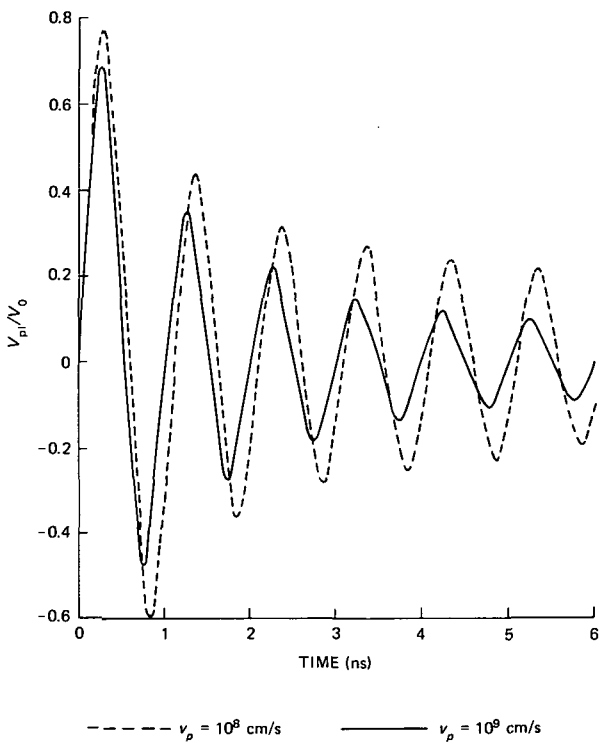

Figure 9—Impulse responses of a nonmagnetoplasma slab for different excitation amplitudes, $\omega_p^2(x) = \omega_p^2(0)[1 - (x/a)^2]$.

Comparison of Anharmonic and Multistreaming Effects

As mentioned earlier, the inhomogeneity in plasma density gives rise to two distinct nonlinear mechanisms, which result in different plasma responses. The two forms of nonlinearity have been identified as (1) that due to the nonlinear trajectory for the electrons and (2) that caused by the singular behavior (i.e., shock formation) of the electron density resulting in electron crossover. The nonlinear trajectory equation (Equation 27) resulted in anharmonic motion for the electrons, producing a plasma response that displays a negative frequency shift; i.e., the frequency of oscillation decreases with increasing impulse voltage or initial electron velocity. It has also been shown that the electron crossover, which begins at the plasma boundaries and propagates toward the center of the volume, acts to randomize the electron motion. Considering that only the coherent (nonrandom) electrons contribute to the plasma response, it was found that the response displays both an initial increase in oscillation frequency and increasing damping for larger impulse amplitude or initial velocity. This nonlinear behavior is consistent with the experimental results reported earlier (Reference 4); i.e., the theoretical and experimental responses both display an increase in frequency and damping with excitation. This proposed mechanism represents one basic contribution of this study.

Linear Equations for a Cylindrical, Cold Magnetoplasma

The cold-fluid equations are analyzed for a cylindrical magnetoplasma column excited by a transverse electric field as shown in Figure 10. Unfortunately, the additional dimensions complicate the nonlinear analysis; thus only the linearized equations are considered. To estimate the nonlinear behavior, reference is made to the previous one-dimensional results and the added effects of cylindrical geometry.

Analysis of the linear interaction of a transverse electric field with a cold, cylindrical magnetoplasma have been performed with varying degrees of clarity and completeness by a number of authors, whose approaches differ according to their backgrounds and motivations (References 1 to 3, 5 to 7, and 15 to 18). These studies are deficient for purposes of this analysis because their results are not readily applicable to the problem of obtaining the impulse response of the plasma, which is the central topic of this investigation.

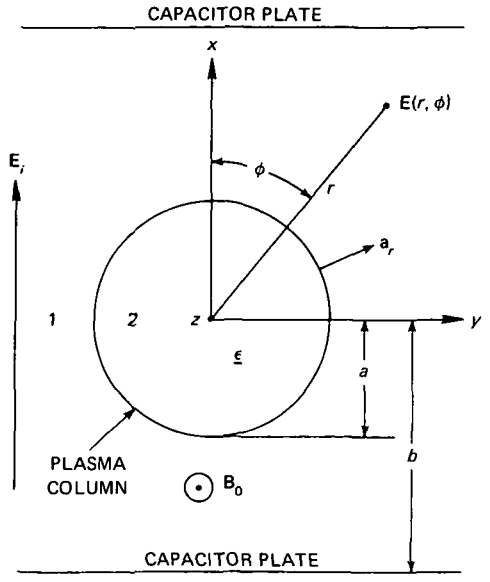

Figure 10--Cylindrical plasma geometry.

To begin the analysis, Equations 1 and 2 are considered, which are linearized by defining a suitable background level and seeking solutions having small deviations about the background. The $n_e \mathbf{v}_e$ and $\mathbf{v}_e \cdot \nabla \mathbf{v}_e$-type nonlinearities are neglected by assuming small deviations about the background ion density $n_i(\mathbf{r})$ and considering $(\partial/\partial t)\mathbf{v}_e \gg \mathbf{v}_e \cdot \nabla \mathbf{v}_e$, respectively; thus the following linear equations are obtained:

$$\frac{\partial}{\partial t} n_e(\mathbf{r}, t) + \nabla \cdot n_i(\mathbf{r}) \mathbf{v}_e(\mathbf{r}, t) = 0 \qquad (40)$$

$$\frac{\partial}{\partial t} \mathbf{v}_e(\mathbf{r}, t) = -\frac{e}{m_e} [\mathbf{E}(\mathbf{r}, t) + \mathbf{v}_e(\mathbf{r}, t) \times \mathbf{B}_0(\mathbf{r})] \; . \qquad (41)$$

Upon taking the Fourier transform ($(\partial/\partial t) \longleftrightarrow i\omega$) of Equations 40 and 41, it is found after some algebraic manipulations that

$$\tilde{n}_e(\mathbf{r}, \omega) = -\frac{\epsilon_0}{e} \nabla \cdot [\mathbf{K} \cdot \tilde{\mathbf{E}}(\mathbf{r}, \omega)] \qquad (42)$$

$$\tilde{\mathbf{v}}_e(\mathbf{r}, \omega) = \frac{e}{m_e} \frac{i\omega}{\omega_p^2} [\mathbf{K} \cdot \tilde{\mathbf{E}}(\mathbf{r}, \omega)] \; . \qquad (43)$$

The tensor quantity $\mathbf{K}$ is given by the following matrix description:

$$\mathbf{K} = \begin{bmatrix} K_{rr} & -iK_{r\phi} & 0 \\ iK_{r\phi} & K_{rr} & 0 \\ 0 & 0 & K_{zz} \end{bmatrix} \qquad (44)$$

where

$$K_{zz} = \frac{\omega_p^2}{\omega^2}$$

$$K_{rr} = \frac{\omega_p^2}{\omega^2 - \omega_c^2}$$

$$K_{r\phi} = \frac{\omega_c}{\omega} \frac{\omega_p^2}{\omega^2 - \omega_c^2}$$

and the parameter

$$\omega_p = \sqrt{\frac{n_i(\mathbf{r})e^2}{\epsilon_0 m_e}}$$

is the plasma frequency and $\omega_c = (e/m_e)\mathbf{B}_0(\mathbf{r})$ is the electron-cyclotron frequency.

Equations 42 and 43 and the linearized Maxwell equations form a complete description for determining the electromagnetic fields associated with the plasma for weak excitation. The linearized, transformed Maxwell equations are—

$$\nabla \times \tilde{\mathbf{E}}(\mathbf{r}, \omega) = -i\omega\mu_0 \tilde{\mathbf{H}}(\mathbf{r}, \omega) \tag{45}$$

$$\nabla \times \tilde{\mathbf{H}}(\mathbf{r}, \omega) = i\omega\epsilon_0 \tilde{\mathbf{E}}(\mathbf{r}, \omega) - en_i(\mathbf{r})\tilde{\mathbf{v}}_e(\mathbf{r}, \omega) \tag{46}$$

$$\nabla \cdot \tilde{\mathbf{E}}(\mathbf{r}, \omega) = -\frac{e}{\epsilon_0} \tilde{n}_e(\mathbf{r}, \omega) \tag{47}$$

$$\nabla \cdot \tilde{\mathbf{H}}(\mathbf{r}, \omega) = 0\,, \tag{48}$$

where the linearization was carried out in the $\nabla \times \mathbf{H}(\mathbf{r}, t)$ original equation in which $n_e \mathbf{v}_e$ was replaced by the linear term $n_i \mathbf{v}_e$.

Substituting Equations 42 and 43 into Equations 46 and 47 results in

$$\nabla \times \tilde{\mathbf{H}}(\mathbf{r}, \omega) = i\omega\epsilon_0 \underline{\epsilon} \cdot \tilde{\mathbf{E}}(\mathbf{r}, \omega) \tag{49}$$

$$\nabla \cdot \underline{\epsilon} \cdot \tilde{\mathbf{E}}(\mathbf{r}, \omega) = 0\,. \tag{50}$$

The term $\underline{\epsilon} = \mathbf{I} - \mathbf{K}$ is the dielectric tensor of the magnetoplasma and has the following matrix description:

$$\underline{\epsilon} = \begin{bmatrix} \epsilon_{rr} & i\epsilon_{r\phi} & 0 \\ -i\epsilon_{r\phi} & \epsilon_{rr} & 0 \\ 0 & 0 & \epsilon_{zz} \end{bmatrix}, \tag{51}$$

where

$$\epsilon_{zz} = 1 - \frac{\omega_p^2}{\omega^2}$$

$$\epsilon_{rr} = 1 - \frac{\omega_p^2}{\omega^2 - \omega_c^2}$$

$$\epsilon_{r\phi} = \frac{\omega_c}{\omega} \frac{\omega_p^2}{\omega^2 - \omega_c^2} .$$

Equations 45, 48, 49, and 50 comprise the complete set of linear equations for the electromagnetic fields $\tilde{\mathbf{E}}$ and $\tilde{\mathbf{H}}$. To simplify the analysis, the quasi-static approximation is used, i.e., $\nabla \times \tilde{\mathbf{E}} = 0$, to obtain the fields. The problem is then formally equivalent to the electrostatic problem with $\tilde{\mathbf{E}} = -\nabla\Phi$, and from Equation 50 is obtained

$$\nabla \cdot \underline{\epsilon} \cdot \nabla\Phi = 0 . \tag{52}$$

This equation is a familiar one in plasma physics and has been applied to many problems to determine the characteristic resonances and steady-state behavior of plasma structures. Transient effects, which are important in the linear experiments, are next discussed.

Linear Response of a Homogeneous Magnetoplasma

Before considering an inhomogeneous magnetoplasma, the response of a homogeneous plasma is analyzed. In this case, Equation 52 reduces to the familiar potential equation $\nabla^2\Phi = 0$ inside the plasma. The dielectric properties of the plasma come to play only at the boundaries.

Referring to Figure 10, the potentials in regions 1 and 2 have the following general forms:

$$\begin{aligned} \Phi_1 &= \left[\sum_{n=1}^{\infty} r^{-n} (A_n \cos n\phi + B_n \sin n\phi) \right] + \Phi_{\text{ext}} \\ \Phi_2 &= \sum_{n=1}^{\infty} r^n (A'_n \cos n\phi + B'_n \sin n\phi) , \end{aligned} \tag{53}$$

where, assuming a dipole mode of excitation,

$$\left.\begin{aligned} \Phi_{\text{ext}} &= -\tilde{E}_i r \cos\phi \\ \tilde{E}_i &= \tilde{E}_i(\omega) . \end{aligned}\right\} \tag{54}$$

This is the lowest possible mode of excitation for the geometry under consideration and is dominant when $b \gg a$ because then the electric field is nearly uniform and polarized in the x direction for distances far from the plasma column.

The boundary conditions at the plasma/vacuum interface $r = a$ are

$$\left.\begin{aligned} \mathbf{a}_r \times \tilde{\mathbf{E}}_2 &= \mathbf{a}_r \times \tilde{\mathbf{E}}_1 \\ \frac{\partial}{\partial\phi}\Phi_2 &= \frac{\partial}{\partial\phi}\Phi_1 , \end{aligned}\right\} \tag{55a}$$

or

and

$$\left.\begin{aligned} \mathbf{a}_r \cdot \underline{\epsilon} \cdot \tilde{\mathbf{E}}_2 &= \mathbf{a}_r \cdot \tilde{\mathbf{E}}_1 \\ \text{or} \\ \epsilon_{rr} \frac{\partial}{\partial r} \Phi_2 + i\epsilon_{r\phi} \frac{\partial}{a\partial\phi} \Phi_2 &= \frac{\partial}{\partial r} \Phi_1 \, . \end{aligned}\right\} \tag{55b}$$

Substituting Φ_1 and Φ_2 into the boundary equations and applying the orthogonality properties for sinusoidal functions, it is found that

$$\left.\begin{aligned} A_n' &= a^{-2n} A_n - \tilde{E}_i \delta_{n_1} \, , \\ \epsilon_{rr} A_n' + i\epsilon_{r\phi} B_n' &= -a^{-2n} A_n - \tilde{E}_i \delta_{n_1} \, , \\ B_n' &= a^{-2n} B_n \, , \\ \epsilon_{rr} B_n' - i\epsilon_{r\phi} A_n' &= -a^{-2n} B_n \, . \end{aligned}\right\} \tag{56}$$

Solving for the mode amplitudes, it is noted that only the $n = 1$ (dipole) amplitudes are non-vanishing:

$$\left.\begin{aligned} A_1 &= a^2 \frac{\epsilon_{rr}^2 - \epsilon_{r\phi}^2 - 1}{(1+\epsilon_{rr})^2 - \epsilon_{r\phi}^2} \tilde{E}_i \, , \\ A_1' &= -2 \frac{1+\epsilon_{rr}}{(1+\epsilon_{rr})^2 - \epsilon_{r\phi}^2} \tilde{E}_i \, , \\ B_1 &= -2a^2 \frac{i\epsilon_{r\phi}}{(1+\epsilon_{rr})^2 - \epsilon_{r\phi}^2} \tilde{E}_i \, , \\ B_1' &= -2 \frac{i\epsilon_{r\phi}}{(1+\epsilon_{rr})^2 - \epsilon_{r\phi}^2} \tilde{E}_i \, . \end{aligned}\right\} \tag{57}$$

The electric field inside and outside the plasma can be derived from the potentials Φ_1 and Φ_2, respectively, using the relationship $\tilde{\mathbf{E}} = -\nabla\Phi$. The following equations result: Inside the plasma (region 2),

$$\tilde{\mathbf{E}}_2 = \tilde{\mathbf{E}}_x + \tilde{\mathbf{E}}_y \, , \tag{58}$$

$$\tilde{E}_x = 2\tilde{E}_i \frac{1+\epsilon_{rr}}{(1+\epsilon_{rr})^2 - \epsilon_{r\phi}^2} \, ,$$

$$\tilde{E}_y = 2\tilde{E}_i \frac{i\epsilon_{r\phi}}{(1+\epsilon_{rr})^2 - \epsilon_{r\phi}^2} \, .$$

Outside the plasma (region 1),

$$\tilde{\mathbf{E}}_1 = \tilde{\mathbf{E}}_x + \tilde{\mathbf{E}}_y \ , \tag{59}$$

$$\tilde{E}_x = \tilde{E}_i + \tilde{E}_i \left(\frac{a}{r}\right)^2 \frac{\epsilon_{rr}^2 - \epsilon_{r\phi}^2 - 1}{(1+\epsilon_{rr})^2 - \epsilon_{r\phi}^2} \left(\cos 2\phi - \frac{i\, 2\epsilon_{r\phi} \sin 2\phi}{\epsilon_{rr}^2 - \epsilon_{r\phi}^2 - 1} \right) ,$$

$$\tilde{E}_y = \tilde{E}_i \left(\frac{a}{r}\right)^2 \frac{\epsilon_{rr}^2 - \epsilon_{r\phi}^2 - 1}{(1+\epsilon_{rr})^2 - \epsilon_{r\phi}^2} \left(\sin 2\phi + \frac{i\, 2\epsilon_{r\phi} \cos 2\phi}{\epsilon_{rr}^2 - \epsilon_{r\phi}^2 - 1} \right) .$$

The electric field in the plasma is uniform, whereas the scattered field outside the plasma varies with angular position and polarization. For $\phi = 0°$, the scattered field polarized in the x direction of the incident field $\tilde{E}_i$ is

$$\frac{\tilde{E}_x - \tilde{E}_i}{\tilde{E}_i} = \left(\frac{a}{r}\right)^2 \frac{\epsilon_{rr}^2 - \epsilon_{r\phi}^2 - 1}{(1+\epsilon_{rr})^2 - \epsilon_{r\phi}^2} \ . \tag{60}$$

In the quasi-static approximation, Equation 60 represents the scattering coefficient $\tilde{\Gamma}(\omega)$ (Reference 24), and for $\phi = 0°$ is a measure of the backscattered radiation from the plasma. Substituting ϵ_{rr} and $\epsilon_{r\phi}$ into Equation 60, then

$$\tilde{\Gamma}(\omega) = \left(\frac{a}{r}\right)^2 \frac{\omega_0^2(\omega^2 - \omega_0^2)}{(\omega^2 - \omega_R^2)(\omega^2 - \omega_L^2)} \ , \tag{61}$$

where

$$\omega_0 = \frac{\omega_p}{\sqrt{2}}$$

$$\omega_R = \sqrt{\omega_0^2 + \left(\frac{\omega_c}{2}\right)^2} + \frac{\omega_c}{2}$$

$$\omega_L = \sqrt{\omega_0^2 + \left(\frac{\omega_c}{2}\right)^2} - \frac{\omega_c}{2} \ .$$

The scattered radiation varies with excitation frequency, having resonances at ω_R and ω_L and an antiresonance at ω_0. For a nonmagnetoplasma, the spectrum of scattered radiation degenerates into a single resonance at ω_0. In the language of plasma physics (Reference 16), the double-peaked spectrum is appropriately classified as a split dipole resonance, whereas the single resonance obtained in the absence of a magnetic field is defined as a dipole resonance. The term dipole refers to the mode of excitation.

These results are different from those determined for the slab geometry as indicated by Equation 22 which, when transformed, becomes

$$\frac{\tilde{V}_{pl}(\omega)}{2a(m_e/e)v_p} = \frac{\omega_p^2}{\omega^2 - \omega_h^2} , \tag{62}$$

which is related to the scattered radiation from the plasma slab.

The difference between the two results (Equations 61 and 62) is due to the dipole mode excited for the cylindrical plasma that is not supported for slab geometry.

Upon taking the inverse transform of Equation 61, the impulse response is obtained for the cylindrical plasma:

$$\Gamma(t) = \left(\frac{a}{r}\right)^2 \frac{\omega_0^2}{\omega_R + \omega_L} (\sin \omega_R t + \sin \omega_L t) , \tag{63}$$

which may also be written as

$$\Gamma(t) = \left(\frac{a}{r}\right)^2 \frac{\omega_0^2}{\sqrt{\omega_0^2 + (\omega_c/2)^2}} \cos \frac{\omega_c}{2} t \left[\sin \sqrt{\omega_0^2 + \left(\frac{\omega_c}{2}\right)^2}\, t\right] . \tag{64}$$

Unlike the slab impulse response given by Equation 22, this equation consists of two oscillations that interfere to produce a modulated oscillatory response.

The scattered radiation and impulse response given by Equations 61 and 63, respectively, contain no damping mechanisms. The following list indicates the damping mechanisms that were neglected in the previous analysis:

(1) Radiation damping was neglected when using the quasi-static approximation.

(2) Damping caused by electron-neutral collisions was neglected.

(3) Phase-mixing damping resulting from inhomogeneity was also omitted by considering a homogeneous plasma.

Of these three mechanisms, the damping produced from inhomogeneity in plasma density is dominant for the experimental conditions employed.

Damping resulting from radiation has been compared with that due to inhomogeneity in plasma density by Greenwald (Reference 7). Equations 45 and 49 were numerically analyzed to obtain the radiation spectrum for a magnetoplasma excited by a uniform plane wave as shown in Figure 10. Comparing these results with those of the electrostatic problem given by Equation 52, it was concluded that radiation damping is negligible compared with the damping caused by plasma inhomogeneity for the condition $k_0 a < 0.5$, where k_0 is the free-space wavenumber and a is the column radius. In this study, a 0.5-cm column radius was used and the maximum frequency observed was below 1.0 GHz, so that $k_0 a < 0.1$, which is well below the condition necessary to neglect radiation damping as compared with damping resulting from inhomogeneity.

The effect of electron-neutral collisions is to elastically scatter the electrons by transferring momentum from the electrons to neutrals. This process is incorporated mathematically in the electron equation of motion by adding the term νv_e to the left side of Equation 41. The quantity ν represents a phenomenological electron-neutral collision frequency and alters the dielectric terms ϵ_{ij} (Equation 51) so that

$$\left.\begin{aligned} \epsilon_{zz} &= 1 - \frac{\omega_p^2}{\omega\tilde{\omega}} , \\ \epsilon_{rr} &= 1 - \frac{\tilde{\omega}}{\omega}\frac{\omega_p^2}{\tilde{\omega}^2 - \omega_c^2} , \\ \epsilon_{r\phi} &= \frac{\omega_c}{\omega}\frac{\omega_p^2}{\tilde{\omega}^2 - \omega_c^2} , \end{aligned}\right\} \tag{65}$$

where $\tilde{\omega} = \omega - i\nu$; and Equation 61 becomes

$$\Gamma(\omega) = \left(\frac{a}{r}\right)^2 \frac{\omega_0^2(\omega\tilde{\omega} - \omega_0^2)}{[(\tilde{\omega} - \omega_c)\omega - \omega_0^2][(\tilde{\omega} + \omega_c)\omega - \omega_0^2]} . \tag{66}$$

The inverse transform of Equation 66 results in an exponentially damped response according to $\epsilon^{-1/2\nu t}$ and oscillates with a waveform similar to that given by Equation 64. Because the experiments performed in this study were carried out within a time scale of 20 ns and for a collision frequency of about 30 MHz, collisional damping is of negligible importance compared with the stronger damping resulting from plasma inhomogeneity.

Effects Due to Inhomogeneity

In this section, an approximate theory of the linear and nonlinear impulse response is developed for an inhomogeneous cylindrical plasma. The important effects due to the combination of cylindrical geometry and inhomogeneity are illustrated.

It has been determined that inhomogeneity results in linear damping of the impulse response because of phase mixing, and at the nonlinear level it causes increased damping with increasing oscillation frequency due to random mixing. These linear and nonlinear phenomena are further explored in this section for cylindrical geometry using the information gained from the previous theoretical sections.

The linear behavior is first considered and Equation 52 is analyzed to obtain the scattered radiation outside the plasma. Unfortunately, the exact solution can only be found numerically; however, an approximate analytical solution is obtained that illustrates and identifies the effects of inhomogeneity for a cylindrical plasma. This analytical formulation is further expanded to obtain the nonlinear plasma response.

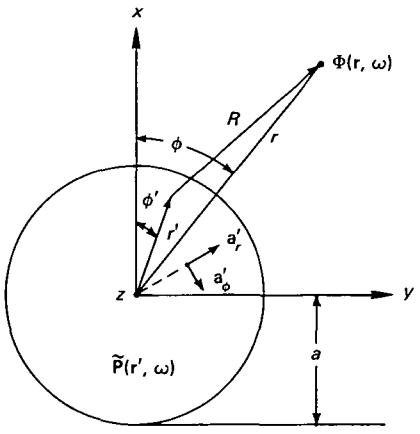

Figure 11—Cylindrical coordinate system.

Equation 52 is rewritten as follows:

$$\nabla^2 \Phi(\mathbf{r}, \omega) = \nabla \cdot \tilde{\mathbf{P}}(\mathbf{r}, \omega) \qquad (67a)$$

$$\tilde{\mathbf{P}}(\mathbf{r}, \omega) = \mathbf{K} \cdot \tilde{\mathbf{E}}(\mathbf{r}, \omega) \qquad (67b)$$

where the term $\tilde{\mathbf{P}}$ physically represents the induced polarization in the plasma and depends on the internal electric field $\tilde{\mathbf{E}} = -\nabla\Phi$. The potential of Equation 67a can then be expressed in terms of the area A integral

$$\Phi(\mathbf{r}, \omega) = \int_A G(\mathbf{r}, \mathbf{r}') \nabla' \cdot \tilde{\mathbf{P}}(\mathbf{r}', \omega)\, dA' , \qquad (68)$$

which is evaluated throughout the cross section of the plasma cylinder shown in Figure 11. The kernel G is the Green function and is the potential at $\mathbf{r}$ due to a line of unit charge located at $\mathbf{r}'$. It is given by

$$\left.\begin{aligned} G(\mathbf{r}, \mathbf{r}') &= \frac{1}{2\pi} \ln R \\ R^2 &= r^2 + r'^2 - 2rr' \cos(\phi - \phi') . \end{aligned}\right\} \qquad (69)$$

Using the identity $\nabla' G\tilde{\mathbf{P}} = \tilde{\mathbf{P}} \cdot \nabla' G + G\nabla' \cdot \tilde{\mathbf{P}}$ and the divergence theorem, Equation 68 becomes

$$\Phi(\mathbf{r}, \omega) = \int_0^{2\pi} G(\mathbf{r}, \mathbf{r}') \tilde{\mathbf{P}}(\mathbf{r}', \omega) \cdot \mathbf{a}'_r a\, d\phi' - \int_0^a \int_0^{2\pi} \tilde{\mathbf{P}}(\mathbf{r}', \omega) \cdot \nabla' G(\mathbf{r}, \mathbf{r}') r'\, dr'\, d\phi' . \qquad (70)$$

The first integral evaluated around the cylindrical surface does not contribute because ω_p and consequently $\tilde{\mathbf{P}}$ is zero at the plasma boundary. Hence, Equation 70 reduces to

$$\Phi(\mathbf{r}, \omega) = -\int_0^a \int_0^{2\pi} \tilde{\mathbf{P}}(\mathbf{r}', \omega) \cdot \nabla' G(\mathbf{r}, \mathbf{r}') r'\, dr'\, d\phi' . \qquad (71)$$

The polarization $\mathbf{P}$ as defined by Equation 67b is written in cylindrical coordinates:

$$\tilde{\mathbf{P}} = \mathbf{a}'_r \tilde{P}_r + \mathbf{a}'_\phi \tilde{P}_\phi , \qquad (72)$$

where

$$\tilde{P}_r = (K_{rr}\tilde{E}_x + iK_{r\phi}\tilde{E}_y) \cos\phi' - (iK_{r\phi}\tilde{E}_x - K_{rr}\tilde{E}_y) \sin\phi'$$

$$\tilde{P}_\phi = -(K_{rr}\tilde{E}_x + iK_{r\phi}\tilde{E}_y) \sin\phi' - (iK_{r\phi}\tilde{E}_x - K_{rr}\tilde{E}_y) \cos\phi' .$$

The electric fields $\tilde{E}_x$ and $\tilde{E}_y$ in the plasma are approximated using Equation 58 and replacing the dielectric terms e_{ij} by their spatially varying counterparts. After substituting the field components

given by Equation 58 into Equation 72, it is found after some algebraic operations that

$$\left.\begin{aligned}\tilde{P}_r &= -2\tilde{E}_i\left[\frac{e_{rr}^2 - e_{r\phi}^2 - 1}{(1+e_{rr})^2 - e_{r\phi}^2}\cos\phi' - \frac{i\,2e_{r\phi}}{(1+e_{rr})^2 - e_{r\phi}^2}\sin\phi'\right] \\ \tilde{P}_\phi &= 2\tilde{E}_i\left[\frac{e_{rr}^2 - e_{r\phi}^2 - 1}{(1+e_{rr})^2 - e_{r\phi}^2}\sin\phi' + \frac{i\,2e_{r\phi}}{(1+e_{rr})^2 - e_{r\phi}^2}\cos\phi'\right]\end{aligned}\right\} \tag{73}$$

where the dielectric terms e_{ij} are given by Equation 51 with $\omega_p = \omega_p(\mathbf{r}')$ and $\omega_c = \omega_c(\mathbf{r}')$. These results are approximate in the sense that they only indicate local spatial variations in polarization and do not display any directional changes due to inhomogeneity.

The remaining term $\nabla' G$ in the integral of Equation 71 is obtained using Equations 69:

$$\nabla' G = \frac{1}{2\pi R^2}\left\{\mathbf{a}_r'[r' - r\cos(\phi - \phi')] - \mathbf{a}_\phi' r\sin(\phi - \phi')\right\} . \tag{74}$$

Equations 73 and 74 can now be substituted into Equation 71 to obtain an approximation to the potential outside an inhomogeneous plasma. To simplify the evaluation of the integral, the potential is determined for $r > r'$, so that $R \cong r$ in Equation 74. It is also considered that variations in plasma density and magnetic field are only dependent on r, so that $e_{ij} = e_{ij}(r')$. For these conditions, the ϕ' integration is easily carried out, resulting in the following simple equation:

$$\Phi(\mathbf{r}, \omega) = \frac{2\tilde{E}_i}{r^2}\left[r\cos\phi\int_0^a \frac{e_{rr}^2 - e_{r\phi}^2 - 1}{(1+e_{rr})^2 - e_{r\phi}^2}\,r'\,dr' - r\sin\phi\int_0^a \frac{i\,2e_{r\phi}}{(1+e_{rr})^2 - e_{r\phi}^2}\,r'\,dr'\right] . \tag{75}$$

This equation reduces to the solution for the homogeneous plasma when e_{ij} are considered constant terms. The backscattered electric field is obtained from the relation $\tilde{\mathbf{E}} = -\nabla\Phi$ and setting $\phi = 0°$. It is then found that

$$\tilde{\Gamma}(\omega) = \frac{2}{r^2}\int_0^a \frac{e_{rr}^2 - e_{r\phi}^2 - 1}{(1+e_{rr})^2 - e_{r\phi}^2}\,r'\,dr' , \tag{76}$$

where after substituting e_{ij} into Equation 76 the final equation becomes

$$\tilde{\Gamma}(\omega) = \frac{2}{r^2}\int_0^a \frac{\omega_0^2(\omega^2 - \omega_0^2)}{(\omega^2 - \omega_R^2)(\omega^2 - \omega_L^2)}\,r'\,dr' , \tag{77}$$

where

$$\omega_0 = \frac{\omega_p(r')}{\sqrt{2}} ,$$

$$\omega_R = \sqrt{\omega_0^2(r') + \frac{\omega_c^2(r')}{4}} + \frac{\omega_c(r')}{2} ,$$

$$\omega_L = \sqrt{\omega_0^2(r') + \frac{\omega_c^2(r')}{4}} - \frac{\omega_c(r')}{2} .$$

Equation 77 reduces to Equation 61 for a homogeneous plasma, where ω_0, ω_R, and ω_L are treated as constants. By taking the inverse transform of Equation 77, the following impulse response is found:

$$\Gamma(t) = \frac{2}{r^2} \int_0^a \frac{\omega_0^2}{\sqrt{\omega_0^2 + (\omega_c/2)^2}} \cos \frac{\omega_c}{2} t \left[\sin \sqrt{\omega_0^2 + \left(\frac{\omega_c}{2}\right)^2} \, t \right] r' \, dr' . \tag{78}$$

Equation 78 contains a phase-mixing integral whose structure is similar to the plasma-slab equation (Equation 21) except for the r' term appearing in the integrand. The similarity between the two integrals can be further seen by considering a homogeneous magnetic field and making the substitution $r'^2 = u$ so that

$$\Gamma(t) = \frac{1}{r^2} \cos \frac{\omega_c}{2} t \int_0^{a^2} \frac{\omega_0^2(\sqrt{u})}{\sqrt{\omega_0^2(\sqrt{u}) + (\omega_c/2)^2}} \sin \sqrt{\omega_0^2(\sqrt{u}) + \left(\frac{\omega_c}{2}\right)^2} \, t \, du . \tag{79}$$

The integral in Equation 79 is equivalent to Equation 21 if $\omega_p(x)$ and $\omega_h(x)$ are replaced by $\omega_p(\sqrt{x})/\sqrt{2}$ and $\sqrt{\omega_p^2(\sqrt{x})/2 + \omega_c^2/4}$, respectively. Hence, for the class of profiles given by Equation 24, the cylindrical plasma response damps asymptotically (see Equation 23) as $t^{-2/N}$. This damping rate is stronger than that for slab geometry $t^{-1/N}$, indicating the influence of geometry on damping resulting from inhomogeneity in density.

This phenomenon is illustrated in Figure 12 where the numerical solutions of Equations 21 and 79 are shown on different normalized voltage and time scales. A nonmagnetoplasma is considered having a parabolic density profile. It is seen that the slab response decays asymptotically as $t^{-1/2}$, whereas the cylindrical plasma response damps according to t^{-1}. The oscillation frequency for the cylindrical plasma is lower than that for the slab geometry; i.e., $f_p(0)/\sqrt{2}$ and $f_p(0)$, respectively.

Because the experimental cylindrical plasma has the addition of a uniform magnetic field along the column axes, the magnetoplasma response is of interest. The response given by Equation 79 is shown in Figure 13 for a uniform magnetic field, where the ratio of electron-cyclotron frequency f_c to frequency $f_0(0) = f_p(0)/\sqrt{2}$ is indicated. To simulate more closely the density distribution found in the plasma, a quartic profile ($N = 4$ in Equation 24) is used rather than the more inhomogeneous parabolic distribution. These responses appear as modulated oscillatory waveforms damping asymptotically as $t^{-1/2}$.

Although the previous results were determined from an approximate analytical theory, the results agree in behavior with the work of Henderson (Reference 6) and Ignat (Reference 25). They have numerically evaluated the electrostatic equation (Equation 52) to obtain the radiation spectrum for an inhomogeneous cylindrical plasma with and without a magnetic field. Because the former

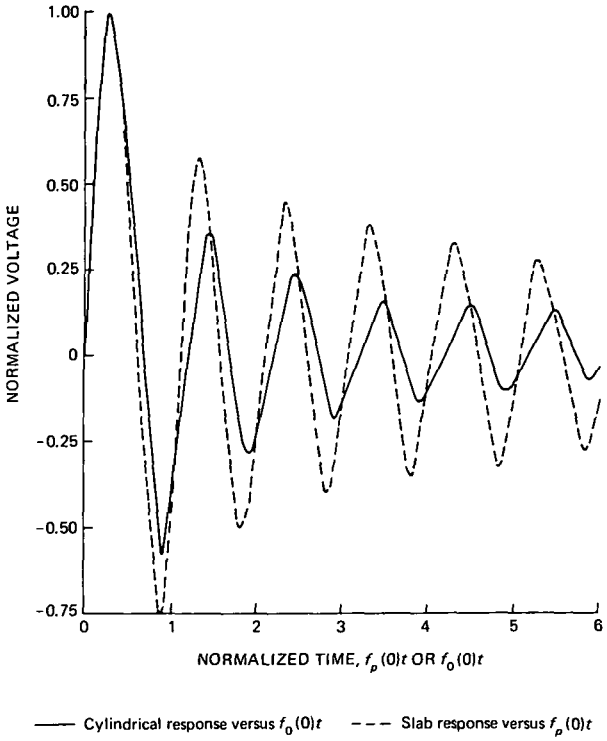

Figure 12—Impulse responses of a nonmagnetoplasma having cylindrical and slab geometry. For the cylindrical geometry, $\omega_p^2(r) = \omega_p^2(0)[1 - (r/a)^2]$; for the slab geometry, $\omega_p^2(x) = \omega_p^2(0)[1 - (x/a)^2]$.

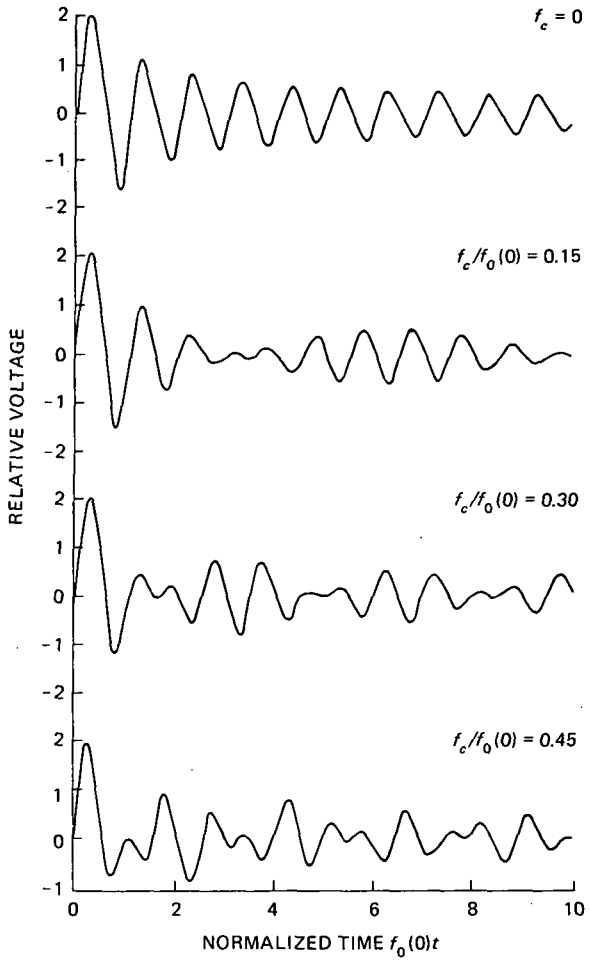

Figure 13—Impulse responses of a cylindrical magnetoplasma for different magnetic fields.

theory agrees qualitatively with the more exact numerical results, it will be now extended to obtain the nonlinear response.

Nonlinear Response

The nonlinear response is obtained following the procedure described earlier for the slab geometry. Thus, the nonlinearity resulting from multistreaming is determined by altering the linear equation (Equation 78) as follows:

$$\Gamma(t) = \frac{1}{\pi r^2} \int_0^{2\pi} \int_0^{r_c} \frac{\omega_0^2}{\sqrt{\omega_0^2 + (\omega_c/2)^2}} \cos \frac{\omega_c}{2} t \left[\sin \sqrt{\omega_0^2 + \left(\frac{\omega_c}{2}\right)^2}\, t \right] r'\, dr'\, d\phi' \qquad (80)$$

where r_c is the electron-crossover position. The ϕ' integration (which was previously carried out (Equation 75)) must be left variable in this expression because the crossover position depends generally on r' as well as ϕ'.

The electron-crossover coordinates may be obtained in general from the uniqueness condition concerning the transformation from Eulerian to Lagrangian coordinates. This condition may be expressed in the form

$$J = \det \begin{bmatrix} 1 + \dfrac{\partial X_1}{\partial x_{0_1}} & \dfrac{\partial X_2}{\partial x_{0_1}} & \dfrac{\partial X_3}{\partial x_{0_1}} \\ \dfrac{\partial X_1}{\partial x_{0_2}} & 1 + \dfrac{\partial X_2}{\partial x_{0_2}} & \dfrac{\partial X_3}{\partial x_{0_2}} \\ \dfrac{\partial X_1}{\partial x_{0_3}} & \dfrac{\partial X_2}{\partial x_{0_3}} & 1 + \dfrac{\partial X_3}{\partial x_{0_3}} \end{bmatrix} = 0 \tag{81}$$

where J is the Jacobian defining the transformation and X_1, X_2, and X_3 are the electron displacements (in directions 1, 2, and 3), each being functions of the initial positions x_{0_1}, x_{0_2}, and x_{0_3}. In the case where the electron motion varies in only one direction, Equation 81 reduces to the simple result $\partial X_1/\partial x_{0_1} + 1 = 0$. This condition was used previously to obtain the electron-crossover position for the one-dimensional slab geometry. As shown later, this same equation is adequate for a cylindrical nonmagnetoplasma and will be used to determine the crossover position for this plasma.

For cylindrical geometry, the linearized (transformed) electron velocity is obtained from Equation 43, where the term $\mathbf{K} \cdot \tilde{\mathbf{E}} = \tilde{\mathbf{P}}$ is given approximately by Equations 73 for an inhomogeneous plasma. In the case of a nonmagnetoplasma, the polarization is in the x direction resulting in the following equations:

$$\left.\begin{aligned} \mathbf{v}(\mathbf{r}, t) &= \mathbf{a}_{x_1} v_p \cos \omega_0(\mathbf{r}) t \\ \omega_0(\mathbf{r}) &= \frac{\omega_p(\mathbf{r})}{\sqrt{2}} \end{aligned}\right\} \tag{82}$$

where $v_p = (e/m_e)E_i t_p$ is the initial electron velocity due to an applied pulse of amplitude E_i and width t_p. The corresponding electron displacement from an initial point $\mathbf{r}_0$ is given by

$$\begin{aligned} \mathbf{X}_1(\mathbf{r}_0, t) &= \int_0^t \mathbf{v}(\mathbf{r}_0, t')\, dt' \\ &= \mathbf{a}_{x_1} \frac{v_p}{\omega_0(\mathbf{r}_0)} \sin \omega_0(\mathbf{r}_0) t \end{aligned} \tag{83}$$

Note that the initial position $\mathbf{r}_0$ and electron position $\mathbf{r}$ are interchangeable for small displacements from equilibrium. Substituting Equation 83 into Equation 81 produces the crossover condition, which

in rectangular coordinates is

$$\frac{\partial X_1}{\partial x_{0_1}} + 1 = 0$$

or

$$\frac{v_p \omega_0'}{\omega_0^2} (\sin \omega_0 t - \omega_0 t \cos \omega_0 t) = 1 , \tag{84}$$

where

$$\omega_0 = \omega_0(x_{0_1}, x_{0_2})$$

$$\omega_0' = \frac{\partial}{\partial x_{0_1}} \omega_0 .$$

Equation 84 is similar to that found for the plasma slab (Equation 35); the main difference lies in the additional spatial dimension in ω_p, which exists for the cylindrical plasma.

As in the plasma-slab case, the crossover position is determined from Equation 84 for $\omega_0 t \gg 1$. For a parabolic density profile, the equation then becomes

$$\frac{r_c}{a} = \sqrt{\left(\frac{T}{\beta} \cos \phi\right)^2 + 1} - \frac{T}{\beta} |\cos \phi| , \tag{85}$$

where $T = f_0(0)t$ and $\beta = f_0(0)(2a/v_p)$.

The nonmagnetoplasma response is given by Equation 80 with $\omega_c = 0$; that is,

$$\frac{\Gamma(T)}{\Gamma_0} = \int_0^{2\pi} \int_0^{r_c/a} \sqrt{1 - u^2} \left(\sin \sqrt{1 - u^2}\, 2\pi T\right) u \, du \, d\phi , \tag{86}$$

where $\Gamma_0 = \omega_0(0)(a/r)^2$.

The numerical evaluation of this equation is shown in Figure 14 for the initial velocities 10^8 cm/s and 10^9 cm/s, where $f_0(0) = 10^9$ s^{-1} and $a = 1/2$ cm. The nonlinear behavior is comparable to the results obtained for slab geometry (Figure 9); i.e., increased excitation produces stronger damping and increased initial frequency of oscillation.

Conclusions and Summary

The linear and nonlinear theories of the interaction of electromagnetic radiation with a cold, inhomogeneous magnetoplasma have been considered. Solutions have been developed in forms appropriate to the experimental work on impulse excitation of a magnetoplasma. It is shown that the essential features of the theoretical results offer an explanation to the experimental observations made

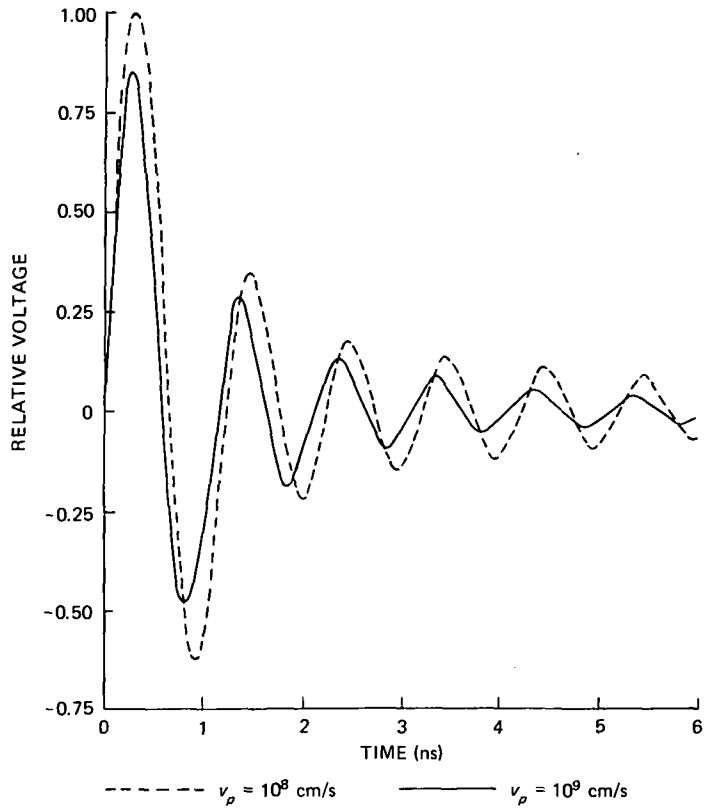

Figure 14—Impulse responses of a cylindrical non-magnetoplasma for different excitation amplitudes; $\omega_p^2(r) = \omega_p^2(0)[1 - (r/a)^2]$.

in this investigation. The damping at the linear level is due to phase mixing of the plasma oscillations. At high nonlinear levels of excitation, the slight increase in oscillating frequency and the increase of damping is due to the random mixing that follows the electron crossover.

The basic linear and nonlinear phenomena resulting from plasma inhomogeneity were obtained by analyzing an inhomogeneous plasma slab. The results of this analysis are clearly shown in Figure 9, displaying the approximately linear and strong nonlinear impulse responses of a nonmagnetoplasma. At the linear level the general impulse response is given by Equation 21:

$$V_{\mathrm{pl}}(t) = \frac{m_e}{e} v_p \int_{-a}^{a} \frac{\omega_p^2(x)}{\omega_h(x)} \sin \omega_h(x) t \, dx \tag{21}$$

For an inhomogeneous plasma, the phase-mixing integral results in a damped oscillatory response, where the damping is due to the interference among the continuum of sinusoidal oscillations. The nonlinear response obtained for large excitation is analyzed by replacing the limits of integration with the electron-crossover position, which is amplitude dependent as shown in Figure 5. This results in a response displaying larger damping and an initial increase in oscillation frequency for stronger impulse excitation.

The laboratory plasma used is of cylindrical geometry and is excited by a transverse electric field as shown in Figure 10. Plasma inhomogeneity complicates the mathematics for cylindrical geometry so that an exact solution can only be obtained numerically. An alternate analytical approach was taken using approximate techniques to obtain useful solutions that can be compared with the results for slab geometry. At the linear level the impulse response is given approximately by Equation 78,

$$\Gamma(t) = \frac{2}{r^2}\int_0^a \frac{\omega_0^2}{\sqrt{\omega_0^2 + (\omega_c/2)^2}} \cos\frac{\omega_c}{2}t\left[\sin\sqrt{\omega_0^2 + \left(\frac{\omega_c}{2}\right)^2}\,t\right] r'\,dr', \qquad (78)$$

and appears completely different from that of the plasma slab. The more complex equation is caused by the dipole mode, which is excited for the cylindrical geometry, and is not supported by the plasma slab. Figure 13 shows the impulse responses for different magnetic fields, displaying the modulated oscillatory waveforms resulting from the interference among the dipole split oscillations. The damping of the responses is due to inhomogeneity in plasma density and is stronger than that found for the plasma slab. This is illustrated in Figure 12 where the impulse responses of a nonmagnetoplasma are displayed for cylindrical and slab geometry, both geometries having the same variation in plasma density. Also observed is the larger frequency of oscillation for the cylindrical plasma as compared with the plasma slab.

At the nonlinear level, the response for the cylindrical plasma is treated with the same mechanism applied to the slab; i.e., the upper limit is replaced by the electron-crossover position. Referring to Figure 14, it is seen that the nonlinear behavior is similar to that found for the slab geometry. The nonlinear response for a cylindrical magnetoplasma has not been performed; however, it can be argued that the response should exhibit the increased damping and initially increased frequency of oscillation as for the nonmagnetoplasma.

These results are applied in Section 4 to explain most of the experimental observations.

3. EXPERIMENTAL DESCRIPTION

The experimental part of this investigation consisted of a series of measurements on the emission (impulse response) from an argon plasma column excited transversely by a narrow (120-ps, 3-dB width) baseband electric field pulse. The peak amplitude of this pulse is 1860 V resulting in a field strength in the plasma region of about 900 V/cm. As mentioned earlier, the key item that made these experiments possible is the BBG with its combined sharpness and high amplitude. In the following sections, a description of the experimental setup and its various components is given. The procedures for the calibration of the overall system and the individual components are also discussed in detail.

Experimental Apparatus

The basic system (part of which is shown in Figure 15) consists of the following principal items:

(1) Plasma and the associated vacuum system

(2) BBG for producing the impulse excitation

(3) Parallel-plate structure for applying the pulse to the plasma

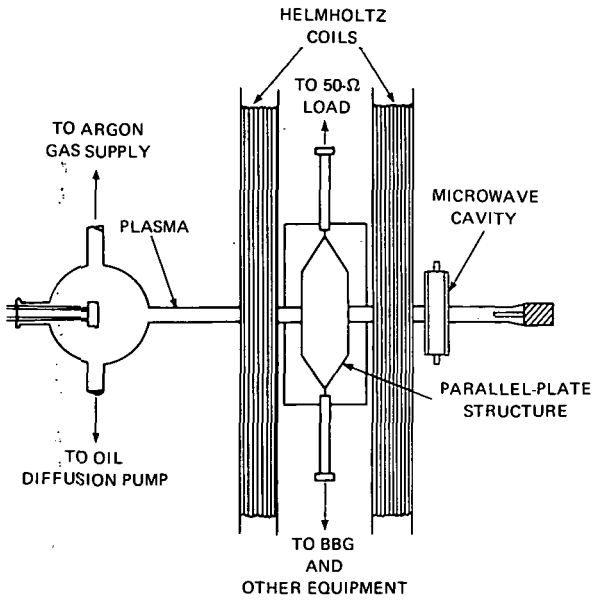

Figure 15—Experimental arrangement (top view).

(4) Helmholtz coils for producing the magnetic field

(5) Sampling scope and the associated X-Y recorder

Consider the system shown in Figure 16, which corresponds to the center portion of Figure 15. The geometry is the same as that employed in Tonks-Dattner resonance experiments except that a parallel-plate structure is used instead of a waveguide. The impulses from the BBG (approximately 0.2 ns wide) form a traveling voltage along the transmission line about 6 cm long. When this electric field is incident on the plasma column (≈1-cm diameter), it can be assumed that an electric field is "turned on" across the plasma as the leading edge of the pulse crosses the tube and is "turned off" as the trailing edge of the pulse passes by. In this small duration of time, the electrons gain a velocity $(eE/m_e)t_p$. This sets up oscillations in the plasma, and the stimulated emission generated by these electron oscillations are observed by the voltage generated across the parallel-plate structure. This voltage is viewed on the sampling scope and displayed on the X-Y recorder.

Plasma

The plasma used in the experiments was a positive-column, hot-cathode dc discharge in argon at pressures ranging from 0.13 to 1.3 N/m^2 (1 to 10 μm Hg). The construction of the discharge tube is indicated in Figure 17, showing the two thyratron cathodes[2] contained in a 2000-ml round-bottom ringed-neck flask, the 9.525-mm-i.d. precision Pyrex glass tube of nominal thickness 1.5 mm, and the oxygen-free high-conductivity (OFHC) copper anode which is joined by means of a copper-to-Pyrex-

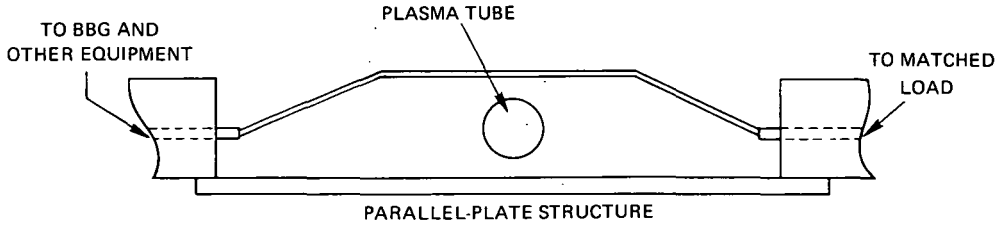

Figure 16—Experimental setup for plasma excitation.

[2]Western Electric 354A cathodes were used.

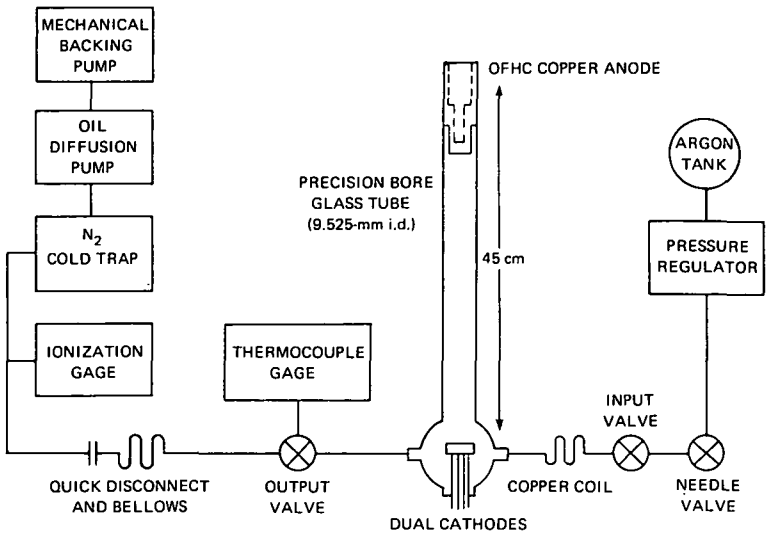

Figure 17—Plasma tube and associated vacuum/gas flow system.

glass graded seal. The vacuum station consists of a 5-cm oil diffusion pump[3] with a 5-cm liquid nitrogen trap and has a pump speed of 0.08 m^3/s.

Argon was allowed to flow through the discharge tube at a slow rate using a needle valve at the gas input port, while gas was removed at the output port by the vacuum station as shown in Figure 17. In this way, contamination of the argon due to outgassing was reduced, because such impurities were constantly being removed from the discharge tube. A short, large-diameter (5-cm) copper tubing and flexible bellows were used to join the vacuum station to the discharge tube at the output port. Pressure as low as 1 $\mu N/m^2$ (10^{-5} μm Hg) was measured using an ionization gage connected to the vacuum station with the input (gas) valve closed; this corresponds to the minimum attainable pressure for the system.

A 6.3-V, 20-A filament transformer was used to supply power to the two cathodes which were connected in series. The cathodes were activated below a pressure of 0.013 N/m^2 (0.1 μm Hg) following the procedure outlined by the manufacturer, after which the discharge tube was ready for plasma production. A steady-operating argon pressure, as measured by a thermocouple gage, was attained by adjusting the needle valve and larger valve at the output port. The plasma discharge power was supplied from a 300-V, 500-mA regulated dc source connected to the anode and cathodes through a 1000-Ω variable rheostat. Stable plasma discharges were obtained by adjusting the dc voltage and rheostat setting to produce plasma currents ranging from 30 to 300 mA.

Measurements were made on the background plasma characteristics, including the electron temperature and average electron density. The electron temperature was obtained using the familiar Langmuir probe method (Reference 26). Figure 18 indicates the data recorded for different argon pressures in the absence of a magnetic field. The plasma frequency (defined later) was set at 1.1 GHz. These

[3]A Veeco pump was used.

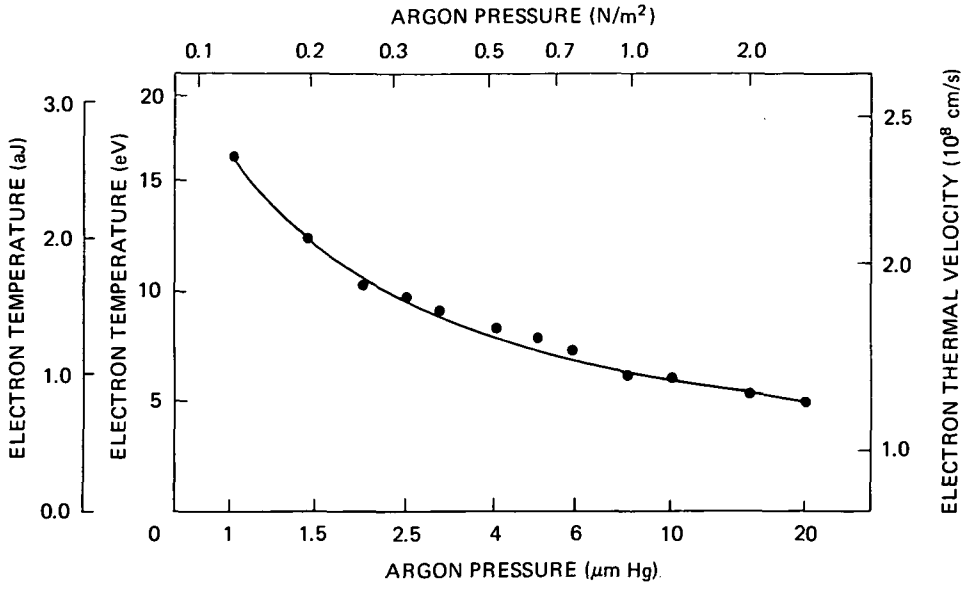

Figure 18—Electron temperature as a function of neutral gas pressure.

temperatures changed with magnetic field; however, because the probe measurements are not very reliable in the presence of a magnetic field, no data were taken for this case.

A major problem encountered when using continuous dc discharges was the appearance of low-frequency spontaneous oscillations (termed striations) in the electron density. These oscillations appear about the average density level and depend strongly on the argon pressure, existing for both low and high pressures. It was found, by monitoring the density fluctuations using the Langmuir probe, that the striations were greatly reduced for pressures within the range of 0.3 to 0.7 N/m^2 (2 to 5 μm Hg). For this reason, the measurements of the plasma given in Section 4 are for pressures within this narrow range at which the plasma is quiet.

The average electron density is given by the following equation:

$$\langle n_e \rangle = \frac{2}{a^2} \int_0^a n_e(r) r \, dr \tag{87}$$

where a is the column radius. The density was measured for different discharge currents using a microwave cavity as described in Appendix B. The results are shown in Figure 19 for an argon pressure of 0.33 N/m^2 (2.5 μm Hg). Also indicated in Figure 19 is the (average) plasma frequency computed from the electron densities as follows:

$$f_p \equiv \langle f_p^2 \rangle^{1/2} = \frac{1}{2\pi} \sqrt{\frac{\langle n_e \rangle e^2}{\epsilon_0 m_e}} \, . \tag{88}$$

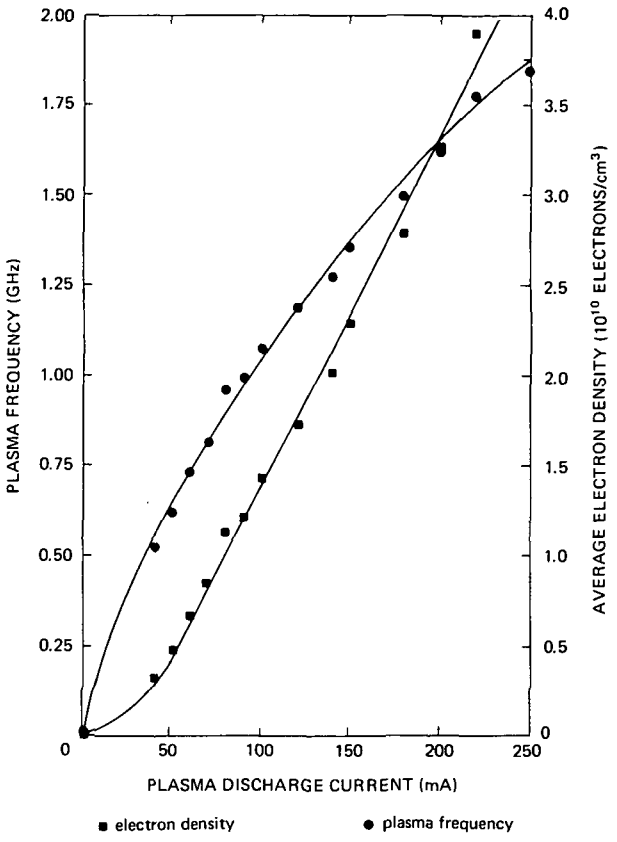

Figure 19—Electron density and plasma frequency for different discharge currents.

The linear relationship found between the electron density and discharge current is well known for such continuous-dc-discharge plasmas (Reference 18). It should be mentioned that no variations in electron density were detected for the magnetic fields used (maximum of 17.5 mT (175 G).

Pulse Generator

A unique part of the experimental system is the BBG used to excite the plasma. The pulse generator is a noncommercial unit built by Dr. P. Pleshko[4] and Dr. J. B. Gunn of IBM Watson Research Laboratories and has the capability of producing an 1860-V (peak voltage), approximately gaussian-shaped, baseband pulse having a 3-dB width of 120 ps.

The pulse is generated by charging a 4.0-mm steel ball bearing that is able to move freely in the gap formed by the split inner conductor of a coaxial section as shown in Figure 20. (For additional details see Pleshko and Palocz.[4])

The ball is charged by making contact with the input conductor, which is connected to a 15-kV dc supply. Having been charged, the ball is accelerated by electrostatic forces toward the output conductor, which is terminated by a matched 50-Ω transmission line (not shown in Figure 20). Upon making contact with this conductor, the ball transfers its charge to the transmission line in the form of a sharp pulse. The electrostatic forces acting on the ball now reverse its direction and accelerate it back to the input conductor, where it is recharged. This charging and discharging process is repeated approximately 100 times per second, resulting in pulses having a very clean waveform and negligible ringing as shown by the measurement displayed in Figure 21. Also shown in Figure 21 is the normalized voltage spectrum of the BBG waveform, which was obtained by Fourier analysis using a digital computer.

The pulse measurement was obtained (Figure 22) by connecting the generator through a 60-ns (4.4-dB loss) RG9U-B delay line and 70 dB of attenuation to a sampling scope having a high-speed (75-ps risetime) head.[5] A fraction of the BBG pulse was used to trigger the scope, after which the delayed pulse arrived and was displayed on the scope. The delay line was necessary to allow adequate time for sampling the BBG pulse. The analog output from the scope was connected to the X-Y recorder resulting in the display shown in Figure 21.

[4]P. Pleshko and I. Palocz: Memorandum M-6, School of Engineering and Science, New York Univ., 1969.
[5]A Tektronix 564 scope was used with a 3S2-S2 sampling head.

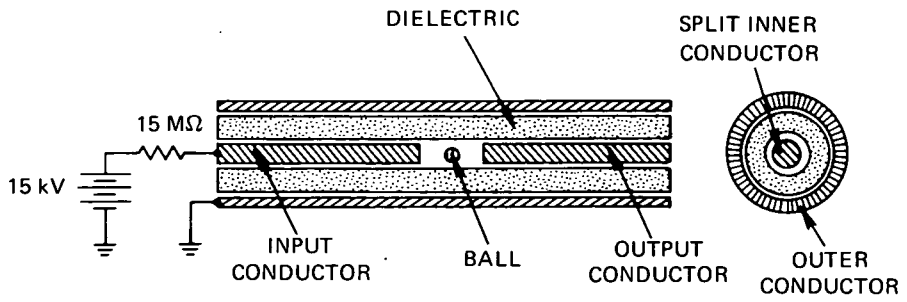

Figure 20—The bouncing ball generator.

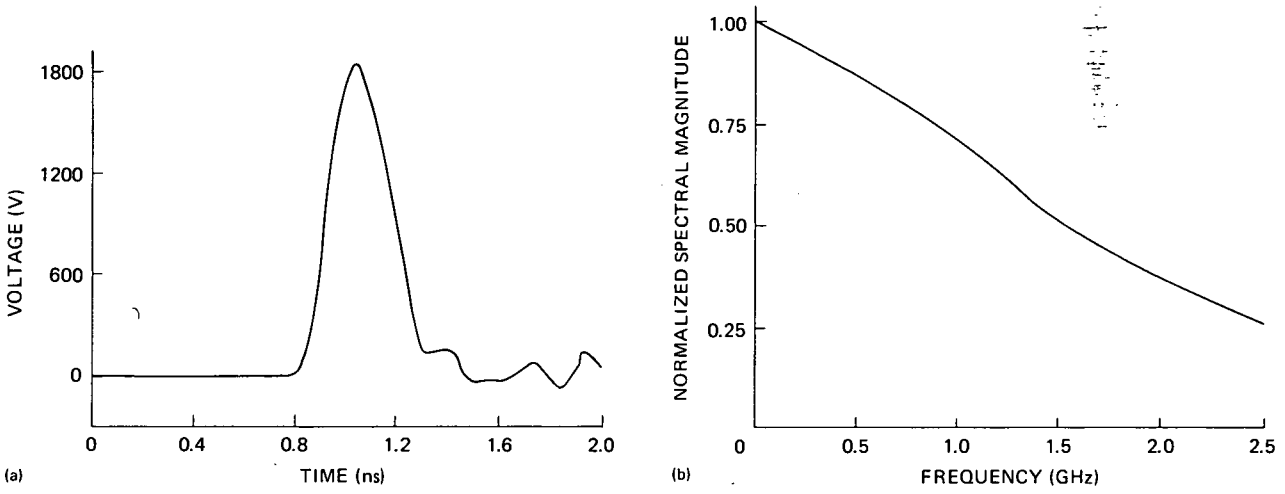

Figure 21—Measurements of BBG. (a) Pulse waveform; V_{pk} = 1860 V. (b) Normalized voltage pulse spectrum.

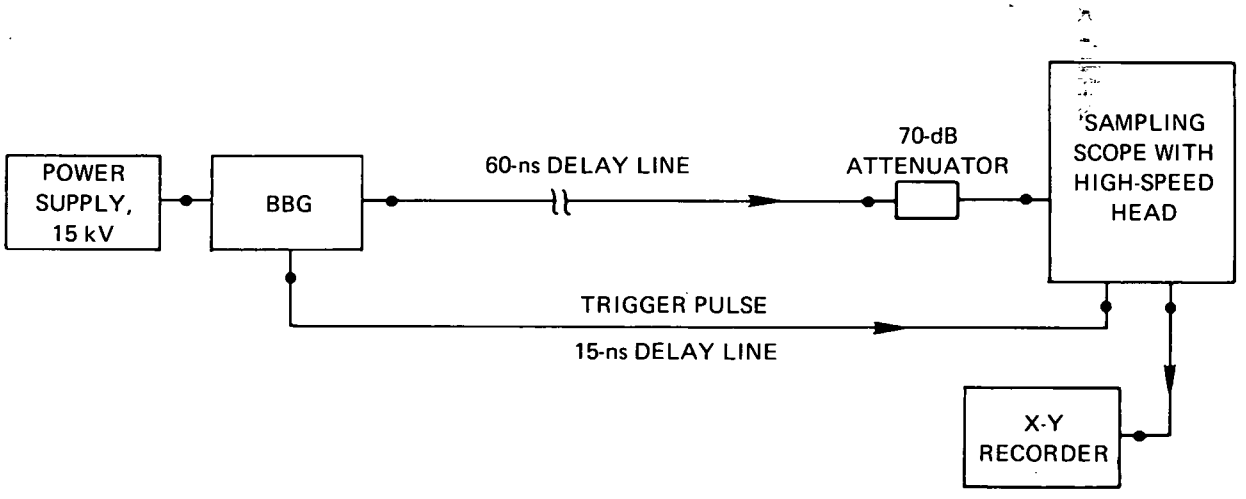

Figure 22—Experimental setup for observation of BBG pulse.

The frequency spectrum of the BBG waveform was determined by Fourier analysis of a 25- by 38-cm X-Y plot using a digital computer. A total of 300 data points, 6.66 ps apart, was used to compute the spectrum. This technique was employed later to obtain the spectrum for the configuration used to monitor the plasma impulse response and to determine the spectrum of the plasma responses. An alternate procedure would be to use an electronic spectrum analyzer; however, such a unit was not available for measuring the extremely fast waveforms encountered in this study.

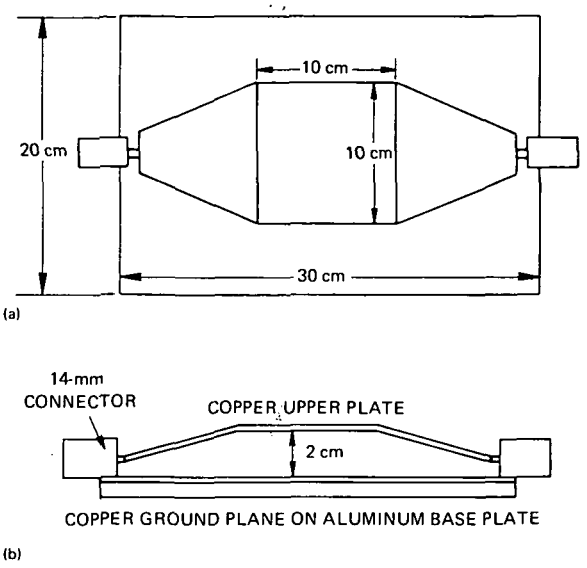

Figure 23—Parallel-plate transmission structure. (a) Top view. (b) Side view.

Transmission Structure

To transmit the BBG pulse with minimum distortion, a parallel-plate transmission structure was chosen in which the plasma column was placed between the plates as shown in Figure 1c. The structure (Figure 23) consists of two copper plates connected[6] to 14-mm air lines. To match the 50-Ω characteristic impedance of the air lines, the upper plate was partially tapered above the flat ground plane; the taper was adjusted to obtain a uniform 50-Ω impedance along the length of the structure. The ratio of upper plate width to separation above the ground plane is approximately 5 to 1, in accordance with transmission line theory (Reference 27). Microwave reflection and transmission measurements performed between 0.25 and 1.10 GHz showed reflections 31 dB below the incident power and transmission losses less than 1 dB.

These measurements were obtained using a sweep generator[7] connected to a wideband (20 dB, 0.25 to 1.10 GHz) directional coupler[8] which in turn was connected to the transmission structure as shown in Figure 24. Reflected signals from the structure were transmitted through the coupling port, detected, and compared with the incident signal after subtracting out the relatively flat, 20-dB coupling loss. Direct transmission through the structure was compared with the input signal to obtain the insertion loss.

Magnetic Field

A magnetoplasma was obtained by applying a static magnetic field along the column axes, as shown in Figure 1c. In choosing a field structure, particular concern was placed on obtaining both a uniform axial and transverse field within the parallel-plate region of 10 cm. To obtain such a field, a Helmholtz pair was designed and constructed having the dimensions shown in Figure 25. The aluminum coil forms are made of 0.4-m^2, 0.6-cm-thick face plates, joined with bronze bolts to a 40-cm-o.d.

[6]A General Radio GR874 14-mm connector was used.
[7]A Gerrald 900 C generator was used.
[8]A Narda coupler was used.

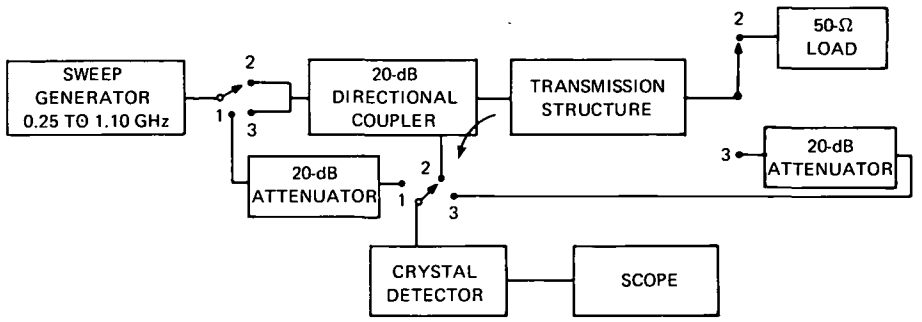

Figure 24—Experimental setup for measuring the transmission structure characteristics. The numbers indicate the types of power: (1) incident, (2) reflected, and (3) transmitted.

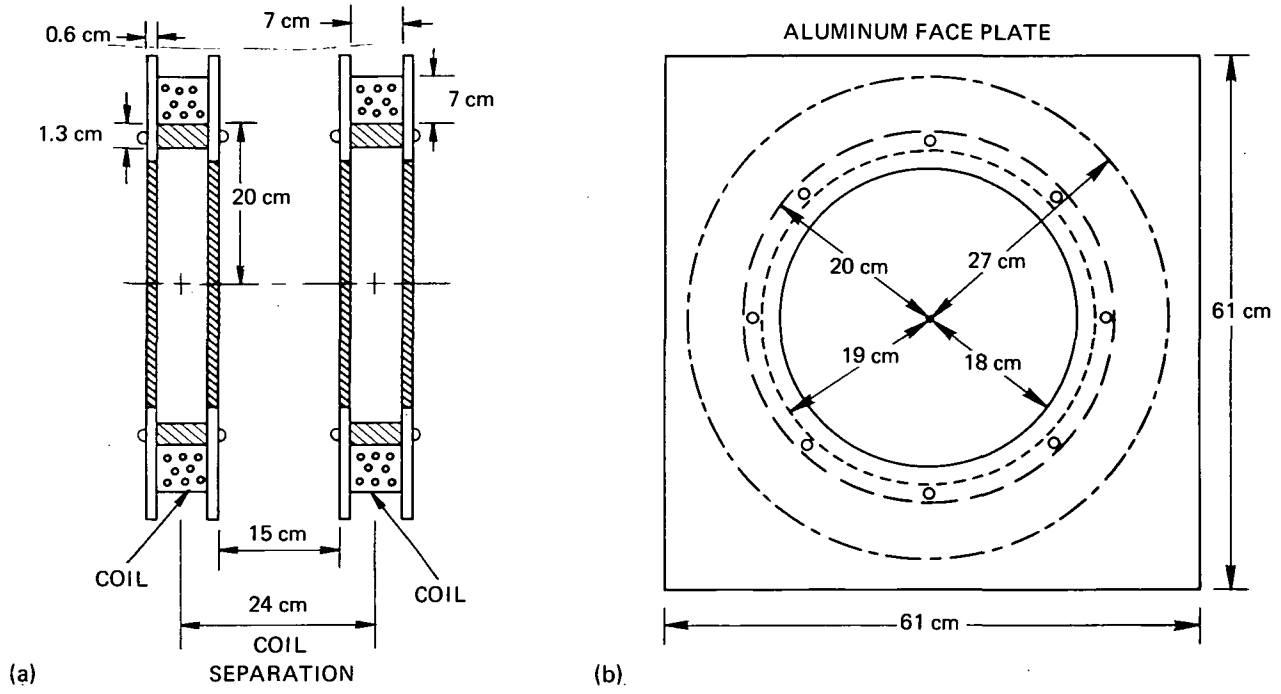

Figure 25—Cross sections of Helmholtz coil construction. (a) Side view. (b) Front view.

tubing, 1.3 cm thick and 7.0 cm long. The forms are wound with 20 layers having 20 turns per layer of No. 8 polyesterine magnet wire. Each coil has an electrical resistance of 1.33 Ω at room temperature and is powered using a 32-V, 40-A regulated dc power supply connected in series with the two identical coils.

Minimum inhomogeneity was obtained by separating the coils a distance approximately equal to their average radius of 23.8 cm. Measurements of the central field strength using a Hall probe

gaussmeter indicated a magnetic field of 1.75 mT/A (17.5 G/A), corresponding to an electron-cyclotron frequency of 50 MHz/A. This measurement is in good agreement with the following equation, which was derived from the Biot and Savart law as contained in Reference 28:

$$B_z = \frac{32\pi}{10 \cdot 5^{3/2}} \frac{NI}{R}, \tag{89}$$

where I is in amperes, R is in centimeters, and B_z is in millitesla (gauss). B_z is the axial magnetic field at the midpoint between two single-loop coils, each having NI ampere turns and separated a distance equal to their radius R. To apply Equation 89 for the experimental coils, an average coil radius R = 23.8 cm is used with N = 400 turns, so that we find B_z = 1.53 mT/A (15.3 G/A).

Measurements of the field inhomogeneity could not be observed using the Hall probe; thus an estimate of the axial field inhomogeneity is computed from the equation developed for the single-loop coils (Reference 28):

$$\frac{\Delta B}{B_z} = \frac{144}{125}\left(\frac{z}{R}\right)^4. \tag{90}$$

This expression gives the axial field variation ΔB about the midpoint, z/R = 0, with respect to the midpoint field B_z. Within the region occupied by the parallel-plate structure ($z \leqslant \pm 5$ cm), Equation 90 indicates an axial field variation of less than 0.3 percent.

The orientation of the plasma, parallel-plate structure, Helmholtz coils, and microwave cavity are shown in Figure 15. This top view of the experimental setup does not show the microwave absorbing material placed around the coils to minimize the amount of radiation reflected back into the parallel-plate structure.

Configuration for Monitoring the Plasma Impulse Response

The impulse responses were monitored using the setup outlined in Figure 26. This configuration was employed to obtain large detection sensitivity.

The plasma column was placed within the parallel-plate structure, which is terminated at one end by a matched 50-Ω load and at the other end is connected to a wideband (10 dB: 0.9 to 2.0 GHz) directional coupler. The BBG pulse incident on the plasma is coupled through the directional coupler to the sampling scope. Because of the isolation provided by the directional coupler, the sampling scope only detects the reflected signal from the plasma so that relatively large incident pulses can be applied without damaging the scope (maximum allowable input of 2 V). Hence, the larger incident pulse results in larger reflected signals, which are above the level of fluctuations from the plasma and scope noise, thus increasing the sensitivity for detecting the plasma response.

The variac connected to the BBG power supply is used to vary the peak output BBG voltage between 1200 and 1860 V without distorting the waveform. To obtain lower peak voltages for weaker excitation of the plasma, fixed attenuators are connected before the directional coupler, as shown in Figure 26. The frequency spectrum characterizing the experimental system was determined using the following technique.

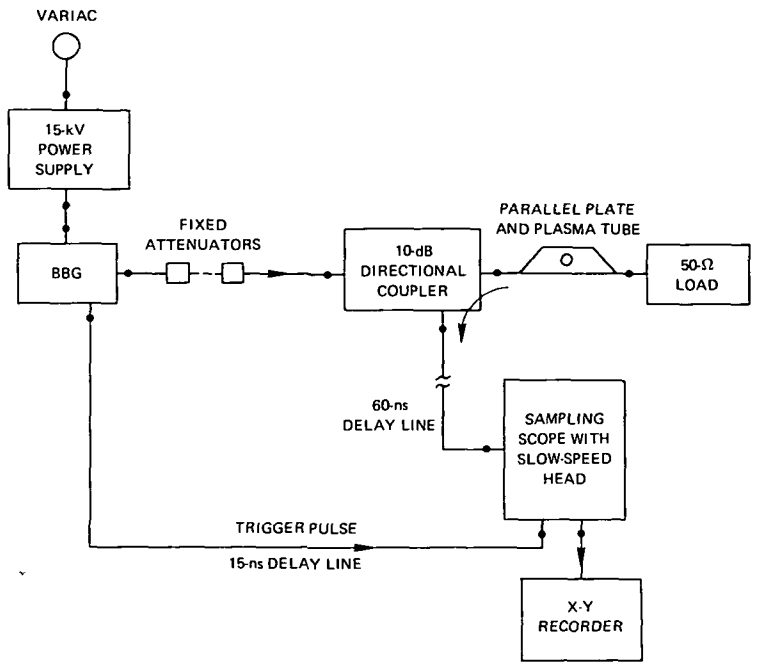

Figure 26—Experimental setup for monitoring the impulse (BBG) response of the plasma.

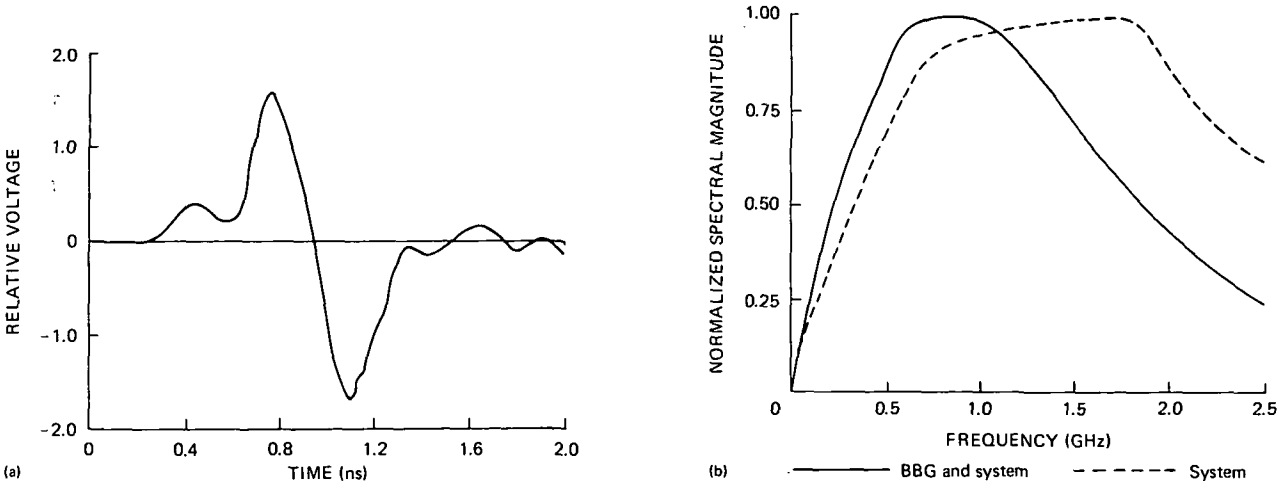

Figure 27—Characteristics of experimental system. (a) BBG response of system. (b) Normalized voltage spectra.

The BBG was used to excite the system (70-dB attenuation and the high-speed scope head were used) with no plasma discharge and with the 50-Ω load replaced by a short circuit. Figure 27 shows the pulse after being reflected from the short and coupled through the directional coupler to the sampling scope. The frequency spectrum of the response was obtained using a computer and is given by the solid curve in Figure 27b. To obtain the frequency spectrum characterizing the system, i.e.,

directional coupler, parallel-plate structure, etc., the BBG spectrum of Figure 21b is divided out, resulting in the dashed curve of Figure 27b. This spectrum is predominately a result of the bandpass characteristics of the directional coupler.

To obtain the frequency (radiation) spectrum of the plasma, the frequency characteristics of the directional coupler and BBG (solid curve of Figure 27b) must be divided out. However, for the frequencies observed (0.5 to 1.2 GHz), the variations due to the BBG and directional coupler combination are less than 10 percent (1-dB power) and can be neglected. Thus, the responses obtained with the plasma on are accurate measurements of the plasma response because of the wideband properties of the BBG, parallel-plate structure, and directional coupler.

As previously mentioned, both the fast BBG pulse (Figure 21) and system response (Figure 27) were monitored by the high-speed (75-ps risetime) sampling head. However, for the purpose of monitoring the lower frequency plasma responses, the slower speed (400-ps risetime) sampling head[9] was found to be adequate. This latter head did not distort the responses produced by the plasma but only reduced the sharp spikes (residuals) resulting from the reflections due to the cable connections, etc. This filtering out of the higher frequency residuals made it easier to identify the plasma response; and therefore the slower speed head was used rather than the high-speed head.

A circuit exists within the scope to smooth out any scattering of sampled data points due to jitter in the plasma response such as that caused by fluctuations in plasma density (striations). This circuit can be connected or removed by setting the smoothing switch to the normal or smooth positions, respectively. Figure 28 shows the plasma response monitored using the slow-speed head which was connected for smooth and normal operation. It is observed that the smoothing circuit acts to average out the fluctuations in the plasma response, making it easier to identify the coherent response of the plasma.

With the combination of the slow sampling head and the smoothing circuit, the coherent response of the plasma could be readily examined without performing any additional signal processing. This reduced the labor involved in determining the digital Fourier spectrum because the residual signals and scattering of sampled data points were small and could sometimes be neglected without introducing large error in the resulting spectrum. (The residual signals were monitored with the plasma off and were subtracted from the response with the plasma on to accurately obtain the response produced by the plasma.)

It is noted in Figure 26 that a 60-ns delay line was placed between the coupler and sampling scope. It was mentioned previously that the delay line was necessary when using the high-speed head to allow adequate time for sampling the BBG pulse. However, in this case the delay line served a different purpose. The slow head, which has an internal delay line, does not need any external delay line for sampling purposes. The delay line was used instead to delay the disturbances from the BBG that radiated into the scope and distorted the measurements. The delay line provided the time necessary for the radiation to damp before the plasma response appeared.

[9]The Tektronix 3S76 sampling head was used.

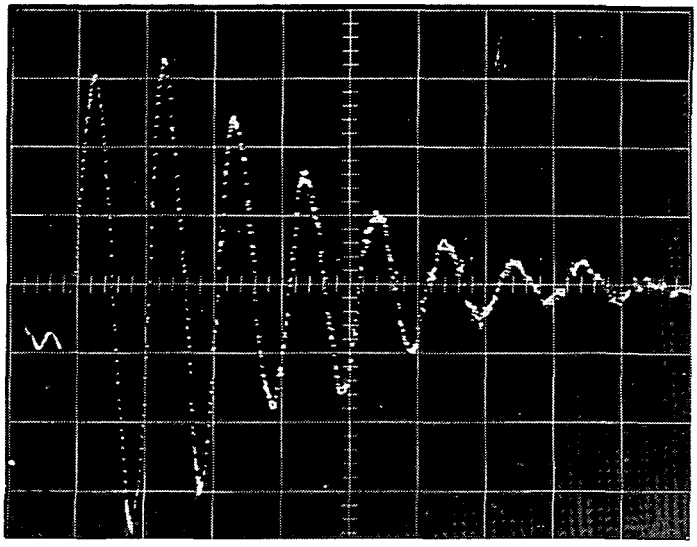

(a)

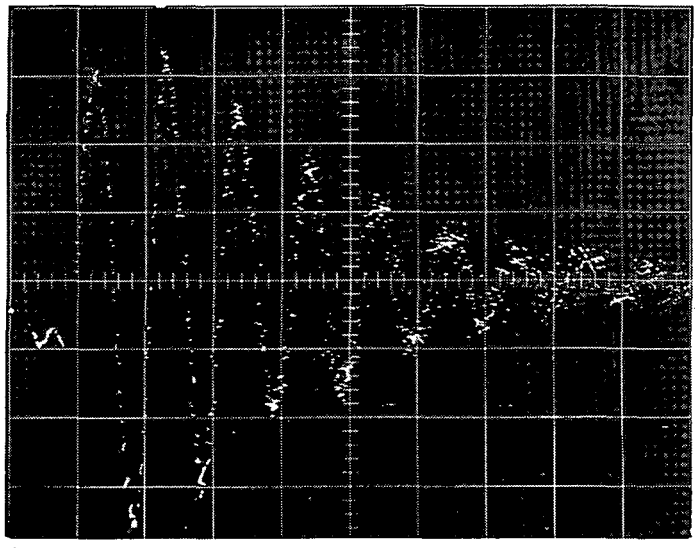

(b)

Figure 28—Plasma response obtained with different samplings. (a) Smooth sampling. (b) Normal sampling.

4. EXPERIMENTAL RESULTS

The linear and nonlinear magnetoplasma responses to impulse excitation were obtained for different plasma discharge currents, magnetic fields, argon pressures, and peak BBG voltages. These four parameters were controlled independently and the different impulse responses as well as their frequency spectra were obtained.

Throughout the following discussion, comparison is made when possible with the theory developed earlier. As previously noted, the measured impulse response (Figure 2) appears as a modulated, damped oscillation. It is shown in this section that the impulse response possesses the general characteristics of the linear theory for a cold, inhomogeneous, cylindrical magnetoplasma. This is ascertained by comparing the results observed for different magnetic fields and plasma discharge currents with those predicted by the theory.

To establish that the damping mechanism is due to phase mixing resulting from inhomogeneity in plasma density, the impulse responses and their frequency spectra obtained for different plasma discharge currents are compared with the theory. The measurements are presented both with and without a magnetic field; the essential damping features are most easily examined for the nonmagnetoplasma.

The magnetic field acts to modulate and alter the oscillation frequencies of the nonmagnetoplasma response. These characteristics are exhibited by both the impulse responses and frequency spectra for different magnetic fields. It is observed that the magnetic field acts to split the single dipole resonance of the nonmagnetoplasma into two separate resonances as predicted qualitatively from the linear theory. For weak magnetic fields (<7 mT (<70 G)) the resonance and antiresonance frequencies compare well with the simpler theory of a homogeneous plasma. However, for larger magnetic fields, the measurements show large discrepancies with the theory. The approximate inclusion of inhomogeneity in plasma density into the theory does not appear to resolve the disagreement for large magnetic fields.

Scattering measurements were made using low-power microwaves incident to the plasma, where the reflected and transmitted power was monitored at different frequencies. The primary purpose of these measurements was to compare the steady-state frequency spectrum with that obtained from the impulse response of the plasma. As expected, the two spectra are approximately the same, agreeing with the well-known convolution principle.

The nonlinear impulse response of the plasma was also studied. As previously noted, from Figure 3, the response for stronger excitation displays larger damping in addition to a small increase in the frequency of oscillation. This nonlinear behavior is compared with the nonlinear theory of a cold, inhomogeneous plasma. It is shown that the experimental results have the general features exhibited by this theory.

The measurements of the nonlinear damping are plotted as a function of the initial velocity imparted to the electrons by the impulse in voltage. This plot is compared with the damping due to electron-neutral collisions to show that the damping observed is not due to increased elastic collisions between electrons and neutrals. This result is important because previously the single-pulse excitation experiments were only able to observe the nonlinear damping due to electron-neutral collisions (Reference 15). According to the nonlinear theory which our measurements seem to correlate, the collisions that are important at the nonlinear level are those involving electrons with electrons in an inhomogeneous plasma.

The Linear Impulse Response

As discussed earlier, the technique used for exciting and monitoring the impulse response of the magnetoplasma employed a continuous dc discharge in argon, and the plasma column was placed within a parallel-plate structure and alined axially with the magnetic field produced by the Helmholtz coils (Figure 15). Throughout the measurements, the argon pressure was kept constant at 0.33 N/m^2 (2.5 μm Hg). The plasma response to the BBG pulse was monitored by the method described in Section 3. To insure that the plasma was linearly excited, the BBG pulse peak amplitude incident on the plasma was reduced to 50 V. This was accomplished by inserting 30 dB of attenuation before the directional coupler (Figure 26). Measurements of the plasma responses were made for different plasma discharge currents and magnetic fields.

Measurements for Various Discharge Currents

Figure 29 shows the responses for discharge currents of 0, 100, 150, and 200 mA, corresponding to plasma frequencies of 0, 1.1, 1.4, and 1.7 GHz, respectively. (See Figure 19.) These responses were obtained for a fixed magnetic field of 7 mT (70 G), which corresponds to an electron-cyclotron frequency of 200 MHz, and are displayed on the same voltage (measured by the sampling scope) and time scales. For the plasma off, $f_p = 0$, the response consists of the small reflected signals (residuals) resulting from the cable connections, the glass plasma tube, etc. With the plasma on, $f_p \neq 0$, the responses are mainly due to the plasma and appear as modulated, damped oscillations.

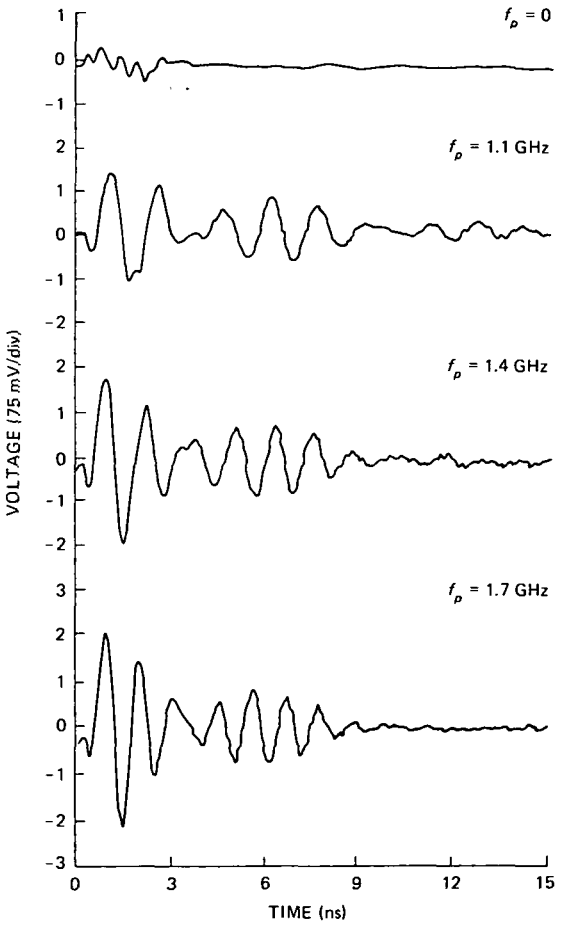

Figure 29—Linear impulse responses, f_c = 200 MHz.

The damping is stronger for larger plasma frequencies. This same form of damping has also been observed in similar experiments performed on a nonmagnetoplasma (Reference 4). Figure 30 shows the responses obtained without magnetic field, $f_c = 0$, for the same plasma frequencies. As seen by comparing Figures 29 and 30, the addition of a magnetic field modulates the nonmagnetoplasma responses without appreciably altering its damping. The results obtained without magnetic field compared well (Reference 29) with the linear theory of a cold, inhomogeneous plasma, for which the damping arises from phase mixing due to inhomogeneity in plasma density. This same damping mechanism also functions in the presence of a magnetic field, although for large homogeneous fields

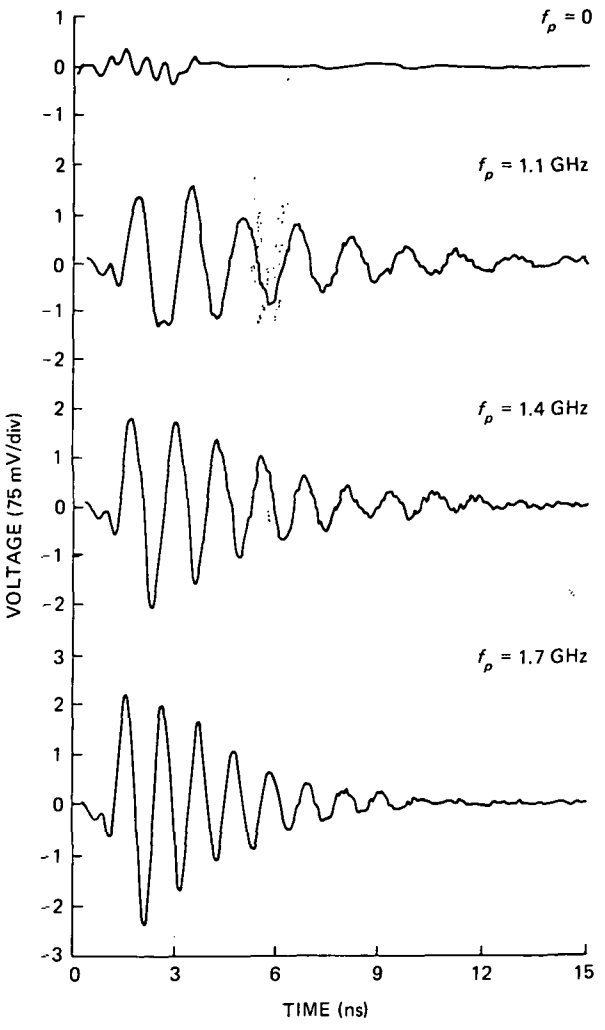

Figure 30—Linear impulse responses, $f_c = 0$.

such that $f_c > f_p$, its effect is reduced appreciably (References 6 and 15). Because the experimental conditions were such that $f_c < f_p$, no reduction in damping was observed for decreasing plasma frequency or for increasing electron-cyclotron frequency (to be shown later).

Besides the damping of the responses, a modulation was observed. It is noted from Figure 29 that the modulation frequency (the envelope) appears to remain unchanged for the different plasma frequencies, but the higher frequency oscillation within the modulation envelope increases with plasma frequency. These two results are compared with the linear theory of a cold, cylindrical magnetoplasma. A homogeneous plasma is considered at this point; the effects due to inhomogeneity in plasma density are considered later.

As shown in the discussion of the theory, the impulse response of a cold, homogeneous, cylindrical magnetoplasma is given by Equation 64:

$$\Gamma(t) = \left(\frac{a}{r}\right)^2 \frac{\omega_0^2}{\sqrt{\omega_0^2 + (\omega_c/2)^2}} \cos \frac{\omega_c}{2} t \times \sin \sqrt{\omega_0^2 + \left(\frac{\omega_c}{2}\right)^2}\, t,$$

where $\omega_0 = \omega_p/\sqrt{2}$. This shows that the response consists of an amplitude-modulated oscillation. The modulation arises from the term $\cos(\omega_c/2)t$ which, as observed experimentally, is independent of the plasma frequency. Also, Equation 64 indicates that the modulated oscillation has a frequency $\sqrt{\omega_0^2 + (\omega_c/2)^2}$ which increases with plasma frequency, as observed experimentally.

To obtain a more quantitative comparison, the frequency spectra of the experimental and theoretical results are employed. Figure 31 contains the normalized frequency (power) spectra of the waveforms in Figure 29. These spectra were determined, as mentioned earlier, by Fourier analysis of a 25- by 38-cm X-Y plot of the waveforms using a digital computer. A total of 300 data points, 50 ps apart, were used to compute the different spectra. Each spectrum consists of two separated resonance peaks at frequencies denoted as f_L and f_R and a minimum at a frequency f_0. The width of the resonances, which is a measure of the plasma absorption, broadens with increasing plasma frequency. This absorption mechanism has previously been identified (from the impulse response measurements) as due to phase mixing resulting from inhomogeneity in plasma density. Of interest are the

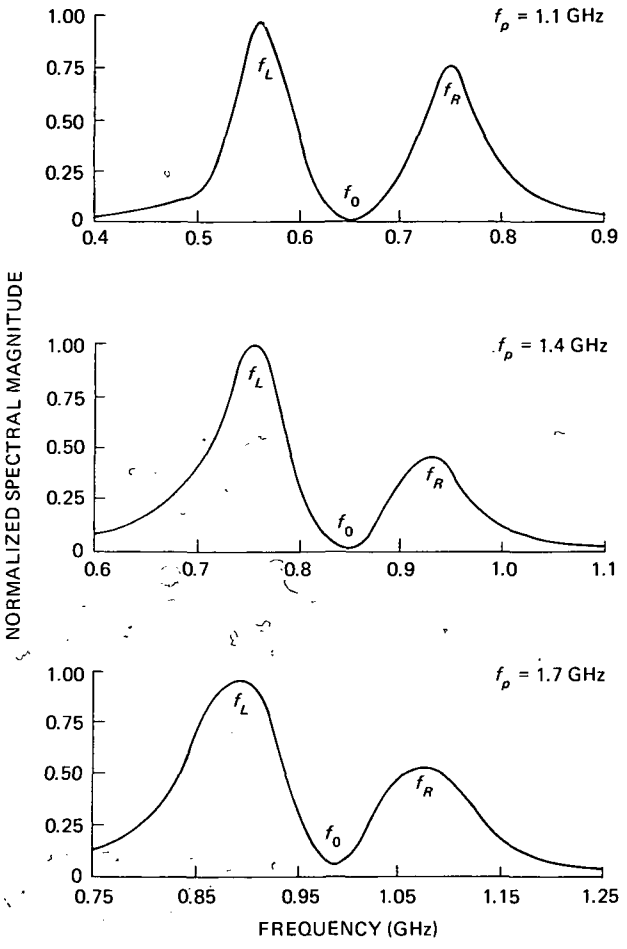

Figure 31—Linear impulse response spectra, f_c = 200 MHz.

relationships between the resonance frequencies f_L and f_R and minimum position f_0 for the different plasma frequencies f_p. The results are to be compared with the frequency spectrum obtained from the Fourier transformation of Equation 64, which was given earlier by Equation 61 and is repeated here:

$$\tilde{\Gamma}(\omega) = \left(\frac{a}{r}\right)^2 \frac{\omega_0^2(\omega^2 - \omega_0^2)}{(\omega^2 - \omega_L^2)(\omega^2 - \omega_R^2)} .$$

This theoretical spectrum contains two resonances at the frequencies $\omega_L/2\pi$ and $\omega_R/2\pi$, where the separation between the resonances is the electron-cyclotron frequency $\omega_c/2\pi$. Also, the spectrum has an antiresonance, corresponding to minimum scattering of incident radiation, at the frequency $\omega_0/2\pi$, which may be written as $\omega_0^2 = \omega_L \omega_R$.

The resonance frequencies were also derived by Crawford et al. (Reference 18), in whose work the inhomogeneity in plasma density was included as well as the presence of the glass (dielectric) surrounding the plasma tube and the coupling of the capacitor plates to the plasma. A variational theory was applied to approximately obtain the resonance frequencies of the system. Their results are the same as those obtained from Equation 61 if the plasma frequency is replaced by the average plasma frequency as defined by Equation 88 (also measured by the microwave cavity technique) and if it is recognized that the proportionality constant between ω_0 and ω_p is always less than $1/\sqrt{2}$ because of the glass capacitive coupling referred to before.

Hence, the relationships to be correlated with the experimental results are as follows:

$$\omega_R - \omega_L = \omega_c , \tag{91}$$

$$\omega_0 = \frac{\omega_p}{\sqrt{K}} , \tag{92}$$

$$\omega_0^2 = \omega_L \omega_R , \tag{93}$$

where $\omega_p/2\pi$ is the plasma frequency measured by the microwave cavity and the constant K is some value (to be determined experimentally) that is greater than 2.

Table 1–Data for linear impulse response spectra, f_c = 200 MHz.

f_p (GHz)	Measured Data			Calculated Results			
	f_L (MHz)	f_R (MHz)	f_0 (MHz)	$f_R - f_L$ (MHz)	$\frac{f_R - f_L}{f_c} - 1$ (percent)	$\frac{f_0}{f_p}$	$\frac{\sqrt{f_L f_R}}{f_0}$
1.1	565	750	650	185	7.5	0.59	1.00
1.4	752	930	850	178	11.0	.60	.99
1.7	890	1080	980	190	5.0	.58	.99

Returning to Figure 31, it is noted that the distance between resonance peaks $f_R - f_L$ is slightly dependent on the plasma frequency f_p; the experimental values are given in Table 1. The separation between peaks varies within 5 to 11 percent of the electron-cyclotron frequency (200 MHz). This is in agreement with Equation 91 within an 11 percent deviation. Also noted in Figure 31 is the increase in the minimum position f_0 with increasing plasma frequency. The ratio f_0/f_p is listed in Table 1 and is seen to vary less than 2 percent for the different plasma frequencies. Hence, this experimental result compares with Equation 92 when the average value of the constant K is 2.85 (greater than 2). From Equation 93 it is seen that the minimum position should be at the geometric mean between the two resonances; i.e., $\sqrt{f_L f_R}/f_0 \equiv 1$. This is shown to be approximately true within a 1 percent variation for the different plasma frequencies (Table 1).

Measurements for Different Magnetic Fields

The responses as shown in Figure 32 were obtained for the electron-cyclotron frequencies of 0, 100, 200, and 300 MHz; the plasma frequency was fixed at 1.1 GHz. In the absence of a magnetic field, f_c = 0, the response appears as an oscillation that is damped because of inhomogeneity in plasma density. The application of the magnetic field is observed to modulate the nonmagnetoplasma response without altering its damping. This same result was noted before by comparing the magnetoplasma responses (Figure 29) with the nonmagnetoplasma responses (Figure 30) for the different plasma frequencies. It was then found that for the condition $f_c < f_p$, there is no reduction in damping for decreasing plasma frequency or (as in this case) for increasing electron-cyclotron frequency.

The responses plotted in Figure 32 are now compared with the linear theory of a cold, cylindrical magnetoplasma. The comparison is begun, as before, by correlating the experimental results in both the time and frequency domains with the theory of a homogeneous plasma, using Equations 64 and 61, respectively. (After this presentation, a further comparison is made by incorporating the theoretical results obtained with inhomogeneity in plasma density included.)

From Equation 64, it is observed that increased f_c results in proportional increases in modulation frequency, as found experimentally in Figure 32. Also noted from the theory is the relatively unchanged higher frequency oscillation for the experimental condition $f_c < f_p$, which is in agreement with the experimental results.

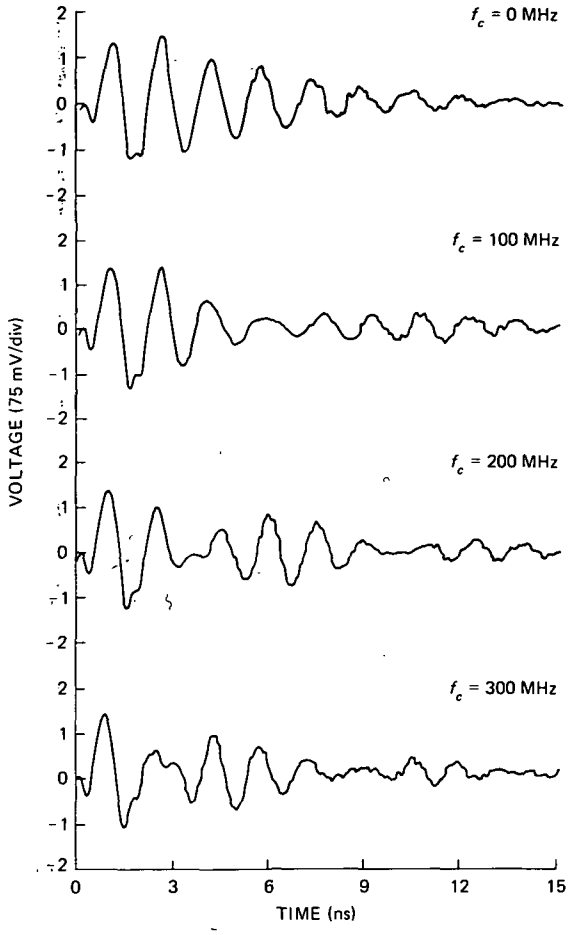

Figure 32—Linear impulse responses, f_p = 1.1 GHz.

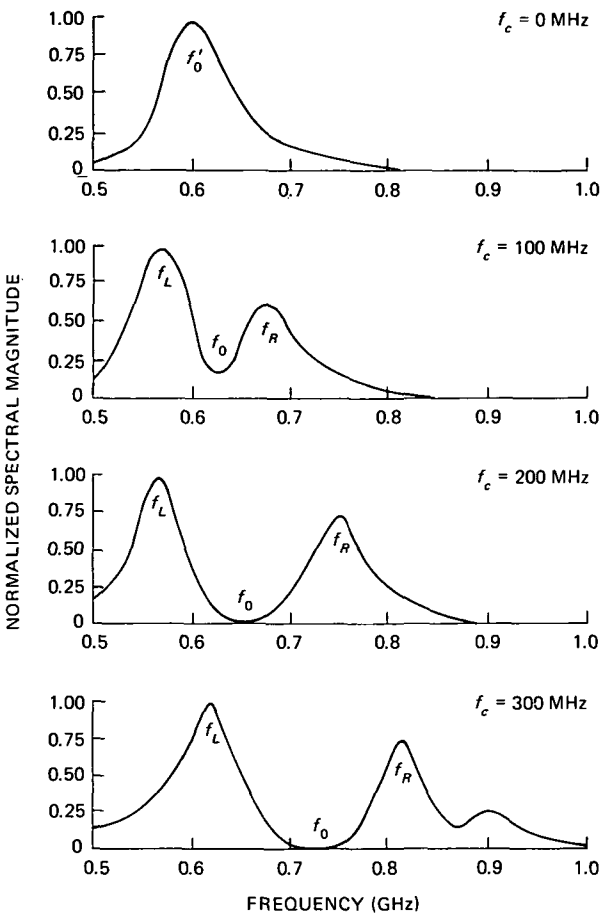

Figure 33—Linear impulse response spectra, f_p = 1.1 GHz.

For a more quantitative comparison, the frequency spectra of the experimental and theoretical results are again compared. Figure 33 shows the normalized frequency (power) spectra of the responses shown in Figure 32. These spectra were determined by digital Fourier analysis as was previously employed to obtain the spectra plotted in Figure 31. With no magnetic field, $f_c = 0$, the spectrum displays a single (dipole) resonance peaked at 605 MHz (denoted as f_0'), the shape of which is due to the plasma absorption resulting from inhomogeneity in plasma density. The effect of magnetic field is seen to split the dipole resonance into two main resonances at the frequencies previously denoted as f_R and f_L, separated by a minimum at the frequency f_0. According to Equation 61, the spectrum for the nonmagnetoplasma consists of a single resonance line at frequency $\omega_0/2\pi$. The application of a magnetic field splits the single resonance into two resonances at frequencies $\omega_L/2\pi$ and $\omega_R/2\pi$ and an antiresonance at $\omega_0/2\pi$. From these theoretical results, the relationships between the measured frequencies f_L and f_R, f_0 and f_0', and the electron-cyclotron frequency f_c are predicted by

$$f_R - f_L = f_c \tag{94}$$

Table 2—Data for linear impulse response spectra, f_p = 1.1 GHz.

f_c (MHz)	Measured Data			Calculated Results		
	f_L (MHz)	f_R (MHz)	f_0 (MHz)	$f_R - f_L$ (MHz)	$\frac{f_R - f_L}{f_c} - 1$ (percent)	$\frac{f_0 - f_0'}{f_0'}$ (percent)
100	575	680	625	105	5.0	3.3
200	565	750	650	185	7.5	7.4
300	620	815	750	195	35.0	19.0

NOTE: f_0' = 605 MHz.

$$f_0 - f_0' = 0 . \tag{95}$$

The separation between resonances $f_R - f_L$ and the difference between the minimum position and dipole resonance $f_0 - f_0'$ are given in Table 2 for the different electron-cyclotron frequencies. It is seen that there is less correlation with Equations 94 and 95 as the electron-cyclotron frequency increases.

It was at first thought that the discrepancy for larger magnetic fields was due to possible changes in plasma frequency with magnetic field. However, accurate microwave cavity measurements of plasma frequency were made showing no such effects. A second mechanism considered was the distortion introduced in the spectrum by spurious resonances. These resonances arise from axial propagation effects (Reference 18) (not included in the theory) and appear as a number of separated, sharp resonances whose frequencies increase with magnetic field. From microwave scattering measurements (to be described later), the spurious resonances were observed to overtake the main resonances (centered at f_L and f_R) producing a distorted spectrum. For the electron-cyclotron frequencies below 250 MHz, no spurious resonances were observed in the spectrum (0.25 to 1.1 GHz). The first evidence of a spurious resonance in Figure 33 is seen to appear at 900 MHz for f_c = 300 MHz. However, because this resonance is beyond the main resonances, there is no apparent distortion of the main resonances.

Having eliminated the possibility of large changes in plasma frequency due to magnetic field and the appearance of spurious resonances produced by the magnetic field, it appears that the discrepancy observed for large magnetic fields (>7 mT (>70 G) f_c > 200 MHz) is due to the inadequacy of the simple theory used. An attempt was made in Section 2 to include the effects due to inhomogeneity in plasma density into the cold plasma model. The approximate impulse response as given by Equation 78 is compared as follows with the experimental responses shown in Figure 32.

Considering a homogeneous magnetic field and inhomogeneous plasma density, the approximate impulse response of Equation 78 is given by

$$\Gamma(t) = \frac{2}{r^2} \cos \frac{\omega_c}{2} t \int_0^a \frac{\omega_0^2}{\sqrt{\omega_0^2 + (\omega_c/2)^2}} \left[\sin \sqrt{\omega_0^2 + \left(\frac{\omega_c}{2}\right)^2}\, t \right] r'\, dr' \tag{96}$$

where $\omega_0 = \omega_p(r')/\sqrt{2}$. This equation is similar to that obtained for a homogeneous plasma (Equation 64). The modulation of the magnetoplasma response comes from the term $\cos(\omega_0/2)t$, which is

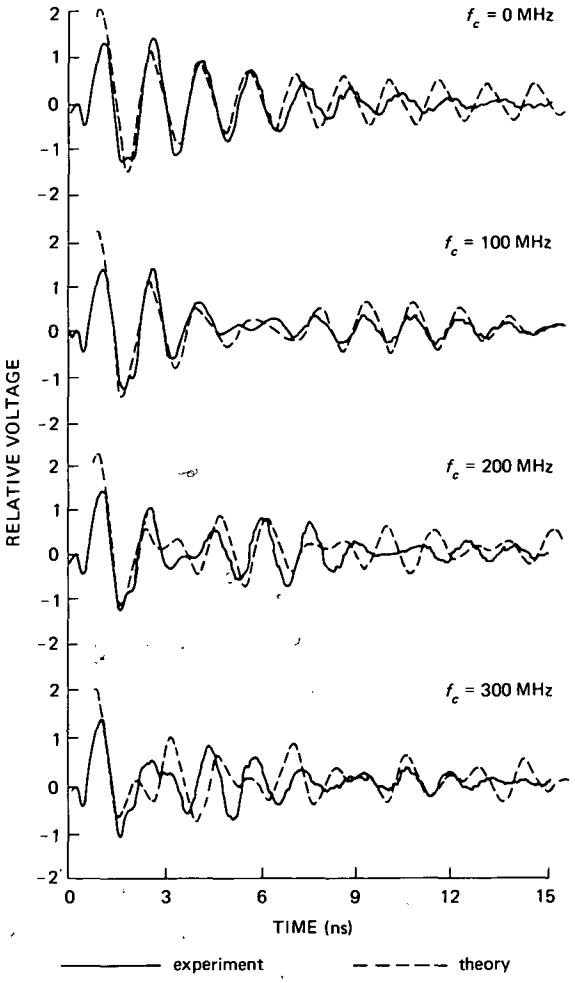

Figure 34—Comparison between theory and experiment.

the same as the homogeneous case. The higher frequency oscillation now appears as a phase-mixing-type integral, resulting in a damping of the plasma response due to the inhomogeneity in density. These effects can be seen from the plots in Figure 13 which were obtained by solving Equation 96 on a computer for a quartic density profile. The different plasma responses are plotted on the same normalized time scale $f_0(0)t$ for the different ratios of electron-cyclotron frequency to frequency $f_0(0) = f_p(0)/\sqrt{2}$; i.e., $f_c/f_0(0)$. For the purpose of comparison, the theoretical responses are superimposed on the experimental responses (Figure 32) as shown in Figure 34. The initial oscillation frequencies of the theoretical and experimental responses are set equal. Also, the amplitude of the theoretical response was adjusted so that its first negative peak is approximately equal to that obtained experimentally. The first negative peak was chosen rather than the initial peak because of the initial reduction of the experimental response due to the finite width of the BBG pulse. In addition, the frequency $f_0(0)$ is equal to 2/3 GHz; therefore, the parameters $f_c/f_0(0)$ of 0.15, 0.30, and 0.45 correspond to the experimentally obtained electron-cyclotron frequencies of 100, 200, and 300 MHz, respectively. Having appropriately scaled the theoretical responses to the experimental responses, the similarities between the two can easily be seen. However, the inclusion of the effect of inhomogeneity has not improved the discrepancy at large values of f_c (300 MHz) mentioned earlier (Table 2); this remains an open question for further investigation.

Scattering Measurements

The steady-state responses of the plasma were obtained using low-power microwaves (<0.1 mW) incident to the plasma and monitoring the reflected and transmitted (scattered) power at different frequencies. The experimental setup employed was similar to that shown in Figure 24, which was used to obtain the frequency characteristics of the parallel-plate transmission structure. In this case, the setup functions to obtain the spectrum of radiation from the plasma, which is within the parallel-plate structure. Because these measurements would be compared with the linear impulse response spectra, the 20-dB directional coupler was replaced by the 10-dB coupler used for the impulse response measurements. Also, the 20-dB attenuators were replaced by 10-dB attenuators.

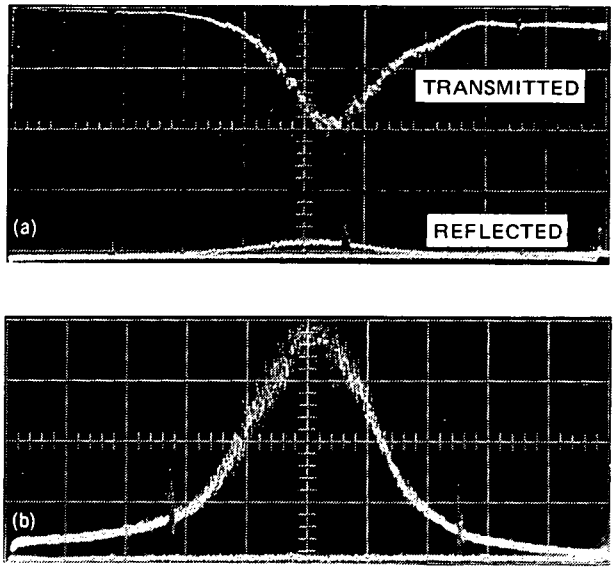

Figure 35—Transmission and reflection measurements, f_p = 1.1 GHz and f_c = 0. (a) Transmitted and reflected power spectra. (b) Normalized reflected power spectrum.

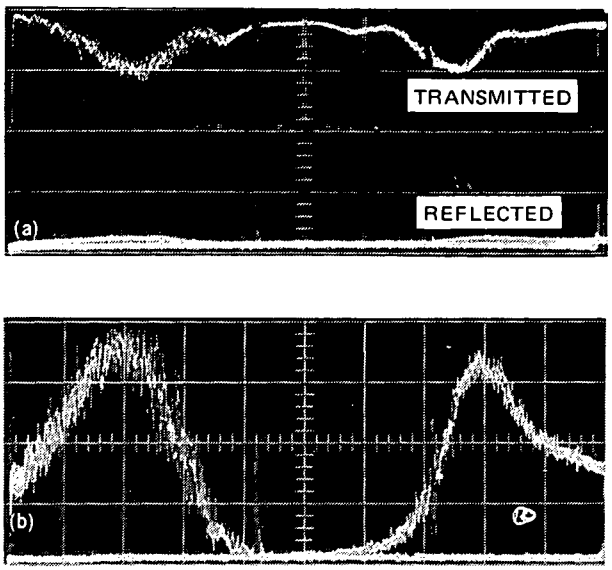

Figure 36—Transmission and reflection measurements, f_p = 1.1 GHz and f_c = 200 MHz. (a) Transmitted and reflected power spectra. (b) Normalized reflected power spectrum.

As in the previous measurements, the argon pressure was set at 0.33 N/m^2 (2.5 μm Hg). Measurements of the reflected and transmitted power from the plasma were made by using the modified setup of Figure 24. These results were used to determine the different amounts of power reflected, absorbed, and transmitted by the plasma. Also, these measurements are used to show the correlation between the steady-state plasma response and its impulse (BBG) response via the Fourier transform principle.

Figures 35 and 36 show the reflected and transmitted power spectra for the plasma parameters indicated. The incident power spectra are approximately flat and are four divisions above the baseline. For the nonmagnetoplasma (Figure 35a) the peak reflected power (600 MHz, at center of the figure) is 50 percent below the transmitted power and 95 percent below the incident power level. This corresponds to 5 percent of the incident power reflected, 45 percent transmitted, and 50 percent absorbed at resonance by the plasma. As discussed earlier, this resonance absorption arises from phase mixing due to inhomogeneity in plasma density. This same form of absorption is observed for the magnetoplasma in Figure 36a (center of figure is 650 MHz) and has been studied extensively (References 6 and 7).

The normalized reflected power spectra are shown in Figures 35b and 36b for the plasma parameters indicated. They are now compared with the spectra obtained from the corresponding impulse responses. The two different spectra cannot be compared side by side because of the slight nonuniformity of the frequency axes introduced by the sweep generator operation. Hence, comparisons are made at only discrete frequency points.

Figure 35b shows the spectrum for the nonmagnetoplasma having a plasma frequency of 1.1 GHz and is compared with that at the top of Figure 33. The impulse response spectrum has its resonance at 605 MHz whereas the reflected spectrum is at 600 MHz. Also, the 3-dB (half power) width is 75

MHz for the impulse response spectrum and 72 MHz for the reflected spectrum. The difference between the two results is less than 5 percent.

The reflected spectrum for the magnetoplasma (Figure 36b) was obtained for the same plasma parameters as that of the impulse response spectrum (Figure 33, f_c = 200 MHz). The minima occur at approximately the same frequency (650 MHz). The two resonances of the reflected spectrum appear at 560 and 760 MHz; those for the impulse response spectrum occur at 565 and 750 MHz, resulting in a difference of less than 2 percent.

The Nonlinear Impulse Response

Nonlinear impulse responses were obtained by exciting the plasma with BBG peak amplitudes (termed excitation voltage) extending up to 1860 V, the maximum BBG output. The experimental setup employed was the same as that used for obtaining the linear impulse responses (Figure 26). To

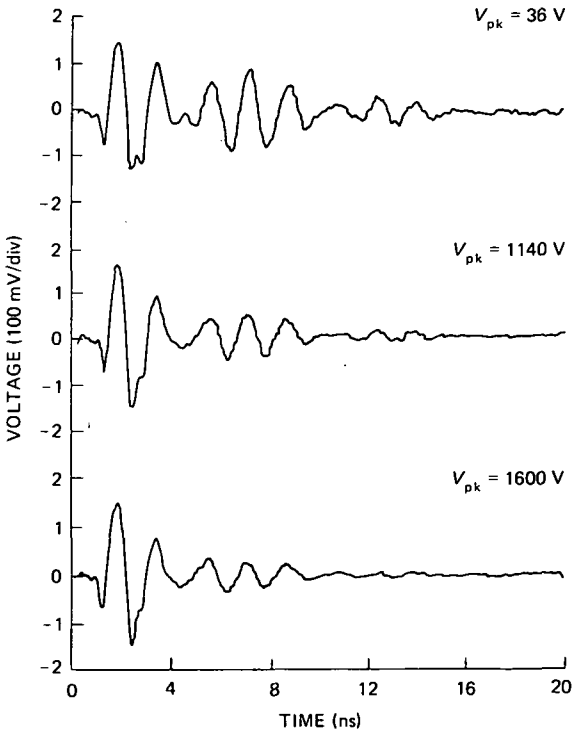

Figure 37—Nonlinear impulse responses for different excitation voltages, f_c = 200 MHz.

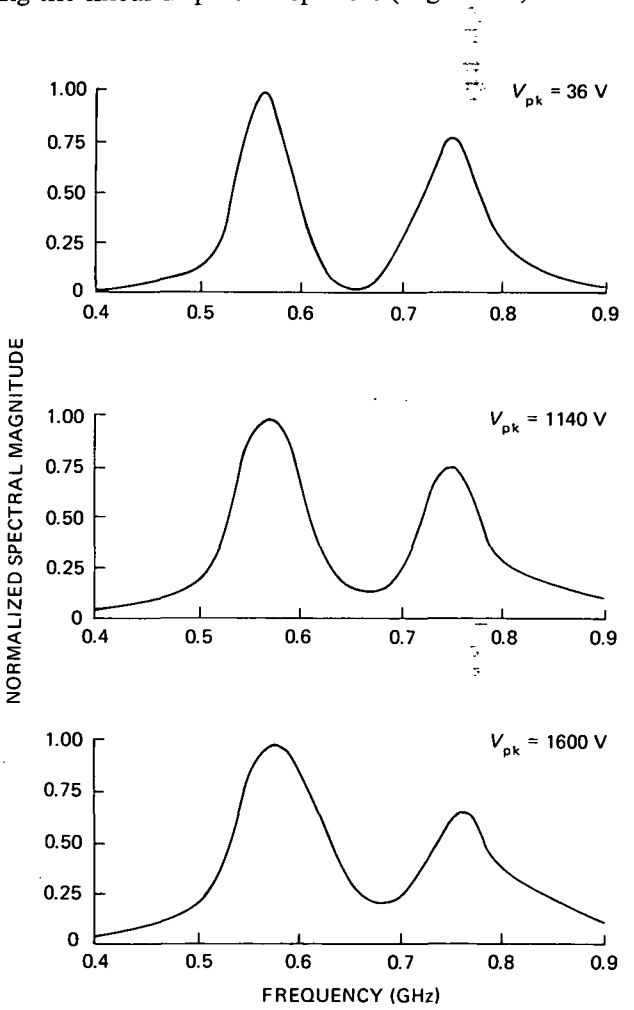

Figure 38—Nonlinear impulse response spectra for different excitation voltages, f_c = 200 MHz.

vary the excitation voltage in discrete steps, fixed attenuators were connected at the output of the BBG. Continuous changes in excitation voltage between steps were obtained by adjusting the variac connected to the BBG power supply.

Measurements were obtained for excitation voltages V_{pk} of 33, 3, and 0 dB below the BBG output of 1600 V (set by the variac); i.e., 36, 1140, and 1600 V, respectively. These excitation voltages were obtained using a 20-, 10-, and 3-dB attenuator and connecting them either at the output of the BBG or before the input to the sampling scope. This sets the attenuation in the circuit to be 33 dB, consequently setting the overall system gain (from BBG output to scope input) to a constant value for the different voltage measurements. Hence, all responses are displayed on the same voltage and time scales, making it a simple matter to compare them. Any changes observed between the different responses can be readily correlated with the nonlinearities in the plasma.

The first series of measurements were obtained for an argon pressure of 0.33 N/m^2 (2.5 μm Hg) and a discharge current of 100 mA, corresponding to a plasma frequency of 1.1 GHz. Also, 7 mT (70 G) of magnetic field was applied, corresponding to an electron-cyclotron frequency of 200 MHz. The responses are shown in Figure 37 on the same voltage (measured by the sampling scope) and time scales for the excitation voltages V_{pk} of 36, 1140, and 1600 V. The increase in damping for the larger excitation voltage is first noted. An increase is also found in oscillation frequency for larger excitation. These same nonlinear features are exhibited by the frequency (power) spectra of the waveforms, as shown in Figure 38, which were obtained using the same technique employed to obtain the linear impulse response spectra.

From these spectra it is clearly seen that the increased excitation results in both an increased nonlinear damping and a positive frequency shift. This same nonlinear behavior was observed for a nonmagnetoplasma (Figure 39) for the same argon pressure, discharge current, and excitation voltages. The nonlinear damping and positive frequency shift are also shown in the frequency spectra (Figure 40) of the nonmagnetoplasma responses.

It is observed from these experiments that the plasma nonlinearity results in a stronger damped response with a small increase in the frequency of oscillation. Additional measurements are presented to display the nonlinear damping as a function of excitation voltage, argon pressure, and plasma frequency. Also shown is the nonlinear frequency shift as a function of plasma frequency. In presenting the data, comparisons are made with the nonlinearity resulting from electron-neutral collisions and the mechanism developed in Section 2.

From the preliminary measurements shown in Figures 37 to 40, it is noted that the nonlinearity exhibits the same characteristics with and without magnetic field. Therefore, only the nonmagnetoplasma responses need to be considered. Experiments were performed (Reference 29) displaying the nonlinear damping of the nonmagnetoplasma responses as a function of excitation voltage, argon pressure, and plasma frequency and are referred to in the following discussion.

To obtain a measure of the damping, the 3-dB (half power) spectral widths were used as determined from the frequency spectra of the different nonmagnetoplasma responses. This damping (frequency) coefficient is compared with that due to electron-neutral collisions in Figure 41. For this purpose, the damping coefficients were obtained for an argon pressure of 0.33 N/m^2 (2.5 μm Hg) and a plasma frequency of 1.1 GHz and are plotted against the initial electron velocity v_e produced by the BBG

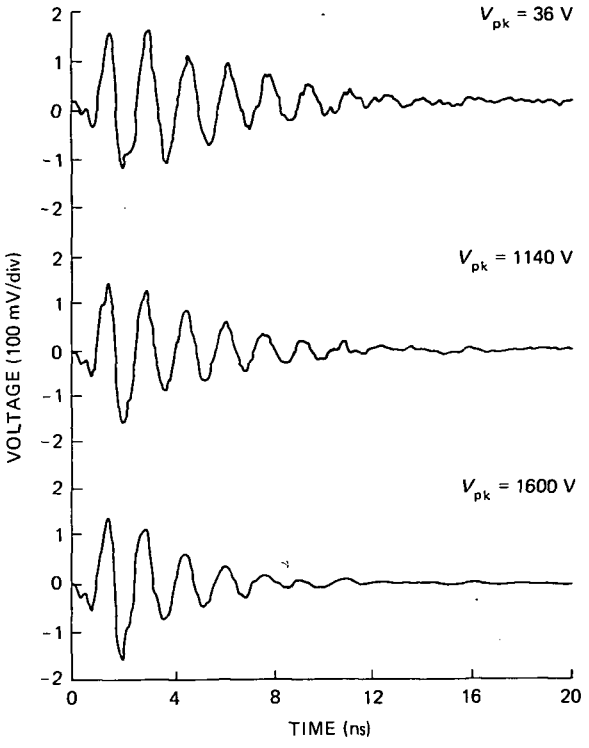

Figure 39—Nonlinear impulse responses for different excitation voltages, f_c = 0.

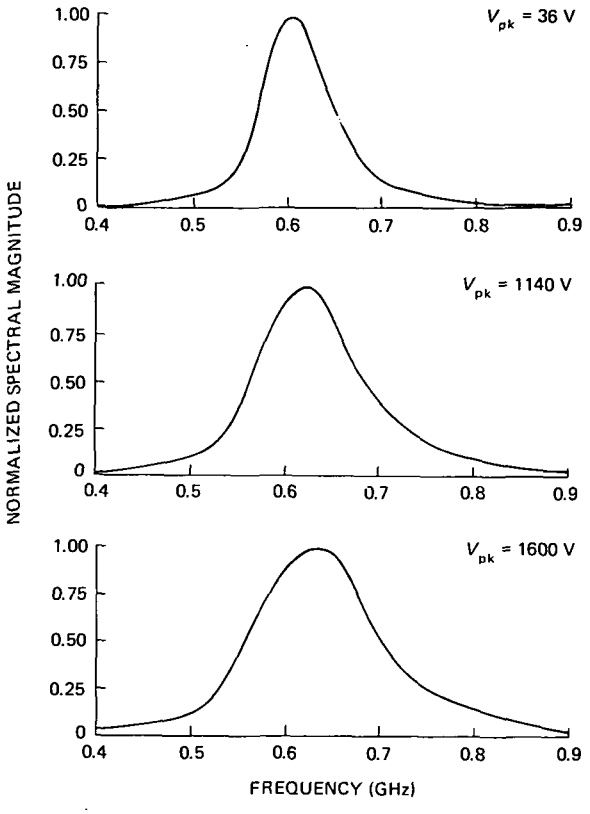

Figure 40—Nonlinear impulse response spectra for different excitation voltages, f_c = 0.

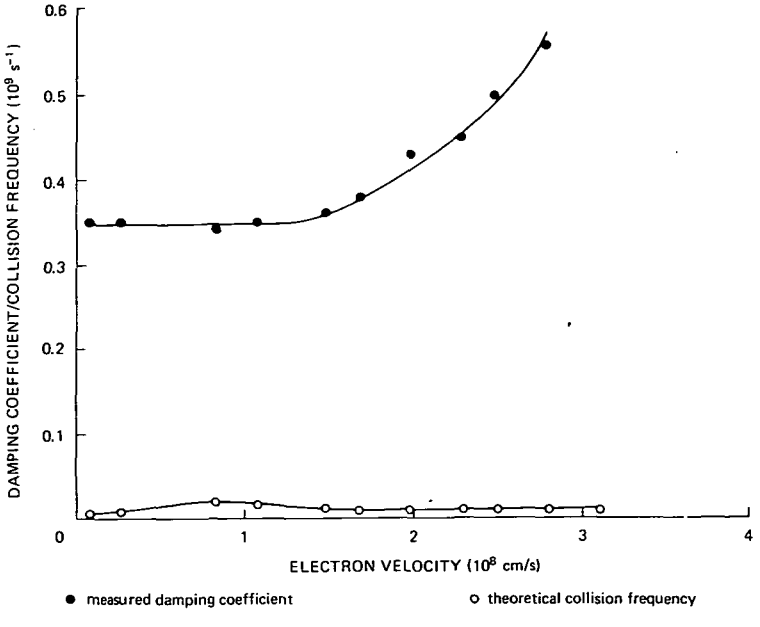

Figure 41—Damping coefficient and collision frequency versus electron velocity.

pulse. The values of v_e corresponding to different V_{pk} were determined from the following equation:

$$v_e = \frac{e}{m_e} \frac{V_{pk}}{2b} t_p \,, \tag{97}$$

where $2b$ = 2 cm and represents the spacing between the parallel plates, and t_p = 200 ps and is the effective pulse width determined by the normalized area (V_{pk} is set to unity) of the BBG waveform in Figure 21a. In obtaining the damping due to electron-neutral collisions, the electron-neutral collision frequency for argon (Reference 30) was employed corresponding to the pressure of 0.33 N/m^2 (2.5 μm Hg) and velocities equal to the thermal speed of 1.7 X 10^8 cm/s (1.6-aJ (10-eV) plasma) plus the additional v_e resulting from excitation. It is evident by comparing these two curves that the nonlinear damping is much larger than that produced by electron-neutral collisions. Besides the large difference in magnitudes, the two curves have completely different characteristics. The nonlinear damping coefficient increases monotonically for larger electron velocities whereas the electron-neutral collision frequency reaches a maximum at about 10^8 cm/s and decreases for larger velocity.

To further eliminate the possibility of nonlinear electron-neutral collisional damping, measurements of the damping coefficient are compared for different argon pressures. Figure 42 displays the damping coefficient measured at the linear level (V_{pk} = 50 V) and nonlinear level (V_{pk} = 1600 V) for different argon pressures. The plasma frequency was maintained at 1.1 GHz by adjusting the discharge current for the different pressures. Except for the uniform shift in the damping coefficient, the linear and nonlinear dampings show the same variation with pressure. The changes observed for the low pressure and high pressure are due to the increase in striations (see previous discussion of the plasma in Section 3) and appear independent of excitation voltage. If the damping were due to electron-neutral collisions, the linear damping would increase linearly with pressure, which it does not. Also, according

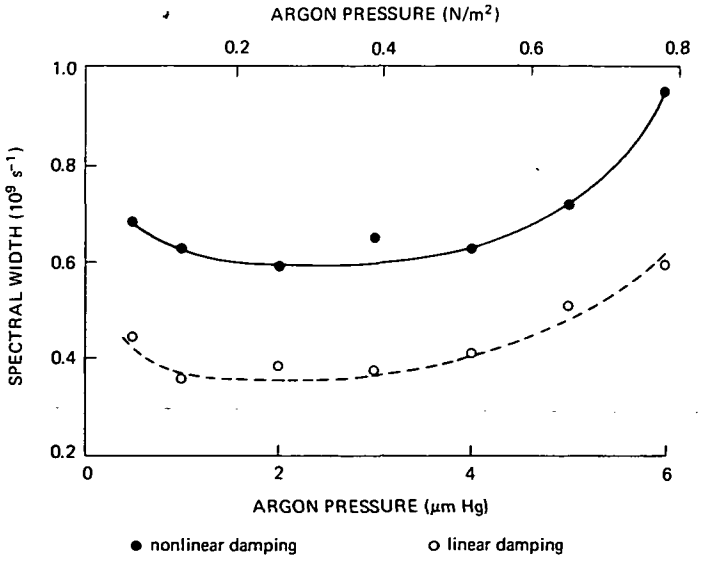

Figure 42—Damping coefficient of nonlinear emission versus pressure.

to Figure 18, the electron velocity is dependent on pressure, decreasing for higher pressures. Hence, the effect due to excitation on electron-neutral collisional damping should show a greater difference between the linear and nonlinear dampings at higher pressures than at lower pressures; this is not observed.

Having established that the nonlinearity is not a result of the velocity-dependent electron-neutral collisions, the mechanism developed in Section 2 offers the best explanation of the strong damping found for larger excitation. In Figure 9, it is observed that there exists a nonlinear mechanism for damping the plasma response due to electron crossover in an inhomogeneous plasma. Unlike that due to electron-neutral collisions, this form of nonlinearity results in increased damping with excitation. Also predicted by this theory is a small increase in the frequency of oscillation for larger excitation. Figure 43 shows the measured frequency shift as found from the frequency spectra (the center frequency (resonance) is used) of the linear (V_{pk} = 50 V) and nonlinear (V_{pk} = 1600 V) impulse responses for different plasma frequencies. Although there is some scattering of data points, the frequency shift is definitely positive, as predicted by theory, and is small (<20 MHz). Hence, at least qualitatively this nonlinear mechanism displays the characteristics of our experimental results.

Additional correlation with the nonlinear theory can be observed from the measurements made of the nonlinear damping for different plasma frequencies. Figure 44 shows the linear and nonlinear damping for different plasma frequencies at a pressure of 0.33 N/m^2 (2.5 μm Hg). It is observed that the linear (V_{pk} = 50 V) and nonlinear (V_{pk} = 1600 V) damping have different behavior as a function of plasma frequency. The linear damping increases with plasma frequency due to the phase mixing resulting from inhomogeneity in density (refer to the theoretical discussion of the linear impulse response

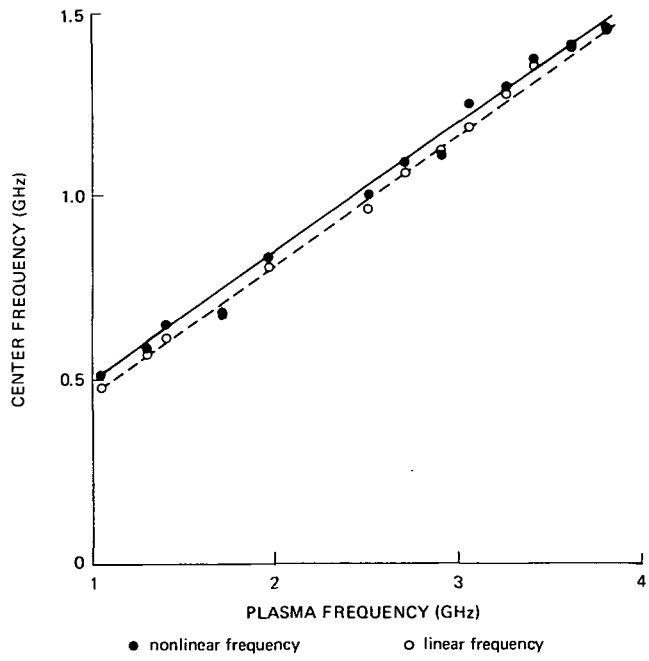

Figure 43—Frequency shift of nonlinear emission versus plasma frequency.

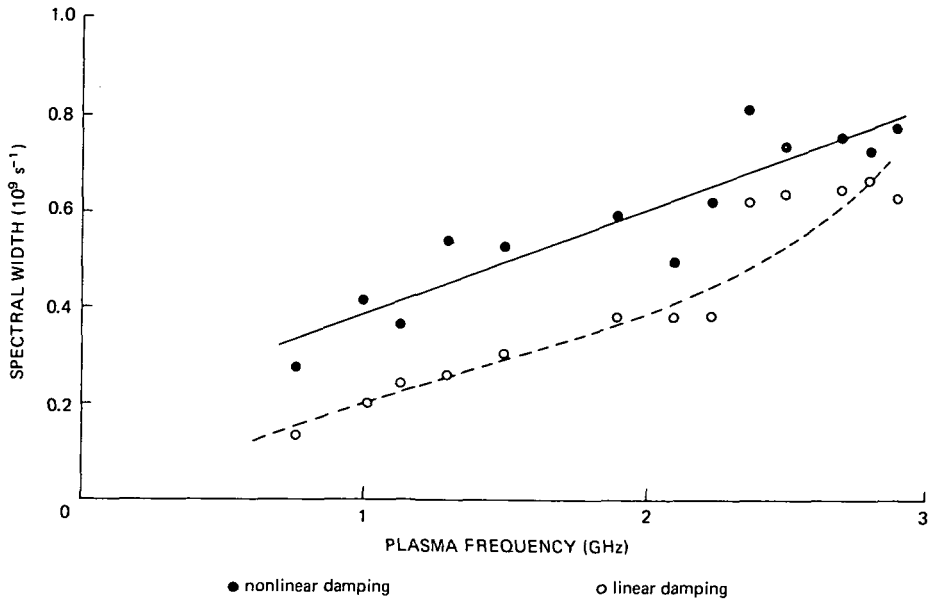

Figure 44—Damping coefficient of nonlinear emission versus plasma frequency.

and Reference 29). The nonlinear damping, however, is much larger than the linear values at low plasma frequencies and approaches the linear damping for larger plasma frequencies. These data support the nonlinear theory, which resulted in Equation 39 (also Equation 86) indicating an increase in damping for larger v_p or lower $f_p(0)$; i.e., for smaller values of the nonlinear parameter $\beta = f_p(0)(2a/v_p)$.

The results of these experiments indicate the close correlation between the nonlinear impulse measurements and the nonlinearity determined by the electron crossover in an inhomogeneous plasma. Both the increased damping and increase in oscillation frequency for larger excitation (or smaller plasma frequency) are explained by this mechanism.

5. CONCLUSIONS

The experimental part of this research provided new results concerning the nonlinear behavior of plasmas. The impulse (BBG) responses displayed both nonlinear damping and a positive frequency shift for initial electron velocities exceeding 10^8 cm/s.. It was established that the nonlinear damping is not due to electron-neutral collisions but results from a much stronger form of nonlinearity. A mechanism was proposed, by considering electron crossover in an inhomogeneous plasma, and accounts for the experimental observations. This nonlinear model results in an impulse response displaying an initial increase in frequency together with increased damping for electron velocities greater than 10^8 cm/s. The nature of the nonlinearity was attributed to the random mixing of the crossed electrons, which acts to remove their phase coherence.

Experiments were also performed to obtain the linear impulse responses corresponding to excitations below 10^8 cm/s. These measurements are found to be comparable with the linear theory of a cold, inhomogeneous plasma in which the damping is due to phase mixing. The magnetic field is seen

to modulate the nonmagnetoplasma response because of dipole splitting. Theoretical and experimental results are shown to correlate well for electron-cyclotron frequencies below 200 MHz.

ACKNOWLEDGMENTS

Grateful acknowledgment is made of the many people who contributed to this work. Prof. B. R. Cheo provided guidance, stimulation, encouragement, and infectious enthusiasm throughout the project.

The many conversations with Dr. R. Stern concerning the conceptual and experimental understanding of plasmas are acknowledged. Prof. N. Marcuvitz is to be thanked for supplying the theoretical background in the form of lectures and notes on plasma dynamics and turbulence. Much of the experimental work was performed in collaboration with Arthur R. Sindoris, who is to be thanked for his many discussions and suggestions during the preparation of this study. Also appreciated are the stimulating discussions with G. Georges and J. Shiue as well as the other members of the electrophysics department of New York University.

The material contained in this report was also used in a dissertation submitted to the Department of Electrical Engineering, New York University, as partial fulfillment for the degree of Doctor of Philosophy.

Goddard Space Flight Center
National Aeronautics and Space Administration
Greenbelt, Maryland, February 24, 1972
630-22-01-01-51

Appendix A

THE NONLINEAR TRANSFORMED EQUATIONS

The fluid equations (Equations 5 to 8), which represent a set of coupled, nonlinear equations, are transformed via Equation 9. The transformed plasma constituents $n_e(x, t)$, $v_x(x, t)$, $v_y(x, t)$, and $E_x(x, t)$ are written as $n_e(x_0, \tau)$, $v_x(x_0, \tau)$, $v_y(x_0, \tau)$, and $E_x(x_0, \tau)$, respectively, and the operators $\partial/\partial t$ and $\partial/\partial x$ when transformed become (using the chain rule)

$$\frac{\partial}{\partial t} = \frac{\partial}{\partial \tau} - v_x(x_0, \tau) \frac{\partial}{\partial x} \tag{A1}$$

$$\frac{\partial}{\partial x} = \frac{\partial/\partial x_0}{1 + (\partial/\partial x_0)X(x_0, \tau)} , \tag{A2}$$

where

$$X = \int_0^\tau v_x(x_0, \tau')\, d\tau' .$$

From Equation A1 it is noted that the transformation has the effect of replacing the convective derivative $\partial/\partial t + v_x\ \partial/\partial x$ by the local derivative $\partial/\partial \tau$. Substituting Equations A1 and A2 into Equations 5 to 8 produces

$$\frac{\partial}{\partial \tau} n_e(x_0, \tau) \left[1 + \frac{\partial}{\partial x_0} X(x_0, \tau)\right] = 0 , \tag{A3}$$

$$\frac{\partial}{\partial \tau} v_x(x_0, \tau) = -\frac{e}{m_e} E_x(x_0, \tau) - \omega_c(x) v_y(x_0, \tau) , \tag{A4}$$

$$\frac{\partial}{\partial \tau} v_y(x_0, \tau) = \omega_c(x) v_x(x_0, \tau) , \tag{A5}$$

$$\frac{\partial}{\partial \tau} E_x(x_0, \tau) = \frac{e}{\epsilon_0} n_i(x) v_x(x_0, \tau) + \frac{d}{d\tau} E_{\text{ext}}(\tau) , \tag{A6}$$

where the parameters ω_c and n_i have not been explicitly transformed.

Employing the relationship $\partial X/\partial \tau = v_x(x_0, \tau)$, Equations A5 and A6 when integrated with respect to τ yield

$$v_y(x_0, \tau) = \int_0^X \omega_c(x')\, dX' \tag{A7}$$

$$E_x(x_0, \tau) = E_{ext}(\tau) + \frac{e}{\epsilon_0} \int_0^X n_i(x')\, dX' , \tag{A8}$$

where $x' = x_0 + X'$.

These equations were obtained for zero initial velocity v_y and field E_x because the excitation arises from the applied field E_{ext}. Equation A8 becomes Equation 12 where

$$\omega_p^2(x) = \frac{n_i(x)e^2}{\epsilon_0 m_e} ,$$

and upon substituting Equations A7 and A8 into Equation A4, the trajectory equation, Equation 10, is obtained. Also, Equation 13 is derived by integrating Equation A3 with respect to τ, and employing the initial condition $n_e(x_0, 0) = n_i(x_0)$.

Appendix B

DENSITY MEASUREMENT

Measurement of the average density is obtained from the frequency shift of a TM 010 microwave cavity. The standard perturbation solution for the frequency shift Δf (Reference 31) gives the density as

$$\frac{\Delta f}{f} = \frac{1}{2} \frac{\int_{\text{plasma}} \omega_p^2(\mathbf{r})/\omega^2 E_0^2(\mathbf{r})\, dv}{\int_{\text{cavity}} E_0^2(\mathbf{r})\, dv}, \tag{B1}$$

where $\mathbf{E}_0(\mathbf{r}) = J_0(\chi_{01} r/r_c)\mathbf{a}_z$ and is the electric field of the empty cavity. Here r_c is the cavity radius, χ_{01} is the first zero of the Bessel function J_0, and $f = \omega/2\pi$ is the resonant frequency of the cavity. Collisions are ignored because $\nu \ll \omega$. The frequency shift is independent of the static magnetic field because the electric field is parallel to the magnetic field in the perturbation solution and fringe fields due to the end holes of the cavity have been ignored.

In the density measurement, a copper microwave cavity with 6.3-cm i.d., 8.5-cm length, and end holes of 16-mm diameter is used. The cavity is resonant at 3.65 GHz.

Measurements are made of densities in the range of $\omega_p^2/\omega^2 < 1/2$ where the perturbation solution is valid. To reduce the fringe fields, a large value of the ratio of cavity length to end-hole radius (approximately 11) is used.

The frequency shift measures the integrated density because the electric field is essentially constant for the value of $a/r_c = 0.15$ used in this experiment (a is the plasma radius). If the field is taken to be constant, which gives a 3 percent error, Equation B1 becomes

$$\frac{\Delta f}{f} = \frac{1}{2} \frac{\langle \omega_p^2 \rangle}{\omega^2} \left(\frac{a}{r_c}\right)^2 \frac{1}{J_1(\chi_{01})} \tag{B2}$$

where

$$\langle \omega_p^2 \rangle = \frac{2}{a^2} \int_0^a \omega_p^2(r) r\, dr\,. \tag{B3}$$

In Figure 19, the average electron density is obtained from Equation B3 which can be rewritten as Equation 87.

The cavity is excited in the TM 010 mode by a microwave signal generator connected to the input of the cavity; coupling in and out of the cavity is provided through magnetic coupling loops in the side walls. Frequency shifts are measured with a wave meter between the output of the cavity and a crystal detector. In all experiments performed, the density is constantly monitored because any drifts in density due to pressure variations (during a measurement) can lead to large errors in the plasma response.

REFERENCES

1. Schmitt, H. J.: "Plasma Diagnostics With Short Electromagnetic Pulses." *IEEE Trans. Nucl. Sci.* 11: 125, 1964.

2. Schmitt, H. J.: "Pulse Dispersion in a Gyrotropic Plasma." *IEEE Trans. Antennas Propagat.* 13: 934, 1965.

3. Baldwin, D. E.; Henderson, D. M.; and Hirshfield, J. L.: "Pulse Stimulated Emission From Plasma Columns." *Phys. Rev. Lett.* 20: 314, 1968.

4. Sindoris, A. R.; Grody, N. C.; and Cheo, B. R.: "Observation of Nonlinear Impulse Stimulated Emission From an Inhomogeneous Plasma Column." *Bull. Amer. Phys. Soc. Ser. II* 16(11): 1267-1268, 1971.

5. Baldwin, D. E.; and Ignat, D. W.: "Resonant Absorption in Zero Temperature Nonuniform Plasma." *Phys. Fluids* 12: 697, 1969.

6. Henderson, D. M.: "Pulse Stimulated Emission and Echoes at Upper Hybrid Resonance." Ph. D. thesis, Yale University, 1970.

7. Greenwald, R. A.: "Scattering of Electromagnetic Waves by a Nonuniform Magnetized Plasma Column." *Phys. Fluids* 13: 1112, 1970.

8. Leavens, W. M.; and Leavens, I. B.: "Quasi-Oscillations of Cold, Sharply Bound Plasmas." *Radio Sci.* 1: 789, 1966.

9. Schneider, H. M.; and Bers, A.: "Nonlaminar Effects in Plasma Slab Oscillations." *Symposium on Simulation of Plasma and Many Body Problems.* NASA SP-153, 1967, p. 41.

10. Hill, R. M.; and Kaplan, D. E.: "Cyclotron Resonance Echo." *Phys. Rev. Lett.* 14: 1062, 1965.

11. Gould, R. W.: "Echo Phenomena." *Phys. Lett.* 19: 477, 1965.

12. Crawford, F. W.; and Harp, R. S.: "Collisional Mechanism for Producing Cyclotron Echoes From Plasmas." *J. Appl. Phys.* 37: 4405, 1966.

13. Harp, R. S.; Bruce, R. L.; and Crawford, F. W.: "Some Studies of Electron Cyclotron Echoes From Plasmas." *J. Appl. Phys.* 38: 3385, 1967.

14. Bauer, L. O.; Blum, F. A.; and Gould, R. W.: "Plasma Echoes at Upper Hybrid Resonance." *Phys. Rev. Lett.* 20: 435, 1968.

15. Bruce, R. L.; Crawford, F. W.; and Harp, R. S.: "Plasma Transient Response and the Determination of Collision Data." *J. Appl. Phys.* 39: 2088, 1968.

16. Tonks, L.: "The High Frequency Behavior of a Plasma." *Phys. Rev.* 37: 1458, 1931.

17. Messiaen A. M.; and Vandenplas, P. E.: "Resonant Behavior of a Cylindrical Column of Plasma in Free Space With and Without Steady Magnetic Fields." *Physica* 28: 537, 1962.

18. Crawford, F. W.; Kino, G. S.; and Cannara, A. B.: "Dipole Resonance of a Plasma in a Magnetic Field." *J. Appl. Phys.* 43: 3168, 1968.

19. Davidson, R. W. C.; and Schram, P. P. J. M.: "Nonlinear Oscillations in a Cold Plasma." *Nucl. Fusion* 8: 183, 1968.

20. Dawson, J. M.: "Nonlinear Electron Oscillations in a Cold Plasma." *Phys. Rev.* 113: 383, 1959.

21. Nickel, J. C.; Parker, J. V.; and Gould, R. W.: "Resonance Oscillations in a Hot Nonuniform Plasma Column." *Phys. Rev. Lett.* 11: 183, 1963.

22. Gould, R. W.; and Blum, F. A.: *Proc. Int. Conf. Phenomena Ioniz. Gases 8th.* Springer-Verlag (Vienna), 1967, p. 405.

23. Cunningham, W. J.: *Introduction to Nonlinear Analysis.* Ch. 6. McGraw-Hill Book Co., Inc., 1958.

24. Vandenplas, P. E.: *Electron Waves and Responses in Bounded Plasmas.* Ch. 3. Wiley-Interscience, 1968.

25. Ignat, D. W.: "Resonant Behavior of a Bound Plasma." Ph. D. thesis, Yale University, 1969.

26. Huddlestone, R. H.; and Leonard, S. L.: *Plasma Diagnostic Techniques.* Ch. 4. Academic Press, Inc., 1965.

27. Saad, T. S.: *The Microwave Engineers' Handbook and Buyers' Guide.* Horizon House–Microwave, Inc. (Dedham, Mass.), 1969, p. 66.

28. Reitz, J. R.; and Milford, F. J.: *Foundations of Electromagnetic Theory.* Ch. 8. Addison-Wesley Pub. Co. (Reading, Mass.), 1960.

29. Sindoris, A. R.: "Nonlinear Impulse Stimulated Emission From a Plasma Column." Ph. D. thesis, New York University, 1971.

30. Brown, S. C.: *Basic Data of Plasma Physics.* MIT Press, 1959.

31. Bushman, S. J.; Mower, L.; and Brown, S. C.: "Interaction Between Cold Plasmas and Guided Electromagnetic Waves." *Phys. Fluids* 3: 806, 1960.

NATIONAL AERONAUTICS AND SPACE ADMINISTRATION
WASHINGTON, D.C. 20546

OFFICIAL BUSINESS
PENALTY FOR PRIVATE USE $300

SPECIAL FOURTH-CLASS RATE
BOOK

POSTAGE AND FEES PAID
NATIONAL AERONAUTICS AND
SPACE ADMINISTRATION
451

U.S.MAIL

POSTMASTER: If Undeliverable (Section 158
Postal Manual) Do Not Return

"The aeronautical and space activities of the United States shall be conducted so as to contribute . . . to the expansion of human knowledge of phenomena in the atmosphere and space. The Administration shall provide for the widest practicable and appropriate dissemination of information concerning its activities and the results thereof."

—NATIONAL AERONAUTICS AND SPACE ACT OF 1958

NASA SCIENTIFIC AND TECHNICAL PUBLICATIONS

TECHNICAL REPORTS: Scientific and technical information considered important, complete, and a lasting contribution to existing knowledge.

TECHNICAL NOTES: Information less broad in scope but nevertheless of importance as a contribution to existing knowledge.

TECHNICAL MEMORANDUMS: Information receiving limited distribution because of preliminary data, security classification, or other reasons. Also includes conference proceedings with either limited or unlimited distribution.

CONTRACTOR REPORTS: Scientific and technical information generated under a NASA contract or grant and considered an important contribution to existing knowledge.

TECHNICAL TRANSLATIONS: Information published in a foreign language considered to merit NASA distribution in English.

SPECIAL PUBLICATIONS: Information derived from or of value to NASA activities. Publications include final reports of major projects, monographs, data compilations, handbooks, sourcebooks, and special bibliographies.

TECHNOLOGY UTILIZATION PUBLICATIONS: Information on technology used by NASA that may be of particular interest in commercial and other non-aerospace applications. Publications include Tech Briefs, Technology Utilization Reports and Technology Surveys.

Details on the availability of these publications may be obtained from:

SCIENTIFIC AND TECHNICAL INFORMATION OFFICE

NATIONAL AERONAUTICS AND SPACE ADMINISTRATION

Washington, D.C. 20546